AMINA-CHIP

A MINIATURIZED MEASUREMENT SYSTEM FOR AMBIENT AMMONIA

Samenstelling promotiecommissie:

voorzitter:
prof.dr. W.H.M. Zijm
promotor:
prof.dr.ir. A. v.d. Berg
assistent Promotor:
dr.ir. W. Olthuis
leden:

prof.dr. N.F. de Rooij	Université de Neuchâtel (CH)
prof.dr. P.J. French	TU Delft (NL)
prof.dr.ir. P. Bergveld	Universiteit Twente (NL)
prof.dr. U. Karst	Universiteit Twente (NL)
dr. J.W. Erisman	ECN (NL)

The described research was carried out at the miniaturized sensor system for biomedical and environmental applications group, BIOS, of the MESA+ Research Institute, University of Twente. The research was financially supported by the Dutch Technology Foundation, STW, project TAC.5093.

Cover: Background: Scanning electron microscope image of the micro-porous polypropylene membrane (figure B.1(B)).
Backside image: structured glass parts of the integrated miniaturized ammonia measurement system (figure 4.18).

Title: AMINA-chip, a miniaturized measurement system for ambient ammonia

Author: Björn Timmer

ISBN: 90-365-2048-7

AMINA-CHIP

A MINIATURIZED MEASUREMENT SYSTEM FOR AMBIENT AMMONIA

PROEFSCHRIFT

ter verkrijging van
de graad van doctor aan de Universiteit Twente,
op gezag van rector magnificus,
prof.dr. F.A. van Vught,
volgens besluit van het College voor Promoties
in het openbaar te verdedigen
op vrijdag 28 mei 2004 om 15.00 uur

door

Björn Herman Timmer

geboren op 25 december 1975

te Nijverdal

Dit proefschrift is goedgekeurd door:

promotor:	prof.dr.ir. Albert van den Berg
assistant-promotor:	dr.ir. Wouter Olthuis

Voor mijn ouders:

"Ik ben toch een heel eind gekomen voor iemand die eigenlijk liever met z'n handen werkt dan met z'n hoofd.
Het is mij langzaam maar zeker duidelijk geworden dat je door je hoofd te gebruiken, ook beter met je handen kunt werken."

"Trust I seek and I find in you
every day for us something new
open mind for a different view
and nothing else matters,

So close no matter how far
couldn't be much more from the heart
forever trusting who we are
and nothing else matters"

Ofwel: "Sta open voor nieuwe dingen maar blijf altijd in jezelf geloven!"

James Hetfield and Lars Ulrich,
METALLICA

Table of contents

CHAPTER 1 SCOPE AND OUTLINE OF THIS THESIS

1.1 Introduction 3
1.2 Evolution of the ammonia measurement system 4
1.3 Research goal 5
1.4 Outline of this thesis 6
1.5 References 8

CHAPTER 2 AMMONIA SENSORS REVIEW

2.1 Introduction 9
2.2 Sources of ammonia 9
2.3 Ammonia toxicity 16
2.4 Application areas of ammonia sensors 16
2.5 Ammonia sensing principles 23
2.6 References 32

CHAPTER 3 "AMINA" AMMONIA MEASUREMENT PRINCIPLE

3.1 Introduction 37
3.2 Analysis of the "AMINA" chemistry 38
3.3 Conclusions 45
3.4 References 46

CHAPTER 4 DESIGN AND REALIZATION

4.1 Introduction 47
4.2 "AMINA" system design 47
4.3 Requirements and boundary conditions 48
4.4 Optimization and design 53
4.5 System realization 66
4.6 References 72

CHAPTER 5 RESULTS AND DISCUSSION

5.1 Introduction 75
5.2 Theoretical 77
5.3 Experimental 78
5.4 Results and discussion 81
5.5 Conclusions 87
5.6 References 89

CHAPTER 6 SOLID-STATE PHASE SEPARATION MEMBRANE

6.1 Introduction 91
6.2 Membrane preparation 91
6.3 Anodic bonding of a Si_3N_4 membrane to glass 98
6.4 References 103

CHAPTER 7 ALTERNATIVE GAS SAMPLER

7.1 Introduction 105
7.2 Experimental 107
7.3 Results and Discussion 111
7.4 Conclusions 113
7.5 References 115

CHAPTER 8 CONCLUSIONS AND RECOMMENDATIONS

8.1 Conclusions 117
8.2 Recommendations for future work 120
8.3 References 124

APPENDIX A MASS TRANSPORT

A.1 Introduction 125
A.2 Diffusive and convective transport of gaseous ammonia 126
A.3 Simulation of ammonia transport 129
A.4 Micro-scale gas sampler optimization 131
A.5 Simulation of ammonium transport 134
A.6 References 139

APPENDIX B MEMBRANE CHARACTERIZATION

B.1 Introduction 141
B.2 Membrane functionality 141
B.3 Porosity of a membrane 142
B.4 Permeability of a membrane 143
B.5 Hydrophobicity of a membrane 146
B.6 References 148

SUMMARY 149

SAMENVATTING 150

DANKWOORD 151

LIST OF PUBLICATIONS 152

Chapter 1

Scope and outline of this thesis

1.1 Introduction

The invention of the ISFET by Bergveld[1], until 2003 the chair holder of the BIOS chair, is an early marker for a whole new field of chemical sensors. With the development of microfluidic components, like pumps and valves, it became possible to integrate miniaturized sensors to form complete chemical analysis systems, known as lab-on-a-chip[2,3] or micro total analysis systems.[4] Since then, many people have worked on parts for the integration of microfluidic systems[5,6] and the first real lab-on-a-chip devices have been presented.[7,8]

Within the BIOS group, over the years, many people have worked on microfluidic systems for biomedical applications, e.g. the comprehensive integration of microdialysis membranes with silicon sensors[8] or a chip to analyze the lithium concentration in whole blood samples.[9] Especially for optimizing biomedical applications, miniaturization and integration can be very useful.[10]

Microfluidic detection systems can also be applied for measuring gasses. Different (dissolved) gas sensors have been made in the BIOS group, e.g. an ^{E}MOSFET-based hydrogen peroxide sensor[11] or a swelling hydrogel-based P_{CO_2} sensor.[12] The sensing system presented in this thesis is a lab-on-a-chip for measuring low concentrations of gaseous ammonia, where ammonia is sampled from an analyte gas into a microfluidic system.

1.2 Evolution of the ammonia measurement system

In the early 1990's an environmental ammonia monitoring system was realized at ECN, the Energy research Centre of the Netherlands. This device used a wet denuder, a rotating tube with a sample solution film. Ambient ammonia is sampled in the film and subsequently separated from interfering gasses and quantified using an electrolyte conductivity measurement. The ammonia monitor, shown in figure 1.1, has a very low detection limit of 6 ng/m^3 or about 5 ppt in air.[13] It proved the best suited apparatus available for a Dutch air quality monitoring network.[14,15]

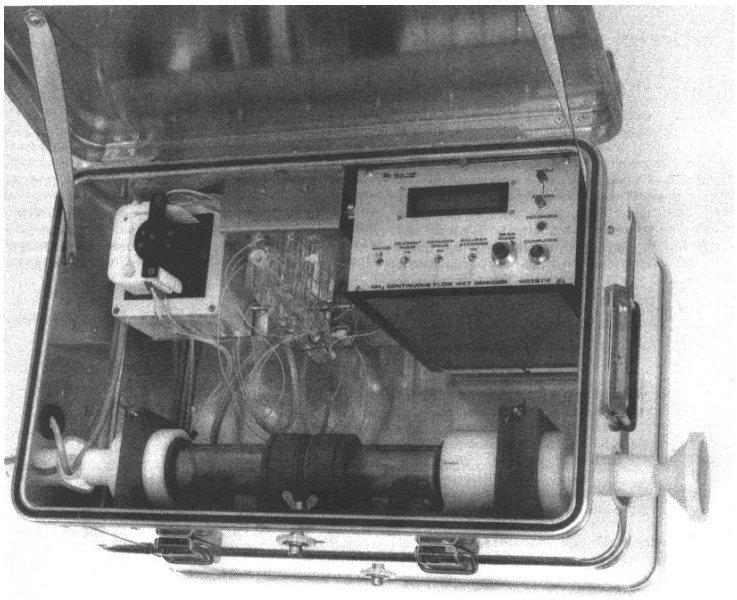

Figure 1.1 *Image of the ammonia monitor with a wet denuder tube.*

Although the ammonia measurement system had very good characteristics, it required intensive maintenance to keep it operational. Furthermore, the consumption of chemicals was rather demanding for usage in the monitoring network.[14] To overcome these problems, a second generation ammonia measurement system was developed, again at ECN.[16] The wet effluent denuder was replaced by a membrane diffusion sampler. This apparatus uses significantly less chemicals and is still very sensitive, with a lower detection limit of 177 ppt of ammonia in air. Since the late 1990's, the device is commercialized by a company called R&R-Mechatronics.[17] A photo of the apparatus called the AiRRmonia is shown in figure 1.2.

Figure 1.2 *Image of the AiRRmonia monitor for ambient ammonia.*[17]

Although the development of the aiRRmonia was a big step forward, for some applications the apparatus is still too cumbersome. Its size of a large carton box is awkward for measuring inside buildings. Furthermore, the apparatus requires about 20 litres of air for one measurement. For applications like breath analysis this required quantity of air is inconvenient. The miniaturization and integration process of the measurement system, described in this thesis, is the next step in the evolution of this type of ammonia monitoring equipment.

1.3 Research goal

The AMINA-chip project aims on miniaturizing the key components of the ambient ammonia measurement system that is developed at ECN.[4] The original macro-scale device comprises three parts, a gas sampler and a selector, that are made up of gas and liquid channels separated by a phase-separation membrane, and an electrolyte conductivity detector that comprises two electrodes. The dimensions of these three components should be reduced in order to decrease the analyte gas and reagents consumption. Miniaturization should also result in a reduced response time. The exact goal of the project will be explained in chapter four of this thesis, where the optimization process of the "AMINA-chip" is discussed.

1.4 Outline of this thesis

In the first part of this thesis, comprising chapter 1 until 5, the development of the "AMINA-chip" is described. First, a general introduction has been given in this first chapter. A review on ammonia sensors is given in chapter 2. After a brief survey on ammonia sources and the health threat caused by ammonia, different application areas for ammonia sensors and different sensing methods are described.

In the two main application areas for miniaturized ammonia measuring systems, environmental and medical ammonia sensing, the concentration levels of acidifying gasses are significantly higher than the alkaline gasses concentration levels, in practice the ammonia concentration. However, when designing an ammonia sensor, the device should always respond selectively to ammonia. How this is accomplished is explained in chapter 3.

When the requirements for the application of interest are known and the measurement principle is clear, an optimized system design can be developed. Both the optimization process and a process scheme for the realization of the resulting design are given in chapter 4.

The results of the measurements with chips that are realized according to the process scheme are given in chapter 5. Measurement results are shown that are used to investigate whether the system responds as expected according to the theoretical discussion in chapter 3 and the design parameters given in chapter 4.

The second part of this thesis is formed by chapter 6 and 7. In these chapters, alternatives are given for parts of the "AMINA-chip". In chapter 6, an exploration is given on a method to make a thin membrane using micro system technology. A bonding method used to integrate such a membrane in a microfluidic system and an optimization technique for the bonding parameters is presented in the second part of chapter 6.

An alternative gas sampler is presented in chapter 7. The gas sampler does not comprise an intermediate membrane layer between the analyte gas and the sample solution stream.

In chapter 8 of this thesis, a summary is given of the drawn conclusions. Subsequently, recommendations are given for future research and for improvements on the presented ammonia measurement system.

The last part of this thesis consists of two appendices. In the first, appendix A, design limitations caused by the required transport time of ions in a solution or gas molecules in a channel or membrane are investigated using simulation results. Subsequently, methods for investigating whether a membrane is suited as a gas-liquid phase separation layer are presented in appendix B.

1.5 References

[1] P. Bergveld, "*Development of an ion-sensitive solid-state device for neurophysiological measurements*", IEEE Transactions on Biomedical Engineering BME-17, pp 70–71, 1970

[2] A. Manz, N. Graber, H.M. Widmer, "*Miniaturized total chemical analysis systems: a novel concept for chemical sensing*", Sensors and Actuators B 1, pp 244-248, 1990

[3] P. Bergveld, "*Bedside clinical chemistry: from catheter tip sensor chips towards micro total analysis systems*", Biomedical Microdevices 2 (3), pp 185-195, 2000

[4] A. v.d. Berg, T.S.J. Lammerink, "*Micro Total Analysis Systems: Microfluidic Aspects, Integration Concept and Applications*", Topics in Current Chemistry 194, pp. 21-50, 1998

[5] P. Gravesen, J. Branebjerg, O. Sondergard Jensen, "*Microfluidics – A review*", Journal of Micromechanics and Microengineering 3, pp 168-182, 1993

[6] M. Elwenspoek, T.S.J. Lammerink, R. Miyake, J.H.J. Fluitman, "*Towards integrated microliquid handling systems*", Journal of Micromechanics and Microengineering 4, pp 227-245, 1994

[7] T.T. Veenstra, "*MAFIAS–An integrated lab-on-a-chip for the measurement of ammonium*", PhD-thesis, University of Twente, 2001

[8] S. Böhm, "*The comprehensive integration of microdialysis membranes and silicon sensors*", PhD-thesis, University of Twente, 2000

[9] E.X. Vrouwe, R. Luttge, A. v.d. Berg, "*Direct measurement of lithium in whole blood using a glass chip with integrated conductivity detection for capillary electrophoresis*", accepted for publication in Electrophoresis, 2004

[10] E. Verpoorte, "*Microfluidic chips for clinical and forensic analysis*", Electrophoresis 23, pp 677-712, 2002

[11] D.T. Van Ahn, "*New hydrogen peroxide sensor based on the ^{E}MOSFET concept*", PhD-thesis, University of Twente, 2003

[12] S. Herber, W. Olthuis, P. Bergveld, "*A swelling hydrogel-based PCO_2 sensor*", Sensors and actuators B 91, pp 378–382, 2003

[13] G.P. Wyers, R.P. Otjes, J. Slanina, "*A continuous flow denuder for the measurement of ambient concentrations and surface fluxes of ammonia*", Atmospheric Environment 27A, pp 2085–2090, 1993

[14] E. Buijsman, J.M.M. Aben, B.G. v. Elzakker, M.G. Mennen, "*An automatic atmospheric ammonia network in the Netherlands, set-up and results*", Atmospheric Environment 32 (3), pp 317-324, 1998

[15] M.G. Mennen, B.G. v. Elzakker, E.M. v. Putten, J.W. Uiterwijk, T.A. Regts, J. v. Hellemond, G.P. Wyers, R.P. Otjes, A.J.L. Verhage, L.W. Wouters, C.J.G. Heffels, F.G. Römer, L. v.d. Beld, J.E.H. Tetteroo, "*Evaluation of automatic ammonia monitors for application in an air quality monitoring network*", Atmospheric Environment 30 (19), pp 3239-3256, 1996

[16] J.W. Erisman, R. Otjes, A. Hensen, P. Jongejans, P. v.d. Bulk, A. Khystov, H. Möls, S. Slanina, "*Instrument development and application in studies and monitoring of ambient ammonia*", Atmospheric Environment 35, pp 1913-1922, 2001

[17] Internet source: http://www.mechatronics.nl/products/airrmonia/

Chapter 2

Ammonia sensors review*

2.1 Introduction

The goal of this review chapter is to explain the relevance of measuring ammonia, to explore possible applications of ammonia sensors and to evaluate different options to make a suitable sensor. To do so, this chapter comprises five parts. In the section following this introduction, different sources of ammonia are discussed, starting with a brief tour into the history of earth's atmosphere. In section three it is described why ammonia is marked as a dangerous chemical. Subsequently, different application areas for gaseous ammonia analyzers are investigated in section four, with a summary of the ammonia concentration levels of interest to these different areas. The last section deals with different techniques that have been described in literature for determining ammonia concentrations, including a summary of the important parameters like detection limits and response time.

2.2 Sources of ammonia

Ammonia is a natural gas that is present throughout the atmosphere. The relatively low concentrations, of low-ppb to sub-ppb levels,[1] have been significantly higher in the past. In this section, a brief discussion of the evolution of the earth's atmosphere is given, concentrating on the important role that ammonia may have played therein. Subsequently, current sources of ammonia are discussed.

**This chapter is submitted for publication as an ammonia sensor review in Sensors and Actuators B, 2004*

2.2.1 History of the earth's atmosphere

Earth history goes back over 4.5 billion years, when it was formed from the same cloud of gas and interstellar dust that created our sun, the rest of the solar system and even the entire galaxy, illustrated in figure 2.1. Earth is still shaping and cooling down from the galactic event that created the other stars and planetary systems in our galaxy, a process which began about 12 billion years ago when the Milky Way began to develop, about 3 billion years after the formation of our universe.[2]

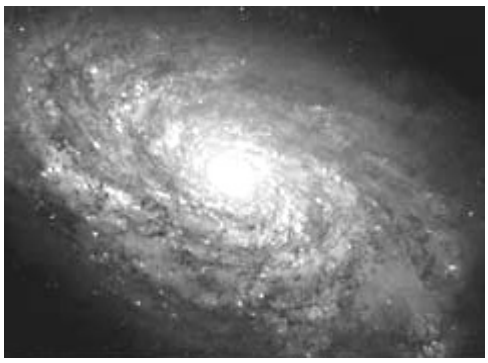

***Figure 2.1**. Earth is part of the Milky Way galaxy.*

As our solar system came into existence 6-7 billion years ago, the sun formed within a cloud of dust and gas that continued to shrink due to its own gravitational forces. This eventually started the fusion process that caused it to give off light, heat and other forms of radiation. During this process, the remaining clouds of gas and dust that surrounded the sun began to coalesce into smaller lumps called planetesimals, which eventually evolved into the planets known today, as illustrated in figure 2.2.

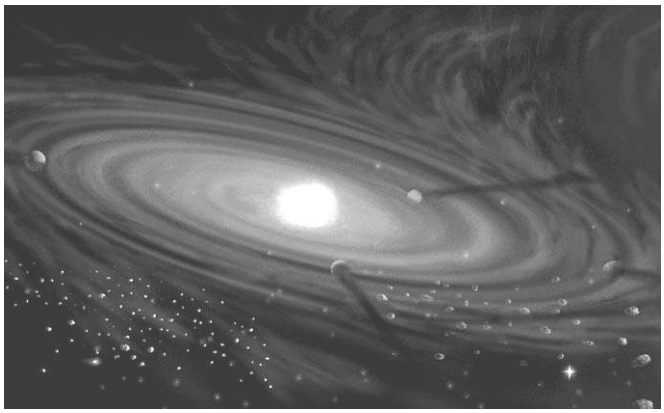

***Figure 2.2.** Earth and the other planets formed from gas and dust in our solar system.*

The larger outer planets had enough gravitational pull to remain covered in clouds of gas. The smaller inner planets, like earth, formed as molten rocky planets with only a thin gaseous atmosphere. For the first billion years of its

existence, earth was heavily bombarded by the remnants of the dust and debris, like asteroids, meteors and comets,[3] illustrated in figure 2.3, and possibly collisions between the planets,[4] until it settled as the current solid sphere in a stable orbit.

Figure 2.3. *Meteors and comets had a great influence on the creation of earth.*

It is thought that 3.8 to 4.1 billion years ago, the early earth had formed an atmosphere that was chemically reducing. Like the atmospheres of the outer planets today, the earth's atmosphere was made up of hydrogen and helium with large concentrations of methane and ammonia. It is known that the red coloration of the atmospheres of the two largest outer planets of our solar system; Jupiter and Saturn, is caused by clouds of ammonia in the gaseous and solid states.

Most of the early atmosphere was lost into space during the history of the planet and the remaining was diluted by a newly forming atmosphere. This new atmosphere was formed mostly from the outgassing of volatile compounds: nitrogen, water vapour, carbon dioxide, carbon monoxide, methane, ammonia, hydrochloric acid and sulphur produced by the constant volcanic eruptions that besieged the earth, illustrated in figure 2.4. Meteors and comets also added material to earth and its atmosphere, like large quantities of rare earth metals but also gaseous compounds like ammonia.[5]

Figure 2.4. *Large quantities of gaseous compounds are released into the atmosphere during volcanic activity.*

The earth's surface began to cool and stabilize, creating the solid crust with its rocky terrain. Clouds of water began to form as the earth began to cool, producing enormous volumes of rain water that formed the early oceans. The combination of a chemically reducing atmosphere and large amounts of liquid water may have led to the origin of life on earth. Earth is the only known life supporting planet. Since Louis Pasteur proved in 1862 that there is no spontaneous generation of life, scientists have made significant progress in understanding which chemical processes may have led to the origin of life on earth, somewhere between 4.0 and 3.5 billion years ago.[6] Ammonia was probably a component of significant importance in this process.[7-10] Earth's initial life forms were primitive bacteria and archea that might have originated from hot springs at the bottom of the ocean.[11] As is the case today, bacteria might have been able to oxidize ammonia as their energy source.[12,13] From these early forms of life it took another billion years before the first organisms capable of photosynthesis began to appear. The oldest fossils found, in fact, were a type of blue-green algae that could photosynthesize. Oxygen appeared in the earth's atmosphere because of the activity of these bacteria. Today, the atmosphere contains such high concentrations of oxygen that the spontaneous generation of complex molecules is impossible.

Since the formation of the early atmosphere, the concentration levels of the available gasses have still changed significantly. This is caused by global temperature changes, comet and asteroid collisions, earthquakes and volcanic activity. Large quantities of nitrogen replaced the hydrogen-helium atmosphere and oxygen and carbon dioxide became the energy sources for plants and animals. Only trace amounts of ammonia remained.

Atmospheric ammonia was discovered only 200 years ago by the French scientist de Saussure (in 1804) when he discovered atmospheric ammonia in rainwater. Only a few decades ago, people started being concerned about health threats by poisonous gasses in the atmosphere, leading to the development of gas analysers.

2.2.2 Today's sources of ammonia

The worldwide emission of ammonia per year was estimated in 1980 by the European community commission for environment and quality of life to be 20-30 Tg.[14] Other investigations, summarized by Warneck,[1] found values between 22 and 83 Tg. Figure 2.5 shows an estimate of the annual ammonium deposition rate world wide, showing a maximum deposition in central- and Western Europe.[1]

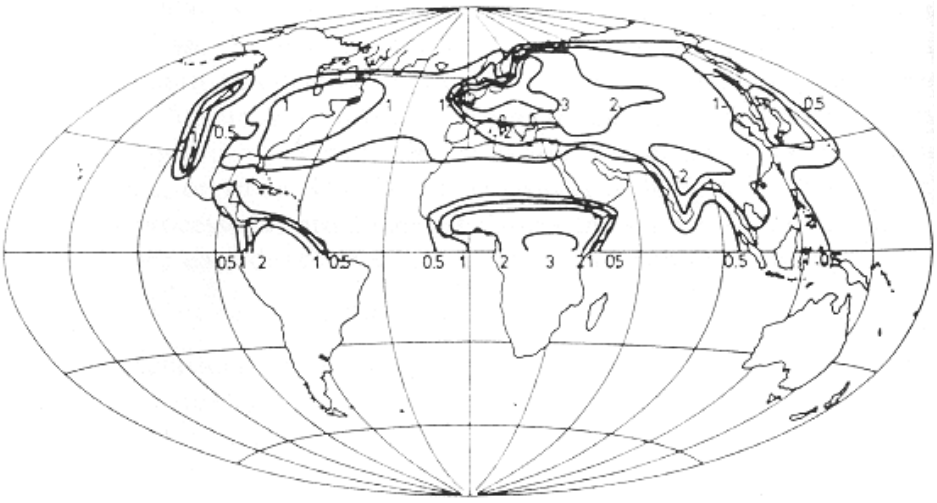

Figure 2.5. *Annual ammonium deposition (100 mg/m²)[1].*

When we take a closer look at these areas, in figure 2.6, it is shown that the atmospheric ammonia concentrations are highest in countries with intensive life-stock, especially in the Netherlands and Belgium. Therefore the Dutch research institute for human health and environment, RIVM, initiated a monitoring network for ammonia, resulting in a demand for very selective and sensitive ambient gas analyzers. This lead to the development of the

ammonia analyzer by the Energy research Centre of the Netherlands, ECN. The miniaturized measurement system described in this thesis is based on the same principle, discussed in detail in chapter 3 of this thesis.

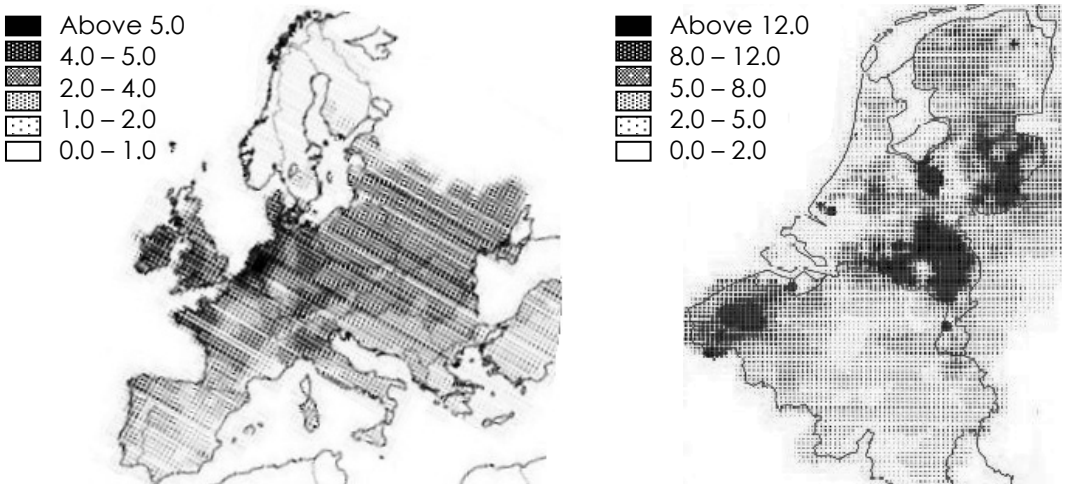

Figure 2.6. *Ambient ammonia levels in µg/m³, taken from the website of the Dutch research institute for human health and environment.*

In literature, three major classes of current ammonia sources are described[1]. Although the earth's atmosphere comprises almost 80% nitrogen, most nitrogen is unavailable to plants and consumers of plants. There are two natural pathways for atmospheric nitrogen to enter the ecosystem, a process called nitrification. The first pathway, atmospheric deposition, is the direct deposition of ammonium and nitrate salts by addition of these particulates to the soil in the form of dissolved dust or particulates in rain water. This is enhanced in the agricultural sector by the addition of large amounts of ammonium to cultivated farmland in the form of fertilizer. However, when too much ammonium is added to the soil, this leads to acidification, eutrophication, change in vegetation[15] and an increase in atmospheric ammonia concentration.[16] The second way of nitrification is bacterial nitrogen fixation. Some species of bacteria can bind nitrogen. They release an excess of ammonia into the environment. Most of this ammonia is converted to ammonium ions because most soils are slightly acidic.[6] The contribution of nitrogen fixation to the total world-wide ammonia emission is approximated to be 1.0 Tg/year.[14]

A larger source in to the overall nitrogen cycle is ammonification, a series of metabolic activities that decompose organic nitrogen like manure from agriculture and wildlife or leaves.[6] This is performed by bacteria and fungi.

The released ammonium ions and gaseous ammonia are again converted to nitrite and nitrate by bacteria.[6,12] The nitrogen cycle is illustrated in figure 2.7. The word-wide ammonia emission resulting from domestic animals is approximated to be 20-35 Tg/year.[1]

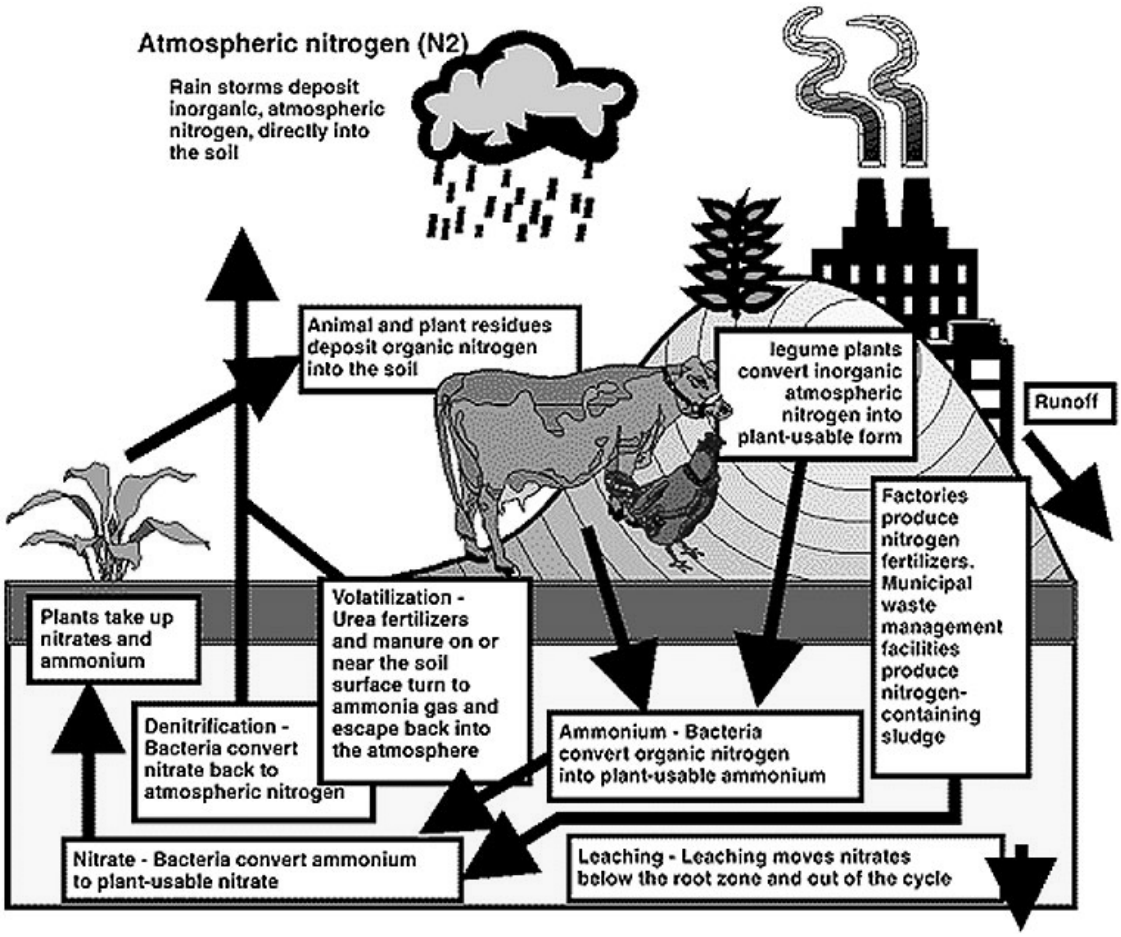

Figure 2.7. *Nitrogen cycle (Copyright University of Missouri, MU Extension WQ252).*

A third source of ammonia is combustion, both from chemical plants and motor vehicles. Ammonia is produced by the chemical industry for the production of fertilizers and for the use in refrigeration systems. The total emission of ammonia from combustion is about 2.1-8.1 Tg/year.[1]

There are numerous smaller sources of ammonia, e.g. surface water. Normally seas and oceans act as a sink for ammonia but occasionally they act as an ammonia source.[17,18] Ammonia is produced because of the existence of ammonium ions that are transformed to gaseous ammonia by acidification through rainwater.[18]

2.3 Ammonia toxicity

The lower limit of human ammonia perception by smell is tabulated to be around 50 ppm, corresponding to about 40 µg/m^3.[19] However, even below this limit, ammonia is irritating to the respiratory system, skin and eyes.[20,21] The long term concentration that is not hazardous for people to work in, is therefore set to be 20 ppm. Immediate and severe irritation of the nose and throat occurs at 500 ppm. Exposure to high ammonia concentrations, 1000 ppm or more, can cause pulmonary oedema; accumulation of fluid in the lungs. It can take up to 24 hours before the symptoms develop: difficulty with breathing and tightness in the chest. Short-term exposure to such high ammonia concentrations can lead to fatal or severe long term respiratory system and lung disorder.[22] Extremely high concentrations, 5000-10000 ppm, are suggested lethal within 5 to 10 minutes. However, accident reconstructions have proven that the lethal dose is higher.[23]

Longer periods of exposure to low ammonia concentration are not believed to cause long-term health problems. There is no accumulation in the body since it is a natural body product, resulting from protein and nucleic acid metabolism. Ammonia is excreted from the body in the form of urea and ammonium salts in urine. Some ammonia is removed from the body through sweat glands.

2.4 Application areas of ammonia sensors

There are many ways to detect ammonia. High concentrations are easy to detect because the gas has a very penetrating odour. With respect to other odorous gasses, the human nose is very sensitive to ammonia. To quantify the ammonia concentration or determine lower concentrations of ammonia, the human nose fails. However, in many occasions, the ammonia concentration has to be known, even at ultra low concentrations of less than parts per billion in air (ppb). This section focuses on four major areas that are of interest for measuring ammonia concentrations; environmental, automotive, chemical industry and medical diagnostics, and describes why there is a need to know the ammonia concentration in these fields. Where possible the concentration levels of interest are given for the different application areas.

2.4.1 Environmental gas analysis

The smell of ammonia near intensive farming areas or when manure is distributed over farmland is very unpleasant. Furthermore, as explained in the toxicity section of this chapter, exposure to high ammonia concentrations is a serious health threat. Concentration levels near intensive farming can be higher than the allowed exposure limit. This results in unhealthy situations for farmers and animals inside stables, where the concentrations are highest.

Another interesting point is the formation of ammonium salt aerosols. Sulphuric acid and nitric acid react in the atmosphere with ammonia to form ammonium sulphate and ammonium nitrate.[24] These salts are condensation nuclei, forming several nanometre sized airborne particles. Therefore, ammonia reduces the quantity of acids in the atmosphere. These aerosols have a sun-blocking function, as can often be seen above large cities or industrial areas. These clouds of smog, illustrated in figure 2.8, have a temperature reducing effect. This effect, however, is presently hardly noticeable due to the more intense global warming caused by the greenhouse effect.

Figure 2.8. *Smog, or clouds of aerosols, has a sun-blocking effect.*

Ammonia levels in the natural atmosphere can be very low, down to sub-ppb concentration levels above the oceans. The average ambient ammonia concentration in the Netherlands is about 1.9 ppb. Very accurate ammonia detectors with a detection limit of 1 ppb or lower are required for measuring such concentrations. Near intensive farming areas, ammonia concentrations are much higher, up to more than ten ppm.[25] It depends on the actual application what concentration levels are of interest. This also

determines the time resolution of the required analysis equipment. Monitoring ambient ammonia levels for environmental analysis does not demand extremely fast detectors. The macro-scale ammonia analyzer that this project is based on is designed for environmental analysis and has a response time of 15-20 minutes. When the analyzer is used in a controlled venting system in stables, a shorter response time is required in the order of a minute.

2.4.2 Automotive industry

The automotive industry is interested in measuring atmospheric pollution for three reasons.[26] First, exhaust gasses are monitored because they form the major part of gaseous pollution in urban sites. For instance, ammonia exhaust is associated with secondary airborne particulate matter, like ammonium nitrate and ammonium sulphate aerosols, as discussed in the previous section. Ammonium aerosols are measured to be up to 17 % of the particulate matter concentration smaller than 2.5 µm.[27] Ammonia emissions have been measured up to 20 mg/s [27] or up to 8 ppm ammonia in exhaust gas.[28]

A second reason for the automotive industry to be interested in detectors for atmospheric pollution like ammonia, is air quality control in the passenger compartment.[26] Modern cars are frequently equipped with an air conditioning system. This system controls the temperature and the humidity of the air inside the car. Fresh air can be taken from the outside of the car or it can be created by conditioning and circulating air inside the car. When there is low quality air outside the car, like air with smoke near a fire or a factory, the system should not take up new air from outside. A major source of unpleasant smell is the smell of manure near farms and meadows. This smell is caused by the increased ammonia concentration in these areas. For indoor air quality monitors, the detection limit should lie at least below the smell detection limit of about 50 ppm. Moreover, for such an application it is important that the sensor responds very fast. The air inlet valve should be closed before low-quality gas is allowed into the car. A response time in the order of seconds is required.

A third application for ammonia sensors in the automotive area is NOx reduction in diesel engines. Modern diesel engines operate at high air-to-fuel ratios that result in an excess of oxygen in the exhaust gas, resulting in large concentrations of NO and NO_2 (NOx).[29,30] Toxic NOx concentrations

are lowered significantly by selective catalytic reduction (SCR) of NOx with NH_3, according to equation 2.1. [31] Therefore, ammonia is injected into the exhaust system.

$$4NO + 4NH_3 + O_2 \rightarrow 4N_2 + 6H_2O \qquad (2.1)$$

It is unfavourable to inject too much ammonia for this is emitted into the atmosphere where it adds to the total pollution. The injected amount can be optimized by measuring the excess ammonia concentration in the exhaust system. The concentration level that is of interest for this application depends on the controllability of the setup. When the controllability of the ammonia injection is very accurate, the used sensor should be able to measure very low ammonia concentrations. The sensors that are currently used have detection limits in the order of a few ppm[29] and a response time of about one minute. Because measurements are performed in exhaust pipes, the sensor should be able to withstand elevated temperatures.

2.4.3 Chemical industry

The major method for chemically producing ammonia is the Haber process. The German scientist Fritz Haber started working on a way to produce ammonia in 1904.[32] In 1918 he won the Nobel Prize in Chemistry for his invention. Ammonia is synthesized from nitrogen and hydrogen at an elevated temperature of about 500˚C and a pressure of about 300 kPa using a porous metal catalyst. The process was scaled up to industrial proportions by Carl Bosch. The process is therefore often referred to as the Haber-Bosch process.

Ammonia production was initiated by the demand for an inexpensive supply of nitrogen for the production of nitric acid, a key component of explosives. Today, the majority of all man made ammonia is used for fertilizers or chemical production. These fertilizers contain ammonium salts and are used in the agricultural sector.

Another substantial part is used for refrigeration. Ammonia was among the first refrigerants used in mechanical systems. Almost all refrigeration facilities used for food processing make use of ammonia because it has the ability to cool below 0˚C.[33,34] The first practical refrigerating machine was developed in 1834 and commercialised in 1860. It used vapour compression as the

working principle. The basic principle: a closed cycle of evaporation, compression, condensation and expansion, is still in use today.[35]

Because the chemical industry, e.g. fertilizer factories and refrigeration systems, make use of almost pure ammonia, a leak in the system can result in life-threatening situations. All facilities using ammonia should have an alarm system detecting and warning for dangerous ammonia concentrations. The maximum allowed workspace ammonia level is tabulated to be 20 ppm. This is a long-term maximum so no fast detectors are not required, a response time in the order of minutes is sufficient. Especially in ammonia production plants, where ammonia is produced, detectors should be able to withstand the high temperature, up to 500˚C, applied in the production process.

2.4.4 Medical ammonia detectors

In the medical community, there is a considerable interest in ammonia analyzers that can be applied to measure ammonia levels in exhaled air for the diagnosis of certain diseases.[36] Measuring breath ammonia levels can be a fast diagnostic method for patients with disturbed urea balance, e.g. due to kidney disorder[37] or bacterial stomach infection causing ulcers.[38-40] For such applications, often only a few hundred ml of exhaled air is available and, at present, no suitable ammonia breath analyzer exists.[41]

In 1984 Marshall and Warren identified stomach bacteria that cause peptic ulcer.[38] The bacterium was named Helicobacter pylori, of which a picture is shown in figure 2.9.

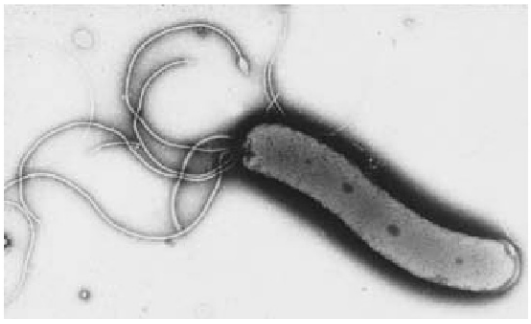

Figure 2.9. *Electron micrograph of H. pylori.*

After infection, the bacterium penetrates the stomach wall through the mucous barrier used by the stomach to protect itself against the digestive acid gastric juice.[39] The bacterium's most distinct characteristic is the abundant production of the enzyme urease.[42] It converts urea to ammonia

and bicarbonate to establish a locally neutralizing surrounding against penetrating acid. This is one of the features that make it possible for the bacterium to survive in the human stomach.

The immune system responds to the infection by sending antibodies.[39] The H. Pylori is protected against these infection fighting agents because it is hidden in the stomach wall protection layer. The destructive compound that is released by the antibodies when they attack the stomach lining cells eventually cause the peptic ulcer, as illustrated in figure 2.10.[39]

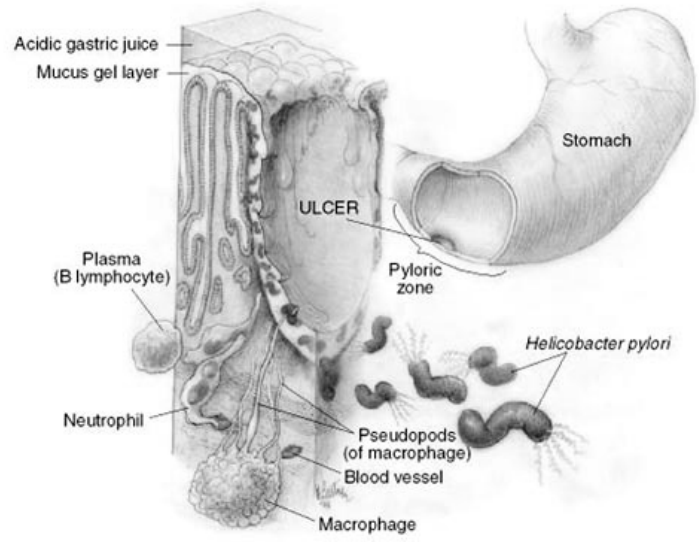

Figure 2.10. *Immune system cells infiltrate the area of the ulcer to attack the bacteria, leading to inflammation and damage.*

The conversion of urea to ammonia and bicarbonate led to H. pylori infection diagnosis tests. A first method is based on a gastric CO_2 measurement, directly related to the bicarbonate concentration. It makes use of an endoscopic procedure.[42] Non-invasive test methods are shown, based on measuring exhaled CO_2 or NH_3 levels.[40,42] Because the normal exhaled CO_2 levels are relatively high, isotopically labelled urea is used. Subsequently, labelled CO_2 concentrations are measured. The results are excellent but the test is expensive and it requires a radionuclide, limiting the applicability. Using a breath ammonia analyzer would be a more appropriate solution. Suitable analyzers should be able to selectively measure down to 50 ppb ammonia in exhaled air, containing CO_2 concentrations up to 3 %.[36] When measuring in exhaled air, the used analysis equipment should have a reasonable response time of at most a few minutes and often only small volumes of analyte gas will be available.

Ammonia levels in blood are also of interest in the sports medicine. During activity the human body produces ammonia. Ammonia can diffuse out of the blood into the lungs when the ammonia levels become higher than the ammonia levels in the air. The expired ammonia levels increase exponential with the workload. The concentration levels of interest, when measuring expired ammonia, are in the range of 0.1 to 10 ppm.[36]

2.4.5 Summary of application areas

The application areas that have been discussed in this section are summarized in table 2.1. The lower ammonia concentration that is of interest is given as the required lower detection limit. Estimations are given for the required response time and operation temperature.

Table 2.1. *Requirements for ammonia analysis equipment in different application areas.*

Application	lower detection limit	required response time	temperature range	remarks
Environmental				
air monitoring	1ppb	minutes	0 – 40˚C	
stables	1 ppm	~1 minute	10 – 40˚C	
Automotive				
exhaust	8 ppm[28]	seconds	Up to 300˚C	
air control	53 ppm[19]	~1 second	0 – 40˚C	
NOx reduction	1 ppm[29]	~1 minute	Up to 300˚C	
Chemical				
leakage alarm	20 ppm[19]	minutes	Up to 500˚C	Might be explosive
Medical				
breath analysis	50 ppb[36]	~1 minute	20 - 40˚C	Small gas volumes

2.5 Ammonia sensing principles

There are many principles for measuring ammonia described in literature. A different sensor is used in the exhaust pipe of automobiles than for measuring ultra-low concentrations of ambient ammonia for environmental monitoring. The most frequently used techniques in commercial ammonia detectors are discussed in this section. First, semiconductor- and metal oxide gas sensors are described. Secondly, conducting polymer ammonia analyzers are dealt with, followed by optical ammonia detection techniques. In the forth sub-section, indirect systems using gas samplers and specific chemical reactions to make a selective ammonia analyzer are discussed, followed by a summary of the described techniques.

2.5.1 Semiconductor- and metal oxide gas sensors

The ammonia sensors that have been manufactured in the largest quantities are without doubt semiconductor-oxide gas sensors, mostly based on SnO_2 sensors. A lot of research has been done on these types of gas sensors,[43] especially in Japan.[44] A great number of papers are published about reactivity of semiconductor- or metal oxide materials to specific gases, for instance ammonia, carbon monoxide or organic vapours.[45] These sensors are rugged and inexpensive and thus very promising for developing gas sensors. Many models have been proposed that try to explain the functionality of these types of sensors.[46] It is well established by now that the gas sensors operate on the principle of conductance change due to chemisorption of gas molecules to the sensing layer.

A common model is based on the fact that metal-oxide films consist of a large number of grains, contacting at their boundaries.[47] The electrical behaviour is governed by the formation of double Schottky potential barriers at the interface of adjacent grains, caused by charge trapping at the interface. The height of this barrier determines the conductance. When exposed to a chemically reducing gas, like ammonia, co-adsorption and mutual interaction between the gas and the oxygen result in oxidation of the gas at the surface. The removal of oxygen from the grain surface results in a decrease in barrier height.[48] The energy band diagram at the grain boundaries is shown in figure 2.11.

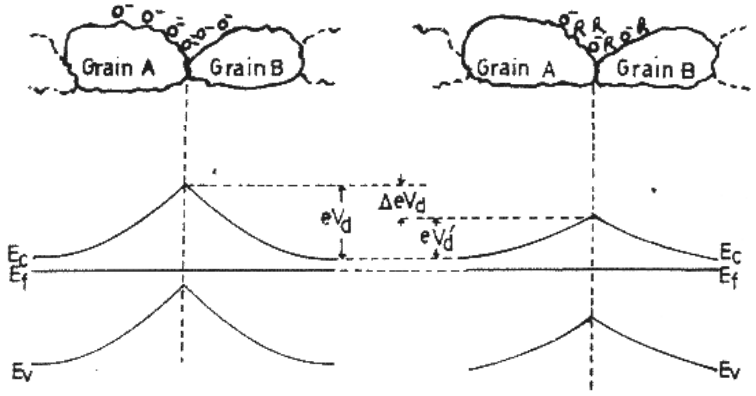

Figure 2.11. *Energy band diagram showing the Schottky barrier height at the grain boundary of tin oxide without and with a chemically reducing gas.*[47]

As can be concluded from this model, metal-oxide and semiconductor-oxide sensors are not selective to one particular gas. This is a major drawback. Different approaches to make selective sensor systems have been applied,[49] like principle component analysis,[50] artificial neural networks, also known as the artificial nose[51] or conductance scanning at a periodically varied temperature.[52] Varying the temperature changes the current density through a Schottky barrier but chemisorption is also a function of the temperature. It is shown that these two effects have a different temperature dependency for different gasses.

A different approach to make selective metal-oxide gas sensors is by using metals or additives that enhance the chemisorption of specific gasses. WO_3 based sensing material is demonstrated to respond to NH_3 and NO.[53,54] Many materials have been added to this sensing material in order to enhance the sensitivity and the selectivity towards these two gasses. The response to the two gasses can be adjusted, as is shown in figure 2.12. Known additives for optimizing the ammonia sensitivity of SnO_2 based ammonia sensors are Pd, Bi and $AlSiO_3$[55] or Pt and SiO_2.[56]

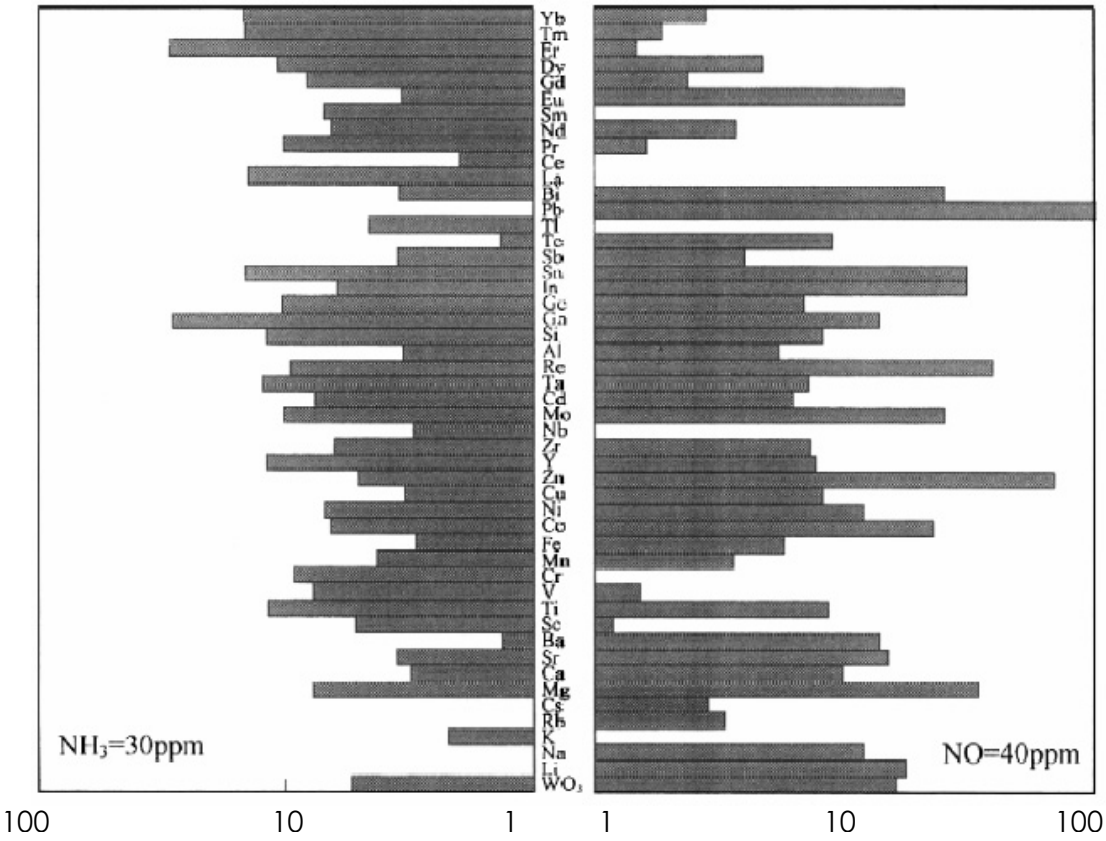

Figure 2.12. *Sensitivity adjustment of a WO_3 metal-oxide gas sensor to NH_3 and NO at 350 °C with 1 wt % additives.*[53]

The lowest ammonia detection limit of these types of sensors found in literature is 1 ppm, using a WO_3 ammonia sensor with Au and MoO_3 additives. The sensor is operated at an elevated temperature of more than 400°C.[54] Normal detection limits of these sensors range from 1 to 1000 ppm.[54,57] These sensors are mainly used in combustion gas detectors[58] or gas alarm systems, for instance for reliable ammonia leakage detection in refrigeration systems.[52]

2.5.2 Conducting polymer gas detectors

A second principle for sensing ammonia makes use of conducting polymers. Different materials have been reported, like polypyrole[59] and polyaniline.[60] The sensing mechanism of polypyrole films is two-fold: first, there is an irreversible reaction between ammonia and the polymer and, secondly, ammonia can reversibly reduce the oxidized form of polypyrole.[61] The reduction of the polymer film causes a change in the conductivity of the material, making it a suitable material for resistometric[62] or amperometric ammonia detection.[59] Response times of about 4 minutes have been shown.[60]

The irreversible reaction with ammonia results in an increase in mass in the polymer film. Sensors have been described that detect ammonia using the change in frequency of a resonator, coated with ammonia sensitive polymer.[63] However, the irreversible nature of the reaction causes the sensitivity of the sensor to decrease over time when exposed to ammonia.[61] Although regeneration mechanisms have been proposed, this is a major drawback of this type of sensors.[64] Polyaniline proved to be a much more stable conducting polymer material. The polymer is believed to be deprotonated by ammonia, resulting in the change in conduction.[65] The lower detection limit of gas sensors based on the two described polymers is about 1 ppm.[60,65]

2.5.3 Optical gas analyzers

There are two main optical principles for the detection of ammonia described in literature. The first is based on a change in colour when ammonia reacts with a reagent. With the second principle optical absorption detection is applied as a method to sense gasses.

Spectrophotometric ammonia detection

Spectrophotometry is a technique where a specific reaction causes a coloration of an analyte. The best known example is pH paper. A piece of this paper in a solution colorizes according to the pH of the solution. There are many commercially available detection kits for all kinds of ions and dissolved gasses.

There are different coloration reactions in use for dissolved ammonia. Best known is the Nessler reaction.[66] This ammonia detection method is applied frequently for determining the total ammonia concentration in water, e.g. in aquaria where too high ammonia levels can cause fish to die. The Nessler reagent consists of dipotassium tetraiodomercurate (II) in a dilute alkaline solution, normally sodium hydroxide. This reagent is toxic. There is not much literature about quantitative measurements with this reaction,[67] probably because of the disadvantages. Besides the toxicity, a second disadvantage is the formation of the non-soluble reaction product, a basic mercury (II) amido-iodide,[66] making the reaction difficult to implement in a miniaturized detection system.

A second coloration method to measure ammonia concentrations in aqueous solutions is the Berthelot reaction. A combination of ammonia, phenol and hypochlorite results in a blue coloration.[68,69] This reaction uses less dangerous chemicals and the reaction products are all soluble in water, making it a suitable technique for integration in miniaturized analysis systems.[70] One drawback of this technique is the rather slow kinetics of the reactions. This was improved by miniaturization in a flow-through analysis system.[71] The detection limit is about 5 µM of ammonia in water or 90 ppb. This technique is still under development in order to lower the detection limit.[72]

To improve the sensitivity, the detection limit of the detector has to be improved. This is done by applying different coloration principles, like thin layers of pH indicator,[73] fluorescent materials that can be used to label ammonia[74] or a combination of the two.[75] A second option is to apply a very sensitive detection principle, like a photon-counting optical sensor[75] or optical waveguide structures[73] to quantify the coloration, resulting in very sensitive, ppt range, ammonia detectors.

Optical absorption ammonia detection

Optical absorption spectroscopy is used in the most sensitive and selective ammonia detectors for ambient ammonia. Systems with a detection limit of 1 ppb, that do a full measurement in 1 second, are reported.[76] Such systems use a laser and a spectrograph. Light travels through air[77] or an ammonia sensitive layer.[78,79] The spectrum of the light reaching the detector is influenced by either the gas composition or the material characteristics as a function of the gas composition. Figure 2.13 shows an absorbance spectrogram found in literature that clearly shows that ammonia can be distinguished from interfering gasses, like CO_2 and water vapor.[80]

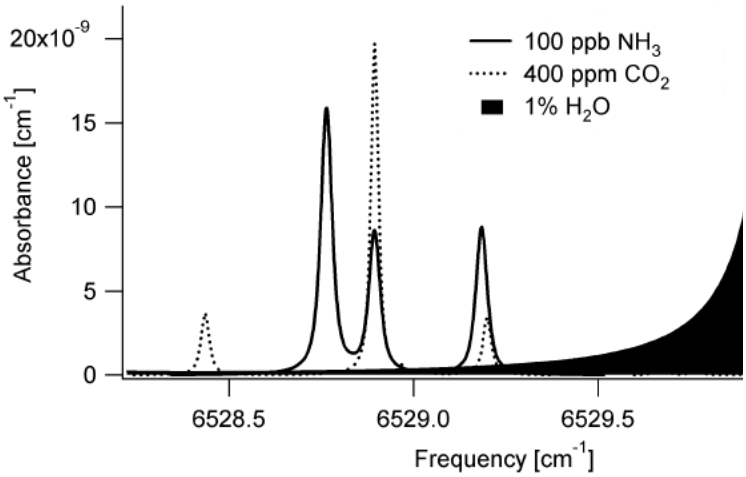

Figure 2.13. *Ammonia absorbance spectogram.*[80]

Although very sensitive and selective ammonia detectors are shown, there are some disadvantages when looking at sensor systems for measuring in small volumes. First, the required equipment is very expensive. It has been tried to use inexpensive diode-lasers to overcome this problem but this also resulted in a decrease in sensitivity.[81,82] Secondly, the sensitivity of absorption spectroscopy is partly determined by the amount of gas between the light source and the detector. For a very accurate analysis the measurement system should be very large. Thus, miniaturization always results in an increase in the lower detection limit. Therefore, this principle is less suited for miniaturized ammonia sensors, e.g. breath analyzers.

2.5.4 Selective gas analyzers using non-selective detectors

One major drawback of most available ammonia sensing principles is the poor selectivity towards ammonia compared to other gasses. However, it is possible to use a non-specific detection principle, like pH-measurement or electrolyte conductivity detection. In that case, the gas analysis system should comprise a selection mechanism that allows only the gas of interest to influence the medium surrounding a detector.[83,84]

These types of air analysis systems make use of gas samplers, like denuders or diffusion scrubbers, to sample ammonia into a sample liquid.[83,85,86] A major advantage of using gas samplers in ammonia sensor systems is the fact that these systems pre-concentrate the ammonia by sampling a large volume of the analyte gas into a much smaller volume of liquid, where ammonium ions are formed.[87] Many accurate ways to selectively measure low concentrations of ammonium have been shown.[88]

One way to separate gasses is by using diffusion separation with gas-permeable membranes.[83,84,88] This principle is used in the ambient ammonia detection system (AMINA) developed at the Energy research Centre of the Netherlands, ECN, in combination with pH-transitions to selectively transport ammonia from an analyte gas stream.[84] The working principle is explained in detail in the next chapter of this thesis. The miniaturized system described in this thesis is based on this principle.

2.5.5 Summary of detection principles and concluding remarks

The ammonia detection principles that are discussed in this section are summarized in table 2.2. The best results found in literature are given for the described detection principles.

Table 2.2. *Parameters of different types of ammonia sensors and sensor systems.*

Principle	lower detection limit	response time	temperature range	remarks
Semiconductor-metal-oxide				
WO_3	1ppm[54]	~5 minutes	400˚C	
Conducting polymer				
polyaniline	1 ppm[60,65]	~3 minutes	Up to 150˚C (regeneration)	Irreversible reactions
Optical gas sensors				
Nessler	50 ⌈M (90 ppb)[71]	~1 minute	37˚C	Ammonia in water
Coulorometric	1 ppt[73]	~5 minutes		Expensive setup
Absorption spectroscopy	1 ppb[76]	~5 minutes		Large and expensive
Non-selective detectors				
Sampler-selector	100 ppt[84]	~20 minutes	0 - 40˚C	Fluidic system

Now, the properties of the described sensors and sensor-systems can be compared with the demands of the described application areas, summarized in table 2.1. The following conclusions can be drawn:

- Environmental air monitoring systems require a detection limit of 1 ppb. Some optical gas sensors are suitable and the AMINA system developed at ECN has a sufficiently low detection limit. However, the optical gas sensors are large and expensive, making them less suited. The AMINA system has the size of a large moving box, not exactly portable. A smaller system would be beneficial. Furthermore, the reagent consumption and maintenance requirements are rather demanding.
- For measuring in stables, a lower detection limit of 1 ppm is required. All described sensor systems can be applied for this purpose. Sensor equipment that requires much maintenance is inconvenient for farmers. For instance, conducting polymer based sensors seem less suited because regular regeneration to prevent loss of sensitivity is required.
- For automotive exhaust applications the required detection limits are not very low, the described sensor systems are all sufficiently sensitive. The elevated temperature in exhaust systems excludes fluidic systems and conducting polymer sensors. Water would evaporate from the fluidic systems and conducting polymers need to be constantly regenerated. The most suitable sensors are semiconductor- and metal-oxide gas sensors. These types of sensors already work at elevated temperatures and have a sufficiently low detection limit.
- Automotive air quality monitoring systems require very fast sensor systems, responding to increasing ammonia concentrations in a few seconds. None of the described sensors is fast enough.
- Chemical alarm systems do not require sensors that are extremely sensitive and selective. Especially in reactors, the operational temperatures can be elevated so the semiconductor- and metal-oxide gas sensors seem the best-suited type of sensors for these applications.
- A diagnostic breath analysis system for medical ammonia requires a rather low detection limit of 50 ppb. The sensor system should be very selective to ammonia. Furthermore, the system should respond to a change in ammonia concentration within a few minutes. The only ammonia sensors performing to these criteria are optical systems. These systems, however, are very large and expensive, making them less suited. The sensitivity and the selectivity of the AMINA principle are adequate but the system requires too much analyte gas to do analysis in a single breath of air and the system is rather slow.

The “AMINA” principle is the best option for a smaller measurement system that is suitable for environmental and medical applications. Miniaturization of the key components would decrease the reagent consumption and the response time of this system. Integration of these components into one chip would increase the functionality. How this is accomplished is described in the following chapters of this thesis.

2.6 References

[1] P. Warneck, "*Chemistry of the natural atmosphere",* Academic Press Inc, 1998

[2] S. Hawking, "*The universe in a nutshell",* (in Dutch), Bert Bakker Amsterdam, 2001

[3] G. Hancock, "*The mars mystery",* Crown Publishers Inc, 1998

[4] Z. Sitchin, "*Genesis revisited",* Bear & Company, 1991

[5] M.K. Bird, W.K. Huchtmeier, P. Gensheimer, T.L. Wilson, P. Janardhan, C. Lemme, "*Radio detection of ammonia in comet Hale-Bopp*", Astronomy and Astrophysics 325, pp L5-L8, 1997

[6] N.A. Campbell, J.B. Reece, "*Biology",* Pearson Education Inc, 2002

[7] A.I. Oparin, "*The Origin of Life",* Dover publications, 1938

[8] J.B.S. Haldane, "*Possible Worlds",* Hugh & Bros, 1928

[9] S. Miller, "*A production of amino acids under possible primitive earth conditions",* Science 117, pp. 528-529, 1953

[10 S. Miller, H. Urey, "*Organic compound synthesis on the primitive earth",* Science 130, pp. 245-251, 1959

[11] P. Davies, "*The fifth miracle",* Simon & Schuster, 1999

[12] G.A. Kowalchuk, J.R. Stephen, "*Ammonia-oxidizing bacteria: a model for molecular microbial ecology*", Annual Review of Microbiology 55, pp 485-529, 2001

[13] I. Schmidt, O. Sliekers, M. Schmid, I. Cirpus, M. Strout, E. Bock, J.G. Kuenen, M.S.M. Jetten, "*Aerobic and anaerobic ammonia oxidizing bacteria – competitors or natural partners?",* FEMS Microbiology Ecology 39, pp 175-181, 2002

[14] J.R. Istas, R. de Borger, L. de Temmerman, Guns, K. Meeus-Verdinne, A. Ronse, P. Scokart, M. Termonia, "*Effect of ammonia on the acidification of the environment*", European communities report No. EUR 11857 EN, 1988

[15] S.V. Krupa, "*Effects of atmospheric ammonia (NH_3) on terrestrial vegetation: a review*", Environmental pollution 124, pp 179-221, 2003

[16] D.A. Oudendag, H.H. Luesink, "*The manure model: manure, minerals (N, P and K), ammonia emission, heavy metals and use of fertiliser in Dutch agriculture",* Environmental pollution 102, pp. 241-246, 1998

[17] D.S. Lee, C. Halliwell, J.A. Garland, G.J. Dollard, R.D. Kingdon, "*Exchange of ammonia at the sea surface – A preliminary study*", Atmospheric environment 32 (3), pp 431-439, 1998

[18] K. Barrett, "*Oceanic ammonia emissions in Europe and their boundary fluxes",* Atmospheric environment 32 (3), pp 381-391, 1998

[19] S. Budarvari, et. al., "*The Merck index, an encyclopedia of chemicals, drugs and biologicals*" 12th edition, Merck&Co, 1996

[20] L.G. Close, F.I. Catlin, A.M. Cohn, "*Acute and chronic effects of ammonia burns on the respiratory tract*", Arch Otolaryngol 106 (3), pp 151-158, 1980

[21] C.M. Leung, C.L. Foo, "*Mass ammonia inhalation burns – experience in the management of 12 patients*", Annals Academy of Medicine Singapore 21 (5), pp 624-629, 1992

[22] R.E. de la Hoz, D.P. Schueter, W.N. Rom, "*Chronic lung disease secondary to ammonia inhalation injury: a report on three cases*", American Journal of Industrial Medicine 29 (2), pp 209-214, 1996

[23] R.A. Michaels, "*Emergency planning and acute toxic potency of inhaled ammonia",* Environmental health perspectives 107 (8), pp 617-627, 1999

[24] C. Baird, "*Environmental Chemistry",* W.H. Freeman and Company, 1995

[25] G.H. Mount, B. Rumburg, J. Havig, B. Lamb, H. Westberg, D. Yonge, K. Johnson, R. Kincaid, "*Measurement of atmospheric ammonia at a dairy using differential*

optical absorption spectroscopy in the mid-ultraviolet", Atmospheric Environment 36, pp 1799-1810, 2002

[26] C. Pijolat, C. Pupier, M. Sauvan, G. Tournier, R. Lalauze, "*Gas detection for automotive pollution control",* Sensors and Actuators B 59, pp 195-202, 1999

[27] T.D. Durbin, R.D. Wilson, J.M. Norbeck, J.W. Miller, T. Huai, S.H. Rhee, "*Estimates of the emission rates of ammonia from light-duty vehicles using standard chassis dynamometer test cycles",* Atmospheric environment 36, pp 1475-1482, 2002

[28] R. Moos, R. Müller, C. Plog, A. Knezevic, H. Leye, E. Irion, T. Braun, K-J. Marquardt, K. Binder, "*Selective ammonia exhaust gas sensor for automotive applications",* Sensors and Actuators B 83, pp. 181-189, 2002

[29] M. Wallin, C-J. Karlsson, M. Skoglundh, A. Palmqvist, "*Selective catalytic reduction of NOx with NH3 over zeolite H-ZSM-5: influence of transient ammonia supply",* Journal of catalysis 218, pp 354-364, 2003

[30] X. Xuan, C. Yue, S. Li, Q. Yao, "*Selective catalytic reduction of NO by ammonia with fly ash catalyst",* Fuel 82, pp 575-579, 2003

[31] S.G. Buckley, C.J. Damm, W.M. Vitovec, L.A. Sgro, R.F. Sawyer, C.P. Koshland, D. Lucas, "*Ammonia detection and monitoring with photofragmentation fluorescence",* Applied optics 37, No. 36, 1998

[32] K.L. Manchester, "*Man of destiny: the life and work of Fritz Haber",* Endavour 26 (2), pp 64-69, 2002

[33] A.T. Bulgan, "*Use of low-temperature energy sources in aqua-ammonia absorption refrigeration systems",* Energy conversation and managment 38 (14), pp 1431-1438, 1997

[34] P. Colonna, S. Gabrielli, "*Industrial trigeneration using ammonia-water absorption refrigeration systems (AAR)",* Applied thermal engineering 23, pp 381-396, 2003

[35] J. Fernandez-Seara, J. Sieres, M. Vazquez, "*Distillation column configurations in ammonia-water absorption refrigeration systems",* International journal of refrigeration 26, pp 28-34, 2003

[36] W. Ament, J.R. Huizenga, E. Kort, T.W. v.d. Mark, R.G. Grevink, G.J. Verkerke, "*Respiratory ammonia output and blood ammonia concentration during incremental exercise",* International Journal of Sports Medicine 20, pp 71-77, 1999

[37] L.R. Narasimhan, W. Goodman, C. Kumar, N. Patel, "*Correlation of breath ammonia with blood urea nitrogen and creatine during hemodialysis",* PNAS 98 (8), pp 4617-4621, 2001

[38] B. Marshall, J.R. Warren, "*Unidentified curved bacillus and gastric Epithaeium in active chonic gastritis",* Lancet 1, pp. 1273-1275, 1993

[39] J.C.E. Underwood, "*General and Systematic Pathology",* Churchill Livingstone Inc, 2nd edition, pp 414-415, 1996

[40] D.J. Kearney, T. Hubbard, D. Putnam, "*Breath ammonia measurement in Helicobacter pylori infection",* Digestive diseases and sciences 47 (11), pp 2523-2530, 2002

[41] E. Verpoorte, "*Microfluidic chips for clinical and forensic analysis",* Electrophoresis 23, pp 677-712, 2002

[42] N.K. Jain, V. Mangal, "*Helicobactor Pyroli infection in children",* J. Nep Med Assoc. 38, pp 140-143, 1999

[43] G. Sberveglieri, "*Recent developments in semiconducting thin-film gas sensors",* Sensors and Actuators B 23, pp 103-109, 1995

[44[N. Yamazoe, "*Chemical sensor Technology",* Elsevier, Amsterdam, 1991

[45] P.T. Moseley, "*Solid state gas sensors*", Measurement Science and Technology 8, pp 223-237, 1997

[46] P.K. Clifford, D.T. Tuma, "*Characteriistics of semiconductor gas sensors I. Steady state gas response",* Sensors and Actuators 3, pp 233-254, 1983

[47] R.K. Srivastava, P. Lal, R. Dwivedi, S.K. Srivastatva, "*Sensing mechanism in tin oxide-based thick film gas sensors*", Sensors and Actuators B 21, pp 213-218, 1994

[48] H.P. Huebner, S. Drost, *"Tin oxide gas sensors: an analytical comparison of gas-sensitive and non-gas-sensitive thin films",* Sensors and Actuators B 4, pp 463-466, 1991

[49] J. Mizsei, *"How can sensitive and selective semiconductor gas sensors be made?",* Sensors and Actuators B 23, pp 173-176, 1995

[50] C. Delpha, M. Siadat, M. Lumbreras, *"Discrimination of a refrigerant gas in a humidity controlled atmosphere by using modeling parameters",* Sensors and Actuators B 62, pp 226-232, 2000

[51] C. Di Natale, F. Davide, A. D'Amico, *"Pattern recognition in gas sensing: well-stated techniques and advances",* Sensors and Actuators B 23, pp 111-118, 1995

[52] A. Jerger, H. Kohler, F. Becker, H.B. Keller, R. Seifert, *"New applications of tin oxide gas sensors II. Intelligent sensor system for reliable monitoring of ammonia leakage",* Sensors and Actuators B 81, pp 301-307, 2002

[53] X. Wang, N. Miura, N. Yamazoe, *"Study of WO_3-based sensing material for NH_3 and NO detection"*, Sensors and Actuators B 66, pp 74-76, 2000

[54] C.N. Xu, N. Miura, Y. Ishida, K. Matuda, N. Yamazoe, *"Selective detection of NH_3 over NO in combustion exhausts by using Au and MoO_3 doubly promoted WO_3 element",* Sensors and Actuators B 65, pp. 163-165, 2000

[55] W. Goepel, K.D. Schierbaum, *"SNO_2 sensors: current status and future prospects",* Sensors and Actuators B 26-27, pp 1-12, 1995

[56] Y-D. Wang, X-H. Wu, Q. Su, Y-F. Li, Z-L. Zhou, *"Ammonia-sensing characteristics of Pt and SiO_2 doped SnO_2 materials"*, Solid-State Electronics 45, pp 347-350, 2001

[57] M. Aslam, V.A. Chaudhary, I.S. Mulla, S.R. Sainkar, A.B. Mandale, A.A. Belhekar, K. Vijayamohanan, *"A highly selective ammonia gas sensor using surface-ruthenated zinc oxide",* Sensors and Actuators A 75, pp 162-167, 1999

[58] A.A. Tomchenko, G.P. Harmer, B.T. Marquis, J.W. Allen, *"Semiconducting metal oxide sensor array for the selective detection of combustion gases",* Sensors and Actuators B 93, pp 126-134, 2003

[59] I. Lähdesmäki, A. Lewenstam, A. Ivaska, *"A polypyrrole-baesd amperometric ammonia sensor",* Talanta 43, pp 125-134, 1996

[60] A.L. Kukla, Y.M. Shirshov, S.A. Piletsky, *"Ammonia sensors based on sensitive polyaniline films"*, Sensors and Actuators B 37, pp 135-140, 1996

[61] I. Lähdesmäki, W.W. Kubiak, A. Lewenstam, A. Ivaska, *"Interference in a polypyrrole-based amperometric ammonia sensor",* Talanta 52, pp 269-275, 2000

[62] E. Palmqvist, C. Berggren Kriz, K. Svanberg, M. Khayyami, D. Kriz, *"DC-resistometric urea sensitivity device utilizing a conducting polymer film for the gas-phase detection of ammonia",* Biosensors & Bioelectronics 10, pp 283-287, 1995

[63] Q. Y. Cai, M.K. Jain, C.A. Grimes, *"A wireless, remote query ammonia sensor",* Sensors and Actuators B 77, pp 614-619, 2001

[64] P.Heiduschka, M. Preschel, M. Rösch, w. Göpel, *"Regeneration of an electropolymerised polypyrrole layer for the amperometric detection of ammonia",* Biosensors and Bioelectronics 12 (12), pp 1227-1231, 1997

[65] V.V. Chabukswar, S. Pethkar, A.A. Athawale, *"Acrylic acid doped polyanailine as an ammonia sensor",* Sensors and Actuators B 77, pp 657-663, 2001

[66] A.I. Vogel, *"Vogel's qualitative inorganic analysis",* Longman Scientific & Technical, 6th ed., 1987

[67] A. Ghauch, J. Rima, A. Charef, J. Suptil, C. Fachinger, M. Martin-Bouyer, *"Quantative measurements of ammonium, hydrogenophosphate and Cu(II) by diffuse reflectance spectroscopy",* Talanta 48, pp 385-392, 1999

[68] M.P.E. Berthelot, Repertoire Chimique Appliquee1, p 284, 1859

[69] P.L. Saerle, *"The Berthelot or indolphenol reaction and its use in the analytical chemistry of nitrogen –A review",* Analyst 109, pp 549-568, 1984

[70] T.T. Veenstra, *"MAFIAS–An integrated lab-on-a-chip for the measurement of ammonium",* PhD-thesis, University of Twente, 2001

[71] R.M. Tiggelaar, T.T. Veenstra, R.G.P. Sanders, E. Berenschot, H. Gardeniers, M. Elwenspoek, A. Prak, R. Mateman, J.M. Wissink, A. v.d. Berg, *"Analysis system for the detection of ammonia base don micromachined components modular hybrid versus monolithic integrated approach",* Sensors and Actuators B 92, pp 25-36, 2003

[72] T. Tsuboi, Y. Hirano, Y. Shibata, S. Motomizu, *"Sensitivity improvement of ammonia determination based on flow-injection indophenol spectrophotometry with manganese(II) ion as a catalyst and analysis of exhaust gas of thermal power plant",* Analytical sciences 18, pp 1141-1144, 2002

[73] A. Yimit, K. Itoh, M. Murabayashi, *"Detection of ammonia in the ppt range based on a composite optical waveguide pH sensor"* Sensors and Actuators B 88, pp 239-245, 2003

[74] N. Strömberg, S. Hulth, *"Ammonium selective fluorosensor based on the principle of coextraction",* Analytica Chimica Acta 443, pp 215-225, 2001

[75] A. Elamari, N. Gisin, J.L. Munoz, S. Poitry, M. Tsacopoulos, H. Zbinden, *"Photon-counting optical-fiber sensor for the detection of ammonia in neurochemical applications",* Sensors and Actuators B 38-39, pp 183-188, 1997

[76] G.H. Mount, B. Rumberg, J. Havig, B. Lamb, H. Westberg, D. Yonge, K. Johson, R. Kincaid, *"Measurement of atmospheric ammonia at a dairy using differential optical absorption spectroscopy in the mid-ultraviolet",* Atmospheric environment 36 (11), pp 1799-1810, 2002

[77] R. Peeters, G. Berden, A. Apituley, G. Meijer, *"Open-path trace gas detection of ammonia base don cavity-enhanced absorption spectroscopy",* Applied Physics B 71, pp 231-236, 2000

[78] Z. Jin, Y. Su, Y. Duan, *"Development of a polyaniline-based optical ammonia sensor",* Sensors and Actuators B 72, pp 75-79, 2001

[79] Y-S. Lee, B-S. Joo, N-J. Choi, J-O. Lim, J-S. Huh, D-D. Lee, *"Visible optical sensing of ammonia based on polyaniline film",* Sensors and Actuators B 93, pp 148-152, 2003

[80] M.E. Webber, M.B. Pushkarsky, C. Kumar, N. Patel, *"Ultra-sensitive gas detection using diode lasers and resonant photoacoustic spectroscopy",* SPIE's international Symposium on optical science and technology 2002, paper no. 4817-11, 2002

[81] M. Fehér, P. A. Martin, A. Rohrbacher, A.M. Soliva, J.P. Maier, *"Inexpensive near-infrared diode-laser-based detection system for ammonia",* Applied optics 32 (12), pp 2028-2030, 1993

[82] G. Modugno, C. Corsi, *"Water vapour and carbon dioxide interference in the high sensitivity detection of NH_3 with semiconductor diode lasers at 1.5 μm",* Infrared physics & technology 40, pp 93-99, 1999

[83] S-I. Ohira, K. Toda, S-I. Ikebe, P. K. Dasgupta, *"Hybrid microfabricated device for field measurement of atmospheric sulfur dioxide",* Analytical Chemistry 74, pp. 5890-5896, 2002

[84] J.W. Erisman, R. Otjes, A. Hensen, P. Jongejan, P. v.d. Bulk, A. Khlystov, H. Möls and S. Slanina, *"Instrument development and application in studies and monitoring of ambient ammonia"*, Atmospheric Environment 35, pp 1913-1922, 2001

[85] P.K. Simon, P.K. Dasgupta, Z. Vecera, *"Wet effluent denuder coupled liquid/ion chromatography systems",* Analytical Chemistry. 63, pp 1237-1242, 1991

[86] P.F. Lindgren, P.K. Dasgupta, *"Measurement of atmospheric sulfur dioxide by diffusion scrubber coupled ion chromatography"*, Analytical Chemistry 61, pp 19-24, 1989

[87] C.B. Boring, R. Al-Horr, Z. Genfa, P.K. Dasgupta, *"Field measurement of acid gases and soluble anions in atmospheric particulate matter using a parallel plate wet denuder and an alternating filter based automatic analysis system",* Analytical Chemistry 74, pp. 1256-1268, 2002

[88] G. Schultze, C.Y. Liu, M. Brodowski, O. Elsholz, *"Different approaches to the determination of ammonium ions at low levels by flow injection analysis",* Analytica Chimica Acta 214, pp 121-136, 1988

Chapter 3

"AMINA" ammonia measurement principle*

3.1 Introduction

At the Energy research Centre of the Netherlands, ECN, the "AMINA" principle is developed for selectively measuring low concentrations of ambient ammonia.[1] The chemical equilibriums that make the system sensitive to gaseous ammonia are discussed in the section following this introduction.[2] The described principle forms the basis of the miniaturization project described in this thesis. The sensitivity and selectivity that can be expected from a system based on the presented principle are investigated.

The central part of the "AMINA" apparatus comprises a gas sampler, a selector and a detector. In the gas sampler, gas is sampled into an acid sample solution through a micro-porous, water-repellent membrane. The solution is transported to the selector where a strong alkaline solution is added. Consequently, all alkaline dissolved gasses, in practice only ammonia, are neutralized and all acidifying gasses are hydrolyzed. A second membrane separates the selector solution from a purified water stream. Gaseous ammonia, which forms from the neutralized ammonia at the membrane interface, diffuses through the membrane into the water stream. Since no acidifying compounds are gaseous in the alkaline selector solution, only ammonia comes in contact with the water. Detection is realized by integrating an electrolyte conductivity sensor. It quantifies the ion concentration that is elevated due to the ionization reaction of

**This chapter is published as part of a article, Analytica Chimica Acta, 2004*

dissolved ammonia with water. A schematic representation of the system, with the pathways of ammonia from the analyte gas to the detector and of acidifying gasses from the analyte gas to the waste outlet of the selector, are shown in figure 3.1.

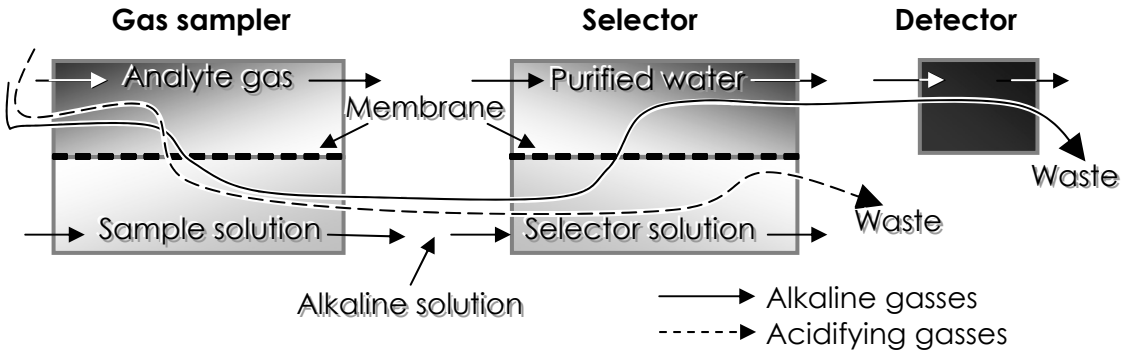

Figure 3.1. *Schematic representation of the "AMINA" ammonia measurement principle developed at ECN[1] showing a gas sampler, a selector and a detector and the pathway for acidifying and alkaline gasses.*

3.2 Analysis of the "AMINA" chemistry

Normal ambient ammonia concentrations are in the low ppb range; an average of 2 ppb is assumed for the Netherlands.[1] Normal CO_2 levels are about 300 ppm, a factor 150.000 higher. Additionally, when an ammonia analyzer is made for exhaled air analysis, the analyte gas can contain up to a hundred fold more CO_2, 30000 ppm and ammonia levels down to 50 ppb should be measurable, a ratio of 600.000.[3-5] The selectivity of the apparatus should be high enough to detect ammonia without too much interference from other gasses, like for instance high levels of CO_2. The following discussion shows how this is accomplished.

3.2.1 The gas sampler

In the gas sampler of the ammonia analyzer, a volume of gas is sampled into a smaller volume of an acid sample solution. The analyte gas is pumped through a gas channel. Opposite to this channel is a second channel where the acid sample solution is pumped through, separated by a water-repellent, gas-permeable membrane. The available gasses can diffuse through the membrane, into the sample solution. If there are any alkaline components available in the analyte gas, they will ionize in the acid solution, e.g. ammonia is converted to ammonium ions. In practice, ammonia is the main alkaline gaseous component in air. Weakly acidifying gasses hardly hydrolyze in the acid environment of the sample stream. CO_2 is used in the following theoretical discussion because it is the acidifying gas

that is available in normal air at the highest concentration levels. The reactions for ammonia and carbon dioxide with the acid sample solution are given in equation 3.1 and 3.2.

$$NH_3(g) + H_2O(l) \leftrightarrow NH_3(aq) \quad (3.1)$$

$$CO_2(g) + H_2O(l) \overset{1}{\leftrightarrow} CO_2(aq) + H_2O(l) \overset{2}{\leftrightarrow} H_2CO_3 \quad (3.2)$$

The solubility of ammonia is extremely high, 52.9 mol/litre at room temperature.[6] Most of the ammonia that comes in contact with the sample solution dissolves, as shown in equation 3.1. In dilute watery solutions, the relation between the NH_3 concentration in the analyte gas, expressed in its partial pressure, P_{NH_3} (Pa), and the dissolved NH_3 concentration in the sample solution, $[NH_3]_{aq}$ (M), is given by Henry's law.[7] The Henry's constant of NH_3, S_{NH_3}, at room temperature is $1.3 \cdot 10^7$ Pa·mol^{-1}·l H_2O,[8] resulting in:

$$P_{NH_3} = S_{NH_3} \cdot [NH_3]_{aq} \quad (3.3)$$

An initial NH_3 concentration of 50 ppb (a partial pressure of $5 \cdot 10^{-6}$ kPa in normal air at a pressure of 100 kPa) results in a low dissolved NH_3 concentration of $3.8 \cdot 10^{-10}$ M, at equilibrium. However, low concentrations of dissolved ammonia are easily converted to ammonium ions in the acid environment in the gas sampler. When there is sufficient time for the ammonia to diffuse into the sample solution and the ammonia concentrations are relatively low, it can be assumed that gaseous ammonia dissolves in the sample solution completely.

This assumption, however, can not be made for carbon dioxide because the solubility in water is far less than for ammonia (e.g. 11.2 µM/l at room temperature and normal partial pressure of CO_2).[6] Furthermore, it only partly reacts with water in an acid environment. An equilibrium between CO_2 in the gas phase and dissolved CO_2 in the sample solution is formed. The relation between the CO_2 concentration in the analyte gas, expressed in its partial pressure, P_{CO_2} (Pa), and the dissolved CO_2 concentration in the sample solution, $[CO_2]_{aq}$ (M), shown in equilibrium 1 in equation 3.2, is given in equation 3.4. Henry's constant for CO_2, S_{CO_2}, at room temperature is $2.97 \cdot 10^6$ Pa·mol^{-1}·l H_2O.[7]

$$P_{CO_2} = S_{CO_2} \cdot [CO_2]_{aq} \quad (3.4)$$

An initial CO_2 concentration of 30000 ppm (a partial pressure of 3 kPa in exhaled breath at a pressure of 100 kPa) results in an equilibrium dissolved CO_2 concentration of 1.0 mM.

After dissolving, the gasses react with water. This causes a shift in the equilibrium towards an increased uptake of the specific gas. The reactions of the two discussed gasses with water are given in equation 3.5 and 3.6:

$$NH_3(aq) + H_2O(l) \leftrightarrow NH_4^+ + OH^- \quad (3.5)$$

$$CO_2(aq) + H_2O(l) \leftrightarrow H_2CO_3 \quad (3.6^a)$$

$$H_2CO_3 + H_2O(l) \leftrightarrow HCO_3^- + H_3O^+ \quad (3.6^b)$$

$$HCO_3^- + H_2O(l) \leftrightarrow CO_3^{2-} + H_3O^+ \quad (3.6^c)$$

The sample solution has an initial pH of 3.5. The ratio between the dissolved state and the ionized state at equilibrium can be calculated from the initial dissolved gas concentration, the initial pH and the equilibrium constant values of the reactions in equations 3.5 and 3.6. For the reaction of ammonia with water, the dissociation constant is used, $K_{b(NH_3)}=([NH_4^+] \cdot [OH^-])/[NH_3]_{aq}=1.8 \cdot 10^{-5}$ M at room temperature.[7]

Before dissolved CO_2 can be ionized, it has to be hydrolyzed. The equilibrium constant of the hydrolyzation reaction shown in equation 3.6^a, $K_{h(CO_2)}=[H_2CO_3]/[CO_2]_{aq}$, is $2.53 \cdot 10^{-3}$ at room temperature,[7] meaning that only a small part of the dissolved CO_2 is available in the hydrolyzed state. From now, the total dissolved CO_2 concentration, $[CO_2^*]=[CO_2]_{aq}+[H_2CO_3]$, is used. The dissociation constant values for the equilibriums shown in equation 3.6^b and 3.6^c are $K_{a(H_2CO_3)}$ and $K_{a(HCO_3^-)}$ respectively, with: $K_{a(H_2CO_3)}=[HCO_3^-] \cdot [H_3O^+]/H_2CO_3]=4.2 \cdot 10^{-7}$ M and $K_{a(HCO_3^-)}=[CO_3^{2-}] \cdot [H_3O^+]/HCO_3^-]=4.8 \cdot 10^{-11}$ M, both at room temperature.[7] Equation 3.7 gives the ratio for ammonia and 3.8 and 3.9 for CO_2.

$$\frac{[NH_4^+]}{[NH_3]_{aq}} = \frac{K_{b(NH_3)}}{[OH^-]} = 5.7 \cdot 10^5 \quad (3.7)$$

$$\frac{[HCO_3^-]}{[CO_2^*]} = \frac{[HCO_3^-]}{[CO_2]_{aq} + [H_2CO_3]} \quad (3.8^a)$$

Since:

$$[CO_2]_{aq} = \frac{[H_2CO_3]}{K_{h(CO_2)}} \quad (3.8^b)$$

and

$$[H_2CO_3] = \frac{[HCO_3^-] \cdot [H_3O^+]}{K_{a(H_2CO_3)}} \quad (3.8^c)$$

$[CO_2^*]$ can be written as:

$$[CO_2^*] = \left(\frac{1 + K_{h(CO_2)}}{K_{h(CO_2)} \cdot K_{a(H_2CO_3)}}\right) \cdot [HCO_3^-] \cdot [H_3O^+] = K_{overall} \cdot [HCO_3^-] \cdot [H_3O^+] \quad (3.8^d)$$

with $K_{overall} = 9.4 \cdot 10^8\ M^{-1}$ and equation 3.8a can be solved to:

$$\frac{[HCO_3^-]}{[CO_2^*]} = \frac{1}{K_{overall} \cdot [H_3O^+]} = 3.4 \cdot 10^{-6} \quad (3.8^e)$$

$$\frac{[CO_3^{2-}]}{[HCO_3^-]} = \frac{K_{a(HCO_3^-)}}{[H_3O^+]} = 1.5 \cdot 10^{-7} \quad (3.9)$$

Because the solubility of ammonia is very high, it is assumed that the ammonia flux from the gas channel through the membrane into the sample solution is directed mainly towards the solution. This is even enhanced because almost all ammonia reacts with water, forming ammonium ions, as shown in equation 3.7. There continues to be a difference in ammonia concentration between the analyte gas and the sample solution so that ammonia continues to diffuse towards the solution. On the other hand, the solubility of carbon dioxide is limited and in the hydrated state it only partly dissociates, as shown in equation 3.8e and 3.9. The sample solution becomes saturated with dissolved CO_2 and no more CO_2 is transported towards the sample solution.

The detector of the ammonia analyzer consists of an electrolyte conductivity detector. It is however not possible to directly measure the changes in conductivity in the sample solution because the difference in ammonium concentration is rather small compared to the absolute ion concentration of the sample solution. This can be enhanced by sampling a larger volume of analyte gas into a small volume of sample solution. However, the resulting high ammonium concentration also causes the pH to increase. This results in a lower dissociation ratio of dissolved ammonia and

a higher dissociation ratio of H_2CO_3, lowering the selectivity. In order to overcome this paradox, a selector is added to the system to make the system both selective and sensitive to ammonia.

3.2.2 The selector

The sample solution is pumped from the gas sampler into a second reaction chamber, the selector. An alkaline 0.25 M NaOH solution is added to increase the pH of the solution to 13. This solution is separated from a purified water stream by a second gas-permeable, water-repellent membrane. The equilibrium reactions, shown in equation 3.10 and 3.11, in an alkaline surrounding, cause ammonium to be neutralized and dissolved CO_2 to dissociate. Since the OH^- concentration is relatively high, it is assumed that no gaseous CO_2 is formed.

$$NH_4^+ + OH^- \overset{1}{\leftrightarrow} NH_3(aq) + H_2O(l) \overset{2}{\leftrightarrow} NH_3(g) + H_2O(l) \quad (3.10)$$

$$CO_2^* + 2OH^- \overset{1}{\leftrightarrow} HCO_3^- + OH^- \overset{2}{\leftrightarrow} CO_3^{2-} + H_2O(l) \quad (3.11)$$

The ratio between the ionized and neutralized state of the dissolved gasses at this elevated pH can be calculated from the equilibrium constants of the reactions and the initial OH^- concentration. For the first equilibrium of equation 3.10, the dissociation constants of the neutralization reaction of ammonium, $K_{b(NH_3)}$, is used. This results in a ratio between the ammonium and the hydrolyzed ammonia concentration, shown in equation 3.12.

$$\frac{[NH_3]_{aq}}{[NH_4^+]} = \frac{[OH^-]}{K_{b(NH_3)}} = 5.6 \cdot 10^3 \quad (3.12)$$

From equation 3.3 it is known that the neutralized ammonia has an accompanying partial pressure.

For calculating the ratios for the two dissociation reactions of H_2CO_3 and HCO_3^-, given in equation 3.11, the $K_{overall}$, see equation 3.8d, and the $K_{a(HCO_3^-)}$ values are used, similar to the description in equation 3.8. The resulting ratios at this pH are shown in equation 3.13 and 3.14:

$$\frac{[CO_2^*]}{[HCO_3^-]} = [H_3O^+] \cdot K_{overall} = 9.4 \cdot 10^{-5} \quad (3.13)$$

$$\frac{[HCO_3^-]}{[CO_3^{2-}]} = \frac{[H_3O^+]}{K_{a(HCO_3^-)}} = 2.1 \cdot 10^{-3} \quad (3.14)$$

It is shown that at this pH value, most of the ammonium is neutralized, as indicated by equation 3.12. The gaseous ammonia that is formed at the membrane interface is transported through the second membrane into the purified water stream in the opposite channel. From the ratios in equation 3.7 and 3.12 it can be calculated that 99.98% of the ammonia is expected to be available as gaseous ammonia in the selector. Carbon dioxide, on the other hand, almost completely ionizes, mainly to CO_3^{2-}, as shown in equation 3.13 and 3.14, and is flushed with the sample solution towards the waste outlet of the system. From the ratios shown in equation 3.8e and 3.13 it can be calculated that at the equilibrium pH values, only $3 \cdot 10^{-6}$ % is available in the neutralized state. As long as the sampled gasses do not significantly change the pH values, the selectivity of 600.000, the ratio between CO_2 and NH_3 in exhaled air, can be reached.

3.2.3 The detector

In the detector, mainly ammonia gas comes in contact with the purified water stream. The gaseous ammonia partly dissolves, where it reacts with water to form ions that can be detected using an electrolyte conductivity detector. The equilibrium reactions are shown in equation 3.15:

$$NH_3(g) + H_2O(l) \overset{1}{\leftrightarrow} NH_3(aq) + H_2O(l) \overset{2}{\leftrightarrow} NH_4^+ + OH^- \quad (3.15)$$

The pH of the purified water stream is about 7.0. The dissolved ammonia to ammonium ratio can be calculated using the base equilibrium constant, $K_{b(NH_3)}$. The ratio is shown in equation 3.16.

$$\frac{[NH_4^+]}{[NH_3]_{aq}} = \frac{K_{b(NH_3)}}{[OH^-]} = 1.8 \cdot 10^2 \quad (3.16)$$

At this pH, almost all dissolved ammonia is ionized and therefore gaseous ammonia continues to diffuse through the membrane into the water stream. At high ammonia concentrations this ratio is lowered due to the increased pH, caused by the formation of ammonium ions and OH^- ions. The influence on the ratio depends on the actual concentration levels.

The resulting concentrations of ammonium and OH^- can be calculated as a function of the ammonia concentration according to the second equilibrium shown in equation 3.15, as shown in equation 3.17. The dissociation constant of ammonia, $K_{b(NH_3)}$, is used and it is assumed that all gaseous ammonia dissolves. Subsequently, the resulting H_3O^+ concentration can be calculated because the water equilibrium states that the product of the OH^- and the H_3O^+ concentration equals 10^{-14} M^2 at room temperature.[7]

$$K_{bNH_3} \cdot [NH_3 - X]_{aq} = [NH_4^+] \cdot [OH^-] = [X] \cdot [10^{-7} + X] \quad (3.17^a)$$

$$[X] = \frac{-(10^{-7} + K_{bNH_3}) + \sqrt{(10^{-7} + K_{bNH_3})^2 + 4 \cdot K_{bNH_3} \cdot [NH_3]_{aq}}}{2} \quad (3.17^b)$$

with X is the amount of ammonia that reacted to form NH_4^+ and OH^- ions.

The conductivity of an electrolyte, κ_{elec} (10^{-3} S/m), is the summation of the concentration, c (M), mobility, λ (10^{-3} S·m²/M) and valence, v, of all ions available in the electrolyte, as given in equation 3.18.[9] The conversion of ammonia to ammonium ions changes the ionic content of the solution and therefore the electrolyte conductivity.

$$\kappa_{elec} = \sum_i (c_i \cdot \lambda_i \cdot v_i) \quad (3.18)$$

Assuming initially pure water, the electrolyte conductivity can be calculated as a function of the ammonia concentration in the detector solution, as shown in figure 3.2.

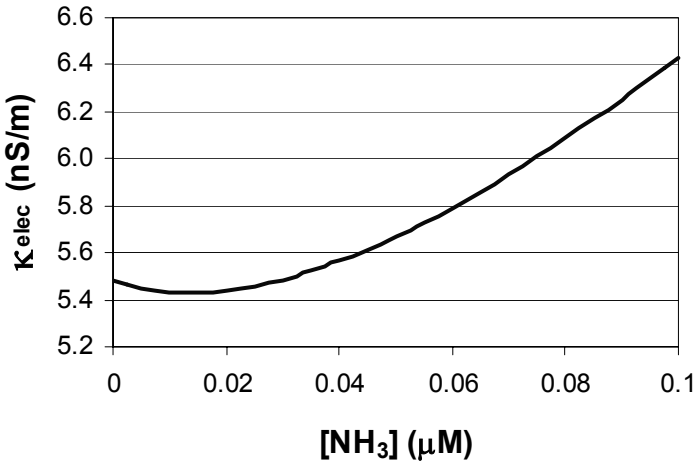

Figure 3.2. *Theoretical electrolyte conductivity of the detector solution as a function of the ammonia concentration.*

The electrolyte conductivity, after an initial decrease due to the lower mobility of NH_4^+ ($7.34 \cdot 10^{-3}$ $S \cdot m^2/M$) compared to H_3O^+ ions ($34.98 \cdot 10^{-3}$ $S \cdot m^2/M$),[7] increases with the concentration of ammonia in pure water. It is shown that the lowest conductivity values are no longer unambiguous. This problem can be solved by the addition of a low ammonium concentration to the alkaline selector solution, resulting in an increased ammonium concentration in the detector.

The method to measure the conductivity of the electrolyte is explained in the next chapter, where the optimization of the key elements of the miniaturized version of the "AMINA" ammonia measurement system is dealt with.

3.3 Conclusions

The "AMINA" principle is an indirect chemical method for determining gaseous ammonia concentrations without interference of acidifying gasses, even when these gasses have elevated concentration levels.[2] Ammonia is sampled into the acid sample solution where it nearly completely reacts with water to form ammonium ions. Acidifying gasses like CO_2 are only partly ionized in the acid environment in the gas sampler. In the selector, the pH is increased to 13 so that the ammonium ions are almost completely neutralized to ammonia. Acidifying gasses are for the most part ionized in this alkaline surrounding. A selectivity of 600.000, the maximum CO_2 to NH_3 ratio in exhaled air, is shown to be expectable as long as the pH values are not significantly altered by the sampled gasses.

3.4 References

[1] J.W. Erisman, R. Otjes, A. Hensen, P. Jongejan, P. v.d. Bulk, A. Khlystov, H. Möls and S. Slanina, *"Instrument development and application in studies and monitoring of ambient ammonia",* Atmospheric Environment 35, pp 1913-1922, 2001

[2] B.H. Timmer, K.M. v. Delft, R.P. Otjes, W. Olthuis, A. v.d. Berg, *"A miniaturized measurement system for ammonia in air",* Analytica Chimica Acta 507 (1), pp. 139-145, 2004

[3] R.M. Berne, M.N. Levy, *"Physiology",* Mosby, 4th edition, 1998

[4] L.R. Narasimhan, W. Goodman, C. Kumar, N. Patel, *"Correlation of breath ammonia with blood urea nitrogen and creatine during hemodialysis",* PNAS 98 (8), pp 4617-4621, 2001

[5] D.J. Kearney, T. Hubbard, D. Putnam, *"Breath ammonia measurement in Helicobacter pylori infection",* Digestive diseases and sciences 47 (11), pp 2523-2530, 2002

[6] R.C. Weast, *"CRC Handbook of chemistry and physics",* The chemical Rubber Co., 65th ed., 1984

[7] R. Chang, *"Physical chemistry for chemical and biological sciences",* University Science Books, 3rd ed., chapter 11, 2000

[8] C.L. Yaws, *"Handbook of vapor pressure",* Gulf Publishing company, volume, 1994

[9] A. Bard, L. Faulkner, *"Electrochemical Methods, Biosensors",* John Wiley & Sons, Chapter 2 & 12, 1980

Chapter 4

Design and realization*

4.1 Introduction

The "AMINA" principle for measuring gaseous ammonia, described in the previous chapter of this thesis, is commercially available for measuring ambient ammonia levels. In this chapter, the design of a miniaturized version of this system and the process that leads to the optimized integrated ammonia analyzer are discussed. The functional design of the system is explained in the first section. In the second section, the boundary conditions of the optimization process are discussed, followed by the optimization process itself. How the optimized analyzer can be realized is explained in the last section.

4.2 "AMINA" system design

As described in chapter 3, the central part of the ammonia measurement system comprises three parts: a gas sampler, a selector and a detector. In the gas sampler, the analyte gas is pumped through a channel over a micro-porous, water-repellent membrane. At the other side of the membrane is a second channel for transportation of an acid sample solution. Gaseous ammonia is transported through the membrane into the sample solution where it is converted to ammonium ions.

Subsequently, the sample solution is pumped into the selector. The selector also comprises a micro-porous, water-repellent membrane between two

**Section 4.4.1 is published in Lab-on-a-chip, 2002*

channels. The sample solution is pumped into one channel of the selector, where an alkaline solution is added to increase the pH to create an alkaline environment. At this elevated pH, the ammonium ions are neutralized. Purified water is pumped through the opposite channel in the selector. The neutralized ammonia in the sample solution becomes gaseous at the membrane interface. This ammonia gas is transported through the membrane into the purified water where it reacts with water and forms ammonium and hydroxyl ions. The purified water with the ions formed in the selector is then pumped into the detector where the ion concentration is quantified using an electrolyte conductivity measurement. An illustration of the involved channels and fluid flows is given in figure 4.1.

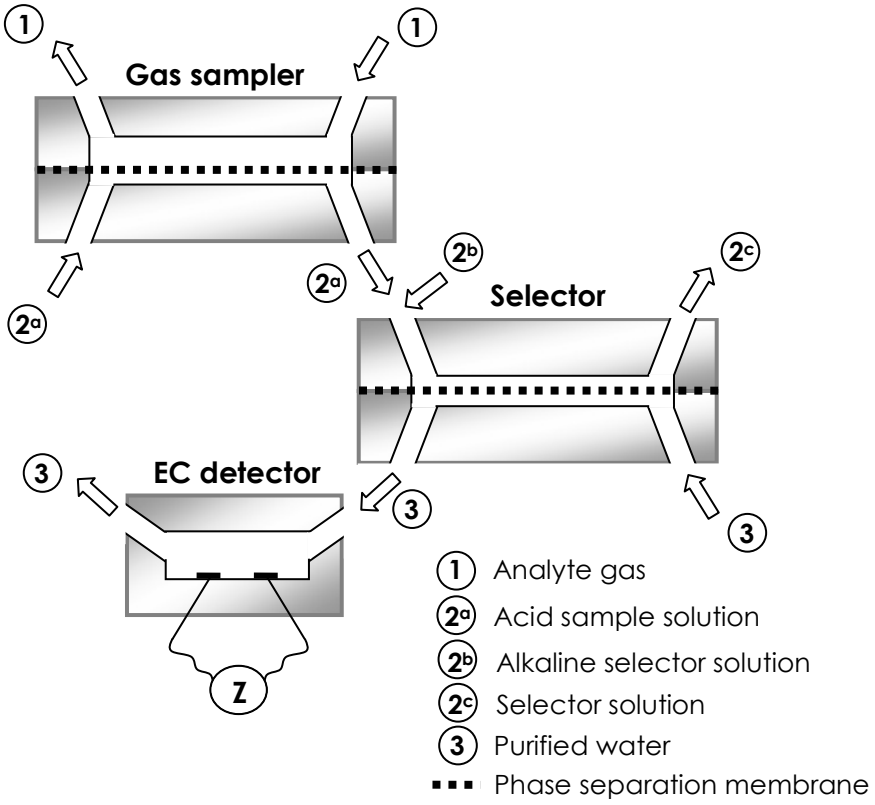

Figure 4.1. *Schematic of the channels and flows of the main "AMINA" components.*

4.3 Requirements and boundary conditions

The boundaries of the optimization process are three-fold. First, the requirements for the miniaturized ammonia measurement system are discussed. Secondly, design rules are discussed that result from technological possibilities and limitations. The third parameter that has to be taken into account is mass-transport, determining the overall response time, as discussed in detail in appendix A.

4.3.1 Requirements

The goal of the project is clear; miniaturize the existing ammonia analyzer without loss of sensitivity and selectivity to decrease the response time and the reagent consumption, which are the main advantages of miniaturization. Because the internal volumes are reduced, the required amount of analyte gas becomes smaller. The macro-scale device uses 1 litre of air per minute and a full measurement takes about twenty minutes. For breath analysis equipment, this response time is rather long and moreover, the required 20 litres of breath is a lot, especially for sick people. Our goal is to do a full measurement within a minute with only a few hundred ml of air.

The detection limit of the macro-scale apparatus is about 0.1 $\mu g/m^3$ or 77 ppt and the selectivity is accurate enough not to be influenced by normal ambient CO_2 concentrations, which are 0.03% or 300 ppm.[1] However, normal ambient ammonia concentrations in the Netherlands are about 2.5 $\mu g/m^3$ or almost 2 ppb. When the detection limit of the miniaturized ammonia analyzer would be about 1 ppb, the system would be accurate enough for environmental monitoring. For medical applications, where the decrease in analyte gas volume is most important, a detection limit of 50 ppb will be sufficient, as discussed in the second chapter of this thesis.

The selectivity results from the chemistry involved in the system, as discussed in the third chapter of this thesis. It is possible to make the system insensitive for normal ambient CO_2 concentrations. A step from 0 to 300 ppm CO_2 should give a response equal or smaller than a step from 0 to 2 ppb NH_3 or the selectivity of ammonia versus carbon dioxide should be 150000:1. However, for breath analysis, the CO_2 concentrations can be up to a hundred times higher. The corresponding requirement for the ammonia detection limit is also higher in that case, 50 ppb. The required selectivity for breath analysis is thus 600000:1.

4.3.2 Technological limitations

Ammonia is a small molecule that easily penetrates all kinds of materials like most plastics and rubbers. When measuring very low ammonia concentrations, desorbing gas from the sensor material can cause significant disturbance. This requires the sensor system to be made from

materials that are ammonia impermeable. The most-used materials for micromachining, silicon and glass, are both very suited.

There are several types of membranes that could be used as an intermediate layer between the channels in the ammonia measurement system. Characterization methods to determine whether a membrane is suited are described in appendix B. The best suited membrane turned out to be micro-porous polypropylene (PP) since it has a high water-repellency while it can still be glued to glass and silicon using epoxy glue. Such membranes have a thickness of about 150 µm.

In order to prevent the membrane to buckle into the channels and block the flow, the channels can not be made too shallow or too wide. Experiments with glass chips glued to a PP membrane showed that a depth of 15 µm and a maximum width of about 1 mm prevented blockage of the channels. In case the width of a channel should be larger, additional posts should be integrated that support the membrane.

Deep channels can be made in glass or silicon using powderblasting.[2] The maximum depth is 100 µm in order to prevent 500 µm thick glass wafers to break during processing.

4.3.3 Mass transport limitation

In the gas sampler, ammonium ions are formed at the membrane interface in the reaction between gaseous ammonia and the excess of protons in the sample solution, resulting in an ammonia concentration gradient over the membrane. This gradient causes transportation of ammonia through the membrane by diffusion. This also results in a concentration gradient inside the gas channel and therefore in diffusive transport of ammonia in the channel towards the membrane. Secondly, the analyte gas is pumped through the channel, causing convective transport of ammonia along the channel. In order to reach the lowest detection limit, the ammonia available in the analyte gas should be sampled into the sample solution as much as possible. The time required to transport the ammonia from the gas stream depends on the channel height, the membrane properties and the flow velocity. Simulation results of gas mass transport investigations are given in appendix A.

The above discussion is also valid for ammonia transport in the selector part of the system. The ammonium ions that are formed in the gas sampler are neutralized in the selector by adding an alkaline solution. The neutralized ammonia will partly turn gaseous at the membrane interface. This gas is transported by diffusion, from the liquid stream inside the selector, through the membrane, into the purified water in the detector. Transport of gaseous ammonia inside the membrane is rather fast because of the high diffusion rate of gaseous ammonia and the short distance. However, ionic transport in the solution is slower due to the much lower diffusion rate. The results of ionic mass transport simulations are also presented in appendix A.

Ionic transport through the membrane should be prevented at any cost. As explained in appendix B, this implies that the pressure difference over the membrane should be kept sufficiently low, below 170 kPa, to prevent water from penetrating the pores. The required pressure difference over a channel, ΔP (Pa), to create a specific flow, Q (m^3/s), is a function of the hydraulic resistance of the channel, R ($N \cdot s/m^5$), according to equation 4.1:[3]

$$\Delta P = Q \cdot R \qquad (4.1)$$

The hydraulic resistance of a channel is a function of the geometry of the channel, length (m), perimeter (m) and cross-section (m^2), and the viscosity, η ($N \cdot s/m^2$), of the fluid that is pumped through:[4]

$$R = \frac{2 \cdot \eta \cdot \text{length} \cdot (\text{perimeter})^2}{(\text{cross - section})^3} \qquad (4.2)$$

Note that very shallow but wide channels result in a high hydraulic resistance and thus in a high pressure drop over the channel.

4.3.4 Summary of the requirements and boundary conditions

The requirements for the system that follow from the possible applications are summarized in table 4.1. The boundary conditions due to technical limitations and residence time limitations due to mass transport are summarized in table 4.2. The next section deals with the optimization process to fulfil these requirements and limitations, resulting in an optimized system design.

Table 4.1. *Overview of requirements that have to be fulfilled in the system optimization and design process.*

	Macro-scale system	**Desired value**
Response time	20 minutes	1-2 minutes
Gas consumption (for full measurements)	20 litres	<500 ml
Detection limit	77 ppt	Atmospheric: 1 ppb
		Breath analysis: 50 ppb
Selectivity (e.g. towards CO_2)	> 150000:1	Atmospheric: 150000:1
		Breath analysis: 600000:1

Table 4.2. *Overview of limitations that have to be taken into account in the system optimization and design process.*

	Comment	**Solution**
Used materials	Gas-impermeable	Glass or silicon
Used membrane	Should be: gas-permeable, water-repellent, suited for integration	150 µm thick micro-porous polypropylene
Shallow channel dimensions	Limited due to buckling of membrane into channel	≥ 15 µm deep at 1 mm width
Deep channel dimensions	Limited due to weakening of substrate	≤ 100 µm depth
Mass transport limitations	A minimum time is required for gas molecules and ions to be transported in the system	Optimize internal volumes and flow velocities
Pressure difference	High water pressure difference causes membrane wetting	$P_{water} \leq 170$ kPa

4.4 Optimization and design

To optimize the miniaturized ammonia analyzer, the required one minute response time has to be divided over the gas sampler, the selector and the electrolyte conductivity detector without losing the required detection limit. This implies that optimal values have to be found for the channel geometries and the flow velocities.

The detection limit is determined by the analyte gas to purified water volume ratio, Q_{gas}/Q_{water}, presuming all gas is extracted into the sample solution and transported to the purified water. The volume inside a channel, V (m^3), can be expressed as a function of the channel geometry, the length l (m), width w (m), and depth h (m), but also from the residence time of the fluid in the channel, τ (s) and the flow, Q (m^3/s):

$$V = l \cdot w \cdot h = \tau \cdot Q \tag{4.3}$$

The gas to water ratio can now be expressed as:

$$\frac{Q_{gas}}{Q_{water}} = \frac{l_{gas} \cdot w_{gas} \cdot h_{gas} \cdot \tau_{water}}{l_{water} \cdot w_{water} \cdot h_{water} \cdot \tau_{gas}} \tag{4.4}$$

Concluding from equation 4.4, the detection limit can be optimized by increasing the gas channel dimensions and the water residence time and by decreasing the water channel dimensions and the gas residence time. The optimal system has a large gas channel with a large gas flow and a small water channel and a small water flow. Together with the technological limitations and the transport requirements, an optimal miniaturized analyzer design can be found.

The optimization process of the three main components of the system will be discussed in the opposite direction, starting with the detector, followed by the selector and the gas sampler, respectively. Miniaturization of these key components implies the need of a detector that can measure low ion concentrations in a small liquid volume.[5] Once the internal volume of the detector is known, the lowest suitable water flow can be chosen. An optimal design of the purified water channel in the selector follows from this flow velocity. Subsequently, the optimal geometries of the sample solution channels of both the selector and the gas sampler can be determined and finally, the geometry of the gas channel of the sampler.

4.4.1 Miniaturized electrolyte conductivity detector

Electrolyte conductivity (EC) detection is a generally applied technique in miniaturized chemical analysis systems[6-10] and lab-on-chip applications.[10,11] The detectors can easily be integrated in systems based on silicon or glass. Although the ion specific temperature dependency of the conductivity can be applied to make the EC detection ion specific,[10] normally EC detection is used as a non-specific measurement method. Conductivity detectors are often used in capillary electrophoresis[6-9,11] where specific ions are separated prior to the detection.

Accurately measuring conductivity on-chip in low electrolyte concentrations is not easy. The conductivity of such electrolytes is very low, resulting in high specific resistance values. Developing reliable interface electronics for high resistance values is highly demanding. A sensor with a low cell constant, K_{cell}, is required to prevent the electrolyte resistance, R_{elec} (Ω), to become too high. K_{cell} (m^{-1}) defines the relation between the measured conductance, G (S), and the conductivity, K_{sol} (S/m), being the product of the concentrations, C_i (mol/m^3), and ion conductivities, λ_i ($S \cdot m^2/mol$), of all the individual types of ions in the electrolyte,[12] as shown in equation 4.5. It should be noted that the ion conductivity values are temperature dependent, causing the sensors to be temperature dependent too.

$$G = \frac{1}{R_{elec}} = \frac{K_{sol}}{K_{cell}} = \frac{\sum_i \lambda_i \cdot C_i}{K_{cell}} \qquad (4.5)$$

The cell constant depends on the geometry of the sensor and generally increases for smaller sensors. For measuring on-chip, using planar electrodes is technologically favourable since these are easier integrated in Microsystems.[13] The cell constant of such sensors can be lowered by using interdigitated electrodes, as illustrated in figure 4.2. A 0.1 cm^2 conductivity sensor is demonstrated with a cell constant of 7.9 m^{-1}. Pure water, with a theoretical conductivity of $5.5 \cdot 10^{-9}$ S/m, results in an electrolyte resistance of 1.4 MΩ, small enough for common conductivity measuring electronics.

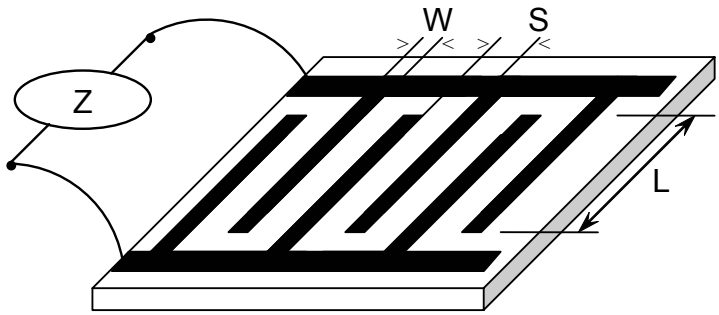

Figure 4.2. *Schematic layout of a planar interdigitated electrode pair with electrode width W (m), spacing S (m) and length L (m).*

Theoretical

An electrical equivalent circuit of the sensor, shown in figure 4.2, is used to calculate the complex impedance, Z (Ω), of the EC detector.[12] Besides the electrolyte solution resistance, R_{elec} (Ω), a lead resistance, R_{lead} (Ω), is present in series with the sensor. This resistance is a result of the resistance in the connecting wires, the bonding wires connected to the bondpads of the sensor and, mainly, the thin film platinum electrodes.

Direct capacitive coupling between the two comb electrodes is represented by the cell capacitance C_{cell} (F). The value of C_{cell} is determined by the dielectric constant of the electrolyte, $\varepsilon \cdot \varepsilon_0$ ($F \cdot m^{-1}$), and the geometry of the electrodes, expressed by the cell constant (m^{-1}).[14]

$$C_{cell} = \frac{\varepsilon \cdot \varepsilon_0}{K_{cell}} \tag{4.6}$$

A double layer capacitance, C_{DI}, is present at the electrode-electrolyte interface. This impedance is determined by the charge distribution caused by physical and chemical interaction between the metal and the ions in the electrolyte. The resulting electrical equivalent model and the mathematical representation are shown in figure 4.3 and equation 4.7.

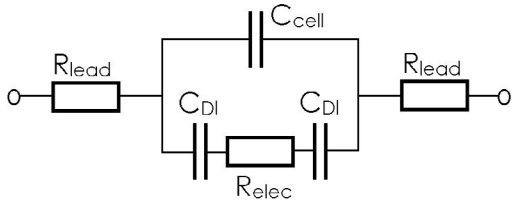

$$Z(j\omega) = 2R_{lead} + \frac{x}{j\omega C_{cell} x + 1} \qquad x = R_{elec} + \frac{2}{j\omega C_{DI}} \tag{4.7}$$

Figure 4.3. *Electrical equivalent circuit and the expression of the impedance of the electrolyte conductivity sensor.*

The radius of (hydrated) ions prevents direct contact between the ions in an electrolyte and the metal electrode. Furthermore, diffusion of ions in the solution causes a nonlinear charge distribution, together resulting in the double layer capacitance, C_{DI}. The charge distribution is described by the Gouy-Chapman model,[12,15] dividing the charge in two layers, a Stern layer and a diffusive layer. Although other models are described in literature,[16] this model is used in this study.

The charge of the ions in the Stern layer is thought to be concentrated at a distance of about 1.0 nm from the electrode surface, determined by the radius of the hydrated ions. This layer can be modelled as a normal capacitor, C_{Stern} (F). The capacitance has a value of about 20μF/cm^2, independent of the ion concentration.[17]

The diffusive layer is present because of the finite amount of charge that can be present in the Stern layer and the need for charge neutrality of the double layer. The diffusive layer capacitance depends on the total thickness of this layer, being a function of the electrolyte concentration. The thickness of this layer is called the Debye length, $1/\kappa$ (cm).[12] The capacitance of the diffusive layer, C_{Diff} (F), equals the absolute dielectric constant divided by the Debye length, multiplied by the electrode area. The equation for the diffusive capacitance value, normalized for the electrode dimensions, is then:

$$C_{Diff} = \varepsilon_{water}\varepsilon_0 \cdot \kappa = \sqrt{\frac{2 \cdot 10^{-3} \cdot z^2 e^2 \varepsilon_{water}\varepsilon_0 \cdot c \cdot N_A}{kT}} \qquad (4.8)$$

with z the valence of the ion, e the electron charge, c the ion concentration (M), N_A the Avogadro constant, $\varepsilon_{water}\varepsilon_0$ the absolute dielectric constant of water, k the Bolzman constant and *T* the absolute temperature (K). Using this equation, the diffusive capacitance can be calculated as function of the ion concentration. It is shown in figure 4.4, where C_{diff} is calculated for room temperature conditions, that the capacitance decreases significantly at decreasing concentration.

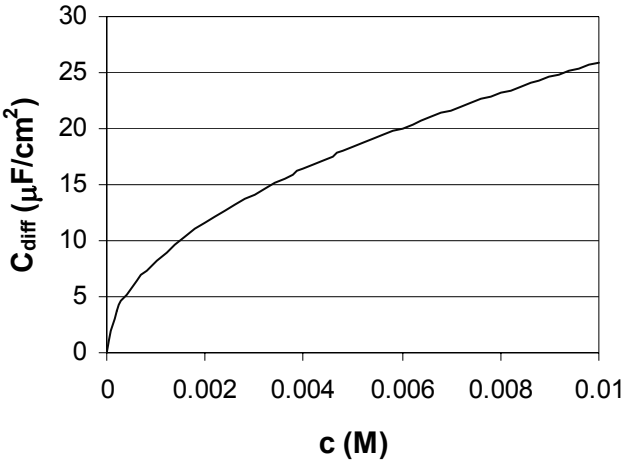

Figure 4.4. *The diffusive capacitance as a function of the electrolyte solution ion concentration.*

The total double layer capacitance is made up of a series connection of the Stern and the diffuse capacitance. The total double layer capacitance is plotted in figure 4.5 as a function of the electrolyte concentration.

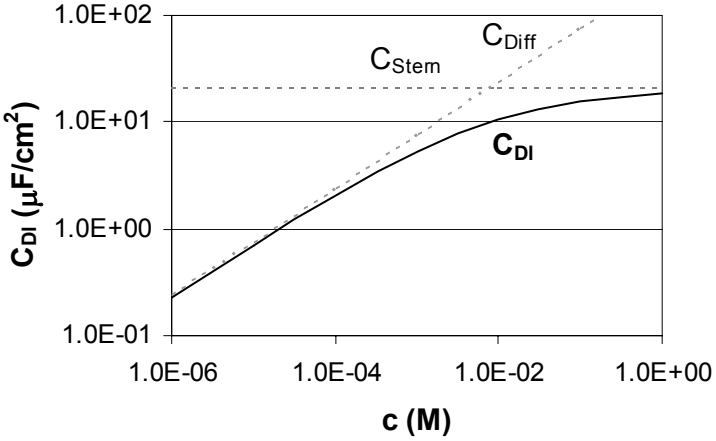

Figure 4.5. *The double layer capacitance as a function of the electrolyte concentration, modelled as a series network of the Stern capacitance and the diffusive capacitance.*

Some textbooks on electrochemistry assume the total double layer capacitance between 10 and 40 µF/cm^2.[18] With the known value of the Stern capacitance, this implies that the diffusive capacitance is assumed to be more than 20 µF/cm^2. When doing so, a large error is made when measuring concentrations below 2 mM where the double layer capacitance is then mainly determined by the relatively small diffusive capacitance, as can be concluded from figure 4.4 and 4.5.

The cell geometry of the EC detector needs to be optimized for both the cell constant and the frequency behaviour. It is important that at least one measurement frequency can be found for the highest and lowest expected conductivity where both the complex impedances are mainly resistive. This can be achieved by making the frequency band between the low and high cut-off frequency as large as possible. This can be obtained by optimizing the ratio between the spacing between the electrodes and the electrode width, the S/W ratio. Previous research shows that a theoretical bandwidth optimum is reached at a ratio of 0.54.[17]

A method to calculate the cell constant of a planar interdigitated electrolyte conductivity sensor is provided in literature:[19]

$$K_{cell} = \frac{2}{(N-1)\cdot L} \cdot \frac{K(k)}{K(\sqrt{1-k^2})} \qquad (4.9^a)$$

with

$$K(k) = \int_0^1 \frac{1}{\sqrt{(1-t^2)\cdot(1-k^2t^2)}}\,dt \qquad (4.9^b)$$

and, for N>>2

$$k = \cos\left(\frac{\pi}{2} \cdot \frac{W}{S+W}\right) \qquad (4.9^c)$$

The cell constant is calculated as a function of the number of electrode fingers, N, and the width of the electrodes, W (m). The space width, S (m), is for technological reasons limited to 10 µm. The smallest cell constant can be realized with a large number of narrow electrode fingers. A nearly optimal electrode width for an optimal S/W ratio would than be 20 µm.

It was our goal was to develop a sensor with a predetermined maximum size of 1.5*5 mm (0.075 cm^2), with a cell constant as low as possible. The optimized sensor would then have 165 electrode fingers, a width of 20 µm, a spacing of 10 µm and a length of 1.2 mm, resulting in a cell constant of 7.9 m^{-1}. A cover is glued over the detector with a channel above the electrodes. The depth of the channel is 25 µm, the width is 2 mm and the length is 5 mm, resulting in an electrolyte volume of 250 nl.

Based on the impedance equation 4.7, the impedance can be calculated as a function of the measurement frequency and the now known values of the components. At low frequency, the impedance is dominated by the

concentration dependent double layer capacitance, C_{DI}. When the measurement frequency is increased, the impedance of this capacitor becomes lower than the resistive impedance of the electrolyte, R_{elec} (Ω). The frequency at which this occurs, f_{lo} (Hz), can be calculated using the following equation:[10]

$$f_{lo} = \frac{1}{2\pi(R_{lead}C_{DI} + 2R_{lead}C_{Cell} + \frac{1}{2}R_{elec}C_{DI})} \approx \frac{1}{\pi R_{elec}C_{DI}} \qquad (4.10)$$

When the measurement frequency is further increased, the impedance of the parallel cell capacitance, C_{cell}, starts to decrease. At a certain frequency the impedance of the cell capacitance becomes lower than the electrolyte resistance. The frequency at which this occurs, f_{hi} (Hz) is given in the following equation:[10]

$$f_{hi} = \frac{1}{2\pi R_{elec}\frac{C_{DI}C_{Cell}}{C_{DI} + 2C_{Cell}}} \approx \frac{1}{2\pi R_{elec}C_{Cell}} \qquad (4.11)$$

This higher cut-off frequency is a function of the cell capacitance and the electrolyte resistance and its value decreases for lower electrolyte concentrations.

Experimental

The measurement setup consists of a HP9194A Impedance/Gain-Phase analyzer connected to a HPIB bus on a personal computer. A home-made Labview conductivity measurement program is used to perform impedance measurements. The impedance analyzer can measure both the absolute value of the impedance and the phase shift of the sensor while sweeping the frequency between 100 Hz and 40 MHz.

The theoretical maximum resistance with pure water is 1.5 MΩ. However, in our lab conditions the practical conductance of deionised water is much higher due to contaminations. The used water has a conductivity of 20 µS/m, taken from the conductivity sensor on the Millipore Elix3 demineralization apparatus. Contamination in the water from glassware and connecting tubes is removed by feeding the water through a mixed bed ion exchange resin, acquired from Baker Analyzed.

The upper conductivity limit to be measured with the developed sensor is 2.5 mS/m for the ammonia detection project. This results in a theoretical resistance of 3.2 kΩ, which can be realized by using a 200 µM NaCl solution.

Results and Discussion

The sensor response is measured with the described method as well as simulated in a mathematical software package, using equation 4.7. The cell constant is experimentally determined to be 8.8 m^{-1} using a 1.0 mM NaCl solution, being about 10 % higher than the calculated cell constant value of 7.9 m^{-1}. The higher value of the cell constant can be caused by small variations in the geometry of the cell. The photolithography and lift-off steps, used in producing the sensors, roughen the sides of the electrode fingers. This causes a concentration dependent influence on the impedance.[20] Another problem is insulation of bonding wires with epoxy glue, influencing the cell constant when parts of the electrodes get covered too.

As described, the lower conductivity limit, with purified water, is measured to be 20 µS/m and the higher limit is prescribed to be 2.5 mS/m. These conductivity values are used for calculating and measuring the impedance as a function of the applied frequency. The result is shown in figure 4.6.

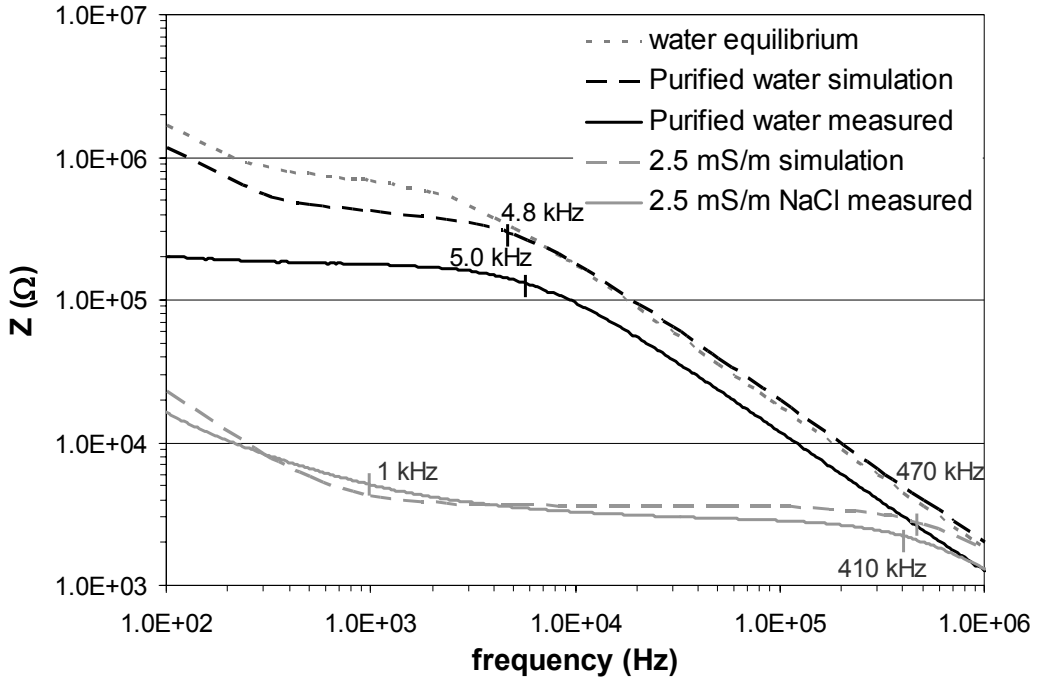

Figure 4.6. *Simulation and measurement results of the frequency response of the electrolyte conductivity sensor in electrolytes with a conductivity of 20 µS/m, the lower limit, and 2.5 mS/m, the higher limit, as well as the theoretical maximum due to the water equilibrium. A 2.5 mS/m solution is realized by using 200 µM NaCl.*

As can be concluded from figure 4.6, the theoretical impedance corresponds reasonably well with the experimentally found impedance of the conductivity sensor. The higher cut-off frequencies can be predicted well with the described theory (4.8 and 5.0 kHz for pure water and 470 and 410 kHz for a 2.5 mS/m electrolyte solution). The experimentally determined impedance at lower frequencies diverges from the theoretically prediction. This is caused by a simplification in the electrical equivalent model. Electrochemical effects at the electrode-electrolyte surface introduce a capacitance, parallel to the double layer capacitance, called the Faradaic impedance.[11] It comprises a charge transfer resistance and a Warburg impedance, a pseudocapacitance.[21] However, for electrolyte conductivity measurements, this lower frequency range is not of interest.

A resistive impedance of about 220 kΩ is found for deionised water at frequencies between 100 Hz and 5 kHz. A resistance of 2.9 kΩ is found for a 2.5 mS/m solution between 1 and 100 kHz. These resistance values are measurable with standard interface electronics. The optimal measurement frequency lies between the lower cut-off frequency of the 2.5 mS/m solution (1 kHz) and the higher cut-off frequency of water (5 kHz). A measurement frequency of 1 KHz frequency is chosen, resulting in the highest accuracy at low ion concentrations, the area that determines the detection limit of the total ammonia measurement system.

Now that the optimal measurement frequency is found, a calibration curve with different NaCl solutions is made with this setting, shown in figure 4.7.

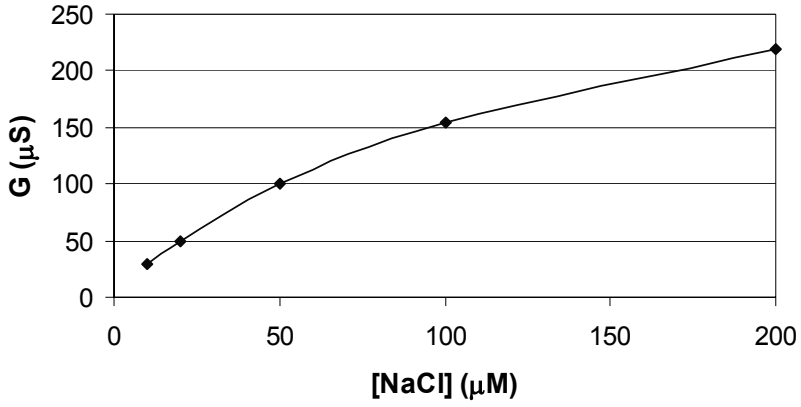

Figure 4.7. *Measurement result of the electrolyte conductivity as a function of the NaCl ion concentration.*

It is shown that the EC detector is very suitable for measuring in the prescribed conductivity range. The relation between the concentration and the conductivity is found to be nearly linear.

The internal volume of the realized detector is calculated to be about 250 nl. In addition, some interconnecting channels between the outlet of the selector and the detector are required. In order to limit the water residence time in the detector to less than 10 seconds, a water flow of about 2 µl/min is used, resulting in a residence time inside the detector of 7.5 seconds.

All measurements have been carried out at room temperature. When using the EC detectors in a measurement system operated at varying temperatures, the temperature dependency has to be taken into account. This can be accomplished by using two detectors. One extra detector is placed in the water stream before the water enters the selector. A change in temperature will have an effect on both detectors while a change in ammonia concentration will only influence the conductivity of the detector at the outlet of the selector.

Conclusions
Theory on the cell constant of planar interdigitated electrolyte conductivity sensors is combined with theory on electrochemical effects at the electrode-electrolyte interface to come to a better description of the sensor. It is known that the double layer capacitance decreases significantly with decreasing electrolyte concentration. Taking this into account it is now possible to predict the sensor response even for low concentrations. A sensor is realized that is optimized for low electrolyte concentrations with a cell constant as low as 8.8 m^{-1} and a total detector area of 0.075 cm^2. The maximum measured resistance value for pure deionised water is about 220 kΩ at 1 kHz. This is a favourable value for common interface electronics.

4.4.2 Selector
The selector comprises two channels, a selector solution and a purified water channel, separated by a phase-separation membrane. A schematic illustration is given in figure 4.8.

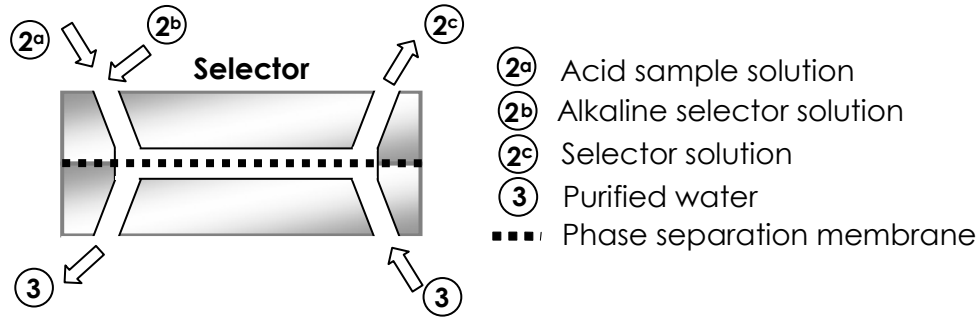

Figure 4.8. *Schematic illustration of the selector (taken from figure 4.1).*

The sample solution that is pumped into the selector contains ammonium ions that are neutralized to ammonia by the addition of an alkaline solution. This dissolved ammonia and remaining ammonium ions have to be transported towards the membrane where gaseous ammonia is formed at the interface layer. This gaseous ammonia diffuses through the membrane into the purified water stream where it reacts very fast with water to form ammonium ions again. In order to reduce the time required for transport of the ions in the channels, the minimum depth of 15 µm will be used. Simulation results with such a channel, given in appendix A, show that a residence time of one second is enough for good mixing and thus for sufficient transport of ammonium in the solution.

The two flows inside the selector have to make contact with the membrane. This implies that also the width and length of the two channels have to be equal. The optimal water flow is determined in the previous section of this chapter to be 2 µl/min.

The flow of the sample and the selector liquid does, within limits, not significantly influence the overall selectivity of the system but it determines the required length of the sample solution channel and the selector channel. As explained before, a large gas sampler is preferred. This means that a very small sample solution flow would only cause the system to become slower. On the other hand, a very large flow demands for a very long or very wide channel. With the macro-scale device at ECN, a selector-to-water flow ratio of ten to one was used and this proved to work fine.[1] This means a 20 µl/min flow through the selector channel resulting in a selector channel volume of 330 nl, with the required residence time of one second. With a known depth of 15 µm, this can be realized with a membrane surface of $22 \cdot 10^{-6}$ m^2.

The length of the total system should be limited to less than 10 cm to fit on a glass substrate that can be processed with our equipment, limiting the selector length to a few centimetres. The width of the channel should be smaller than the length of the channel to make sure the flow will be mainly in the direction of the channel. This prevents a large flow difference between different parts of the channel.

One way to realize the selector geometry in a rectangular shaped channel is to make the channel 9 mm long and 2.5 mm wide. The selector solution requires 1 second to flow through the channel and the water ten seconds. The pressure difference over the selector channel with these parameters can be calculated using equation 4.1 and 4.2 to be 2.85 kPa, well below the maximum of 170 kPa determined in appendix B and mentioned in table 4.2.

4.4.3 Gas sampler

The gas sampler also comprises two channels, a gas channel and a sample solution channel, separated by a phase-separation membrane. A schematic illustration is given in figure 4.9.

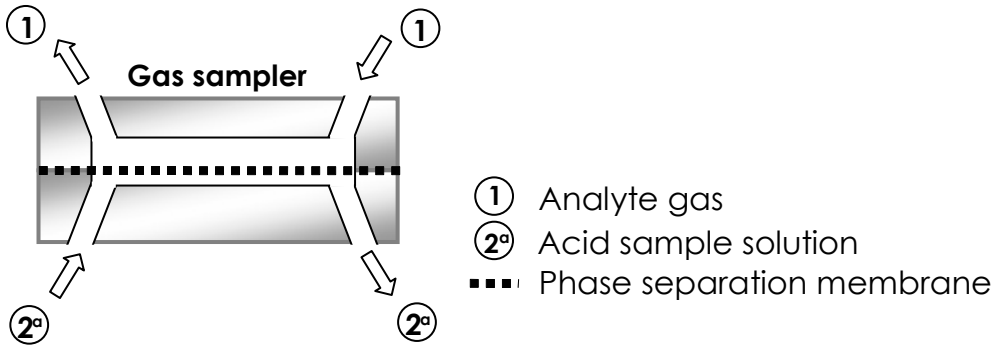

Figure 4.9. *Schematic illustration of the gas sampler (taken from figure 4.1).*

As shown before, the detector requires about 7.5 seconds for the water to flow through the channel. The water inside the selector uses ten seconds to flow through the channel. The water flow and the selector flow are in opposite direction so the residence time of the selector flow does not add to the total flow-through time. This means that 42.5 seconds are left for the gas sampler.

The sample solution and the alkaline solution together form the selector solution. The alkaline solution should not be too concentrated because this would cause the solution to erode the interconnect materials. The sample

solution has an initial pH of about 3. An addition of 20 % alkaline solution with a pH of 13 is applicable. A selector solution flow of 20 µl/min therefore implies a sample solution flow of about 16 µl/min. With the total available time of 42.5 seconds, this results in a sample solution volume inside the gas sampler of 11.3 µl. As will be explained in the realization section of this chapter, the sample solution channel and the selector channel are made on the same glass chip, in the same process step. This implies that the depth of the two channels is also the same. With the known depth and internal volume of the sample solution channel, the required membrane surface can be calculated to be $7.6 \cdot 10^{-4}$ m^2. One way to realize this in a rectangular shaped channel is by making the gas sampler 35 mm long and 22 mm wide. The pressure difference over the channel can be calculated using equation 4.1 and 4.2 to be 1.1 kPa, again well below the maximum allowed 170 kPa.

Simulation results, given in appendix A, show that a gas channel with a depth of 100 µm over a 150 µm thick membrane requires a residence time of 14.6 ms. Therefore, the volume of the gas channel can be calculated to be 77 µl. This results in a maximum gas flow of 300 ml/min.

4.4.4 Summary of the designed system geometry

The dimensions of the channels that have been found in the optimization process are summarized in table 4.3. How the optimized analyzer can be realized is described in the next section.

Table 4.3. *Overview of the geometry and flow parameters of the optimized miniature ammonia analyzer.*

	length	**width**	**depth**	**flow**
Gas sampler Gas channel	35 mm	22 mm	100 µm	① Up to 300 ml/min
Gas sampler Sample channel	35 mm	22 mm	15 µm	②ᵃ 16 µl/min
Selector Selector channel	9 mm	2.5 mm	15 µm	②ᶜ 20 µl/min
Selector Water channel	9 mm	2.5 mm	15 µm	③ 2 µl/min
detector	5 mm	2 mm	25 µm	③ 2 µl/min

4.5 System realization

In this section, it is explained how the chips with the optimized dimensions can be realized. The gas sampler and the selector are made by creating channels in a glass substrate. The techniques used for making these channels are discussed in the first section. In order to minimize interconnect volumes, the gas sampler and the selector are integrated on the same chip. Because it is extremely difficult to make holes in the membranes without causing leakage, the detectors are placed on the outside of these chips, covered with a channel in a cover chip. The technique used for making detectors is addressed in the second section. Subsequently, the process scheme for the total miniaturized ammonia measurement system and the technique used for assembling the different parts are discussed.

4.5.1 Gas sampler and selector channel realization

The shallow liquid channels are made with chemical etching of glass in HF. The process scheme is schematically shown in figure 4.10.

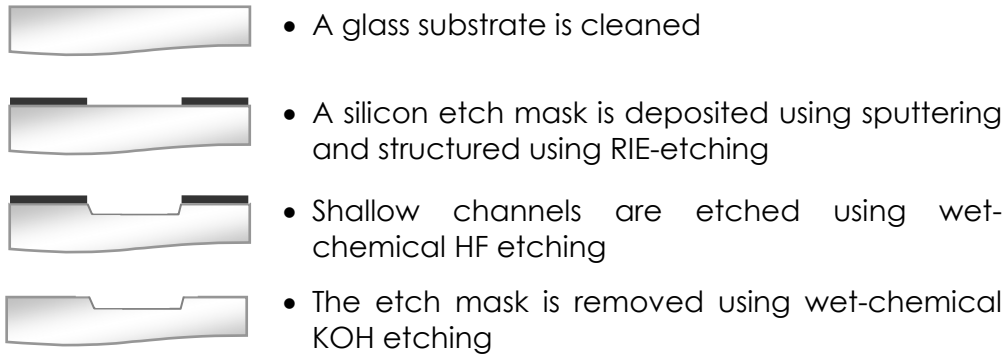

Figure 4.10. *Process scheme for etching shallow channels in glass.*

As described in the technological limitations section, deep channels, through-holes, the gas channel and all interconnect holes are made with powderblasting.[2] A photosensitive protection foil is laminated to a cleaned glass substrate, illuminated with UV light through a mask and developed in sodium carbonate. Subsequently, the channels are blasted into the glass. The process is repeated to make interconnect through-holes. The process scheme is schematically shown in figure 4.11.

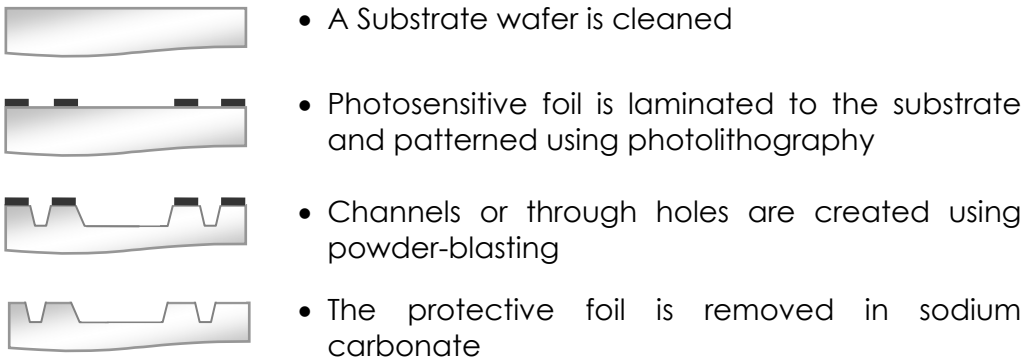

Figure 4.11. *Process scheme for powderblasting channels or through-holes.*

4.5.2 Electrolyte conductivity detector

Planar interdigitated conductivity sensors and bondpads are made on a standard Pyrex glass wafer using a technique called lift-off. First, the substrate is cleaned in fuming nitric acid for 10 minutes. A photoresist layer is deposited in a spin coater and structured using standard photolithography. A 20 nm thick tantalum adhesion layer and a 100 nm thick platinum electrode layer are deposited using sputtering. The excess metal is removed by dissolving the photoresist in acetone in an ultrasound bath. This lift-off technique is illustrated in figure 4.12. A photo of a realized detector is shown in figure 4.13.

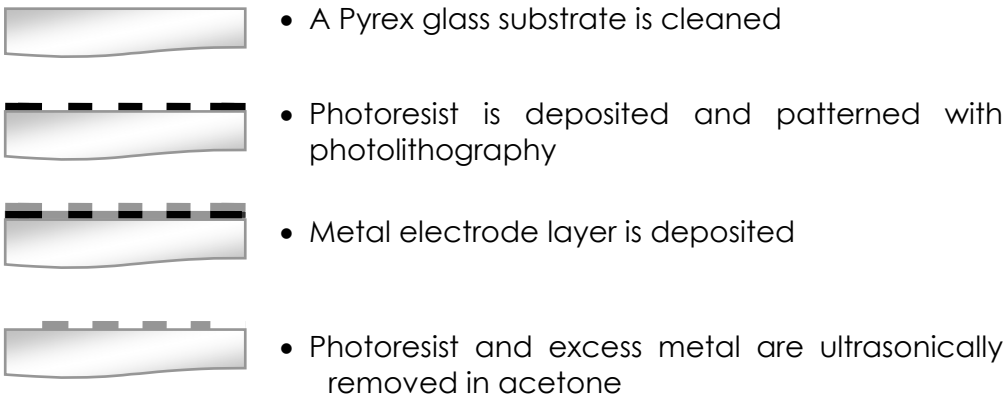

Figure 4.12. *Process scheme for lift-off production of planar electrodes.*

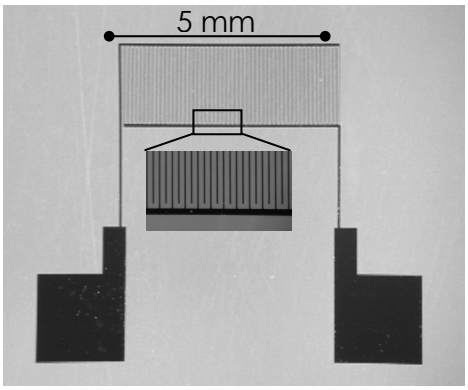

Figure 4.13. *Photograph of an interdigitated planar electrolyte conductivity detector with, in the inset, a close-up of part of the electrodes.*

The detectors are covered with a glass chip with connection holes and a channel therein. The glass covers are made using powderblasting according to the process scheme shown in figure 4.14. A photo of a realized cover chip is given in figure 4.15.

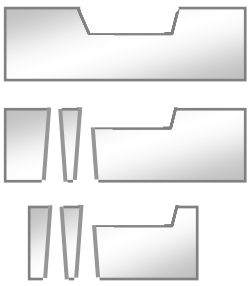

- A 25 µm deep channel is created using powderblasting
- Through-holes are created using powderblasting
- The cover chips are diced from the wafer and cleaned

Figure 4.14. *Process scheme for the powderblasted electrode covers.*

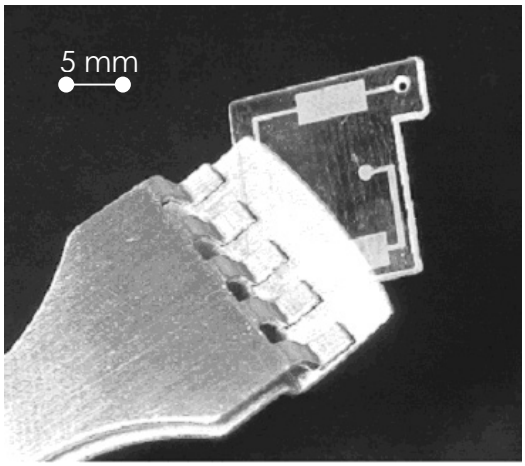

Figure 4.15. *Cover chip for two conductivity sensors.*

4.5.3 System integration

A miniaturized ammonia measurement system can be realized by using the techniques discussed in the previous sections. First, the EC electrodes are created on the back side of a glass substrate. Subsequently, the shallow channels are created, followed by the deep gas channel and the through-

holes. The process scheme for the production of the cover for the electrodes is given in the previous section, see figure 4.14. The scheme for making the gas sampler and selector channels and the detector electrodes is given in figure 4.16. Subsequently, the individual chips are diced from the wafer and the parts are assembled. The resulting stack is shown schematically in figure 4.17. A photo of the realized chips is given in figure 4.18. Note that the realized chips contain two detectors. As discussed briefly in the section dealing with the optimization of the EC detector, the addition of a second detector in the water stream before the selector can be used to detect conductivity changes in the water, other than changes caused by an altered ammonia concentrations, like changes in temperature.

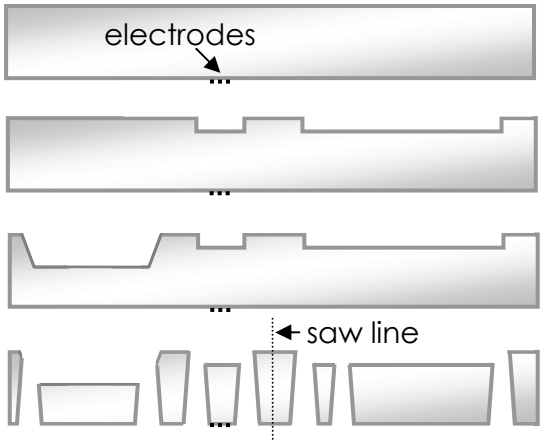

- A Substrate wafer is cleaned and electrodes are made using lift-off
- Shallow channels are etched using wet-chemical HF etching
- Deep channels are made using powderblasting
- Through-holes are made using powderblasting and the chips are diced and cleaned

Figure 4.16. *Process scheme for the realization of the selector and the gas sampler.*

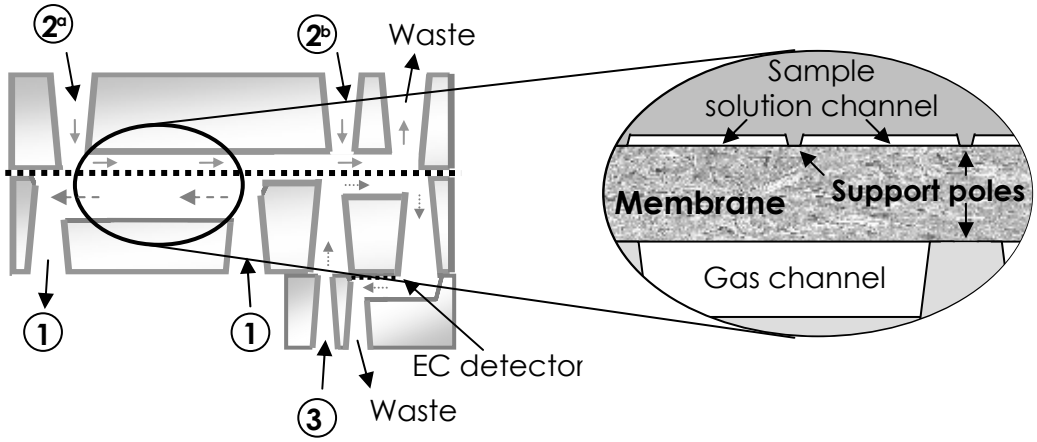

① Analyte gas
②ᵃ Acid sample solution
②ᵇ Alkaline selector solution
③ Purified water
▪▪▪ Phase separation membrane

Figure 4.17. *Impression of the assembled parts with a scaled close-up of the channels, the membrane and the support posts in the gas sampler.*

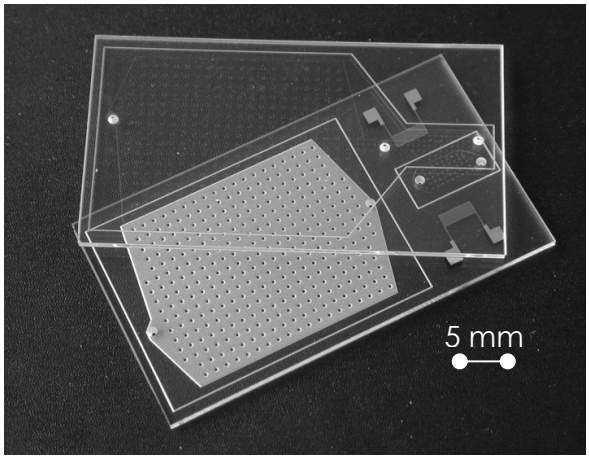

Figure 4.18. *Realized glass chips.*

4.5.4 Assembly of the integrated miniaturized system

The two glass chips are glued to a polypropylene membrane with thermo-hardening epoxy glue. The glass around the channels is covered with a thin glue layer by hand. The membrane adsorbs most of the glue, preventing it from entering the channels. Furthermore, as can be seen in figure 4.18, a deep trench is made around the channels using powderblasting. This trench prevents glue from penetrating the channels. Once a thin layer of glue is applied on both chips, the system is assembled and slightly pressed together.

Subsequently, the glass cover is glued over the electrolyte conductivity sensors using epoxy glue. A very thin glue layer has to be applied to the glass cover in order to prevent glue entering the channels.

The last step in the assembly of the miniaturized ammonia analyzer is making interconnects. Fluid connectors are glued to the glass chips at the through-holes and wires are bonded to the bondpads of the electrodes. The result is shown in figure 4.19.

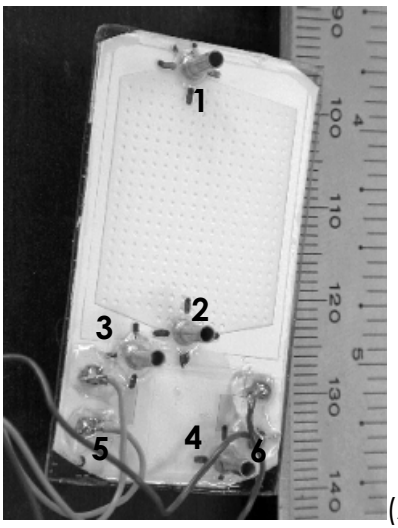

(A)
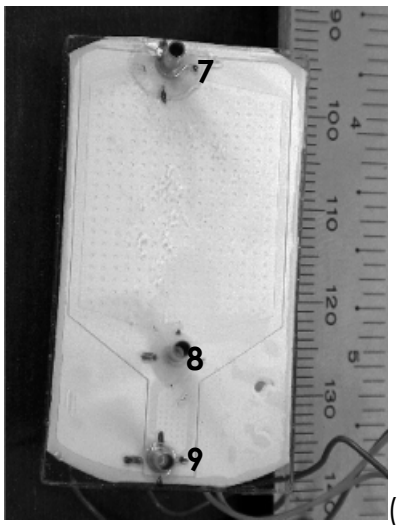

(B)
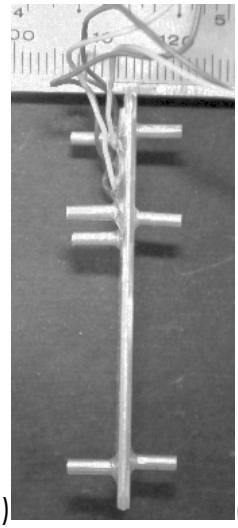
(C)

Figure 4.19. *Photographs of an assembled miniaturized ammonia analyzer, showing (A) a top view, (B) bottom view and (C) side view of the chip with 1-gas outlet, 2-gas inlet, 3-purified water inlet, 4-water outlet, 5- EC detector at the water inlet, 6-EC detector at the water outlet, 7-sample solution inlet, 8-alkaline selector solution inlet and 9-solution outlet.*

4.6 References

[1] J.W. Erisman, R. Otjes, A. Hensen, P. Jongejan, P. v.d. Bulk, A. Khlystov, H. Möls and S. Slanina, *"Instrument development and application in studies and monitoring of ambient ammonia",* Atmospheric Environment 35, pp 1913-1922, 2001

[2] S. Schlautmann, H. Wensink, R.B.M. Schasfoort, M. Elwenspoek, A. v.d. Berg, *"Powder Blasting Technology as an Alternative Tool for Microfabrication of Capillary Electrophoresis Chips with Integrated Conductivity Electrodes",* Journal of Micromechanics and Microengineering 11(4), pp 386-389, 2001

[3] N. Goedecke, J. Eijkel, A. Manz, *"Evaporation driven pumping for chromatography application"*, Lab on a chip 2, pp 219-223, 2002

[4] P. Gravesen, J. Branebjerg, O. Sondergard Jensen, *"Microfluidics – A review",* Journal of Micromechanics and Microengineering 3, pp 168-182, 1993

[5] B. Timmer, W. Sparreboom, W. Olthuis, P. Bergveld, A. V.d. Berg, *"Optimization of an electrolyte conductivity detector for measuring low ion concentrations",* Lab on a chip 2, pp 121-124, 2002

[6] H. Zhao, R. Dadoo, R. J. Reay, G. T. A. Kovacs, R. N. Zare, *"Electrically floating conductivity detection system for capillary electrophoresis",* Journal of Chromatography (A) 813, pp 205-208, 1998

[7] Y. Liu, D. O. Wipf, C. S. Henry, *"Conductivity detection for monitoring mixing reactions in microfluidic devices",* Analyst, 126, pp 1248-1251, 2001

[8] A. J. Zemann, E. Schnell, D. Volgger, G. K. Bonn, *"Contactless conductivity detection for capillary electrophoresis",* Analytical Chemistry 70, pp 563-567, 1998

[9] K. Mayrhofer, A. J. Zemann, E. Schnell, G. K. Bonn, *"Capillary electrophoresis and contactless conductivity detection of ions in narrow inner diameter capillaries",* Analytical Chemistry 71, pp 3828-3833, 1999

[10] G.R. Langereis, W. Olthuis, P. Bergveld, *"A demonstration of acquiring specific concentration data by variations in the operating conditions of a non-specific sensors",* Chemometrics and intelligent Laboratory systems 50, pp 211-223, 2000

[11] R.M. Guijt, E. Baltussen, G. v.d. Steen, R.B.M. Schasfoort, S. Schlautmann, H.A.H. Billiet, J. Frank, G.W.K. v. Dedem, A. v.d. Berg., *"New approaches for fabrication of microfluidic capillary electrophoresis devices with on-chip conductivity detection",* Electrophoresis 22 (2), pp 235-241, 2001

[12] A. Bard, L. Faulkner, *"Electrochemical Methods, fundamentals and applications",* John Wiley & Sons, Chapter 2 & 12, 1980

[13] P. Jacobs, A. Varlan, W. Sansen, *"Design optimisation of planar electrolytic conductivity sensors",* Medical & biological engineering and computing, pp 802-810, 1995

[14] M. Lambrechts, S. Sansen, *"Biosensors: Microelectrochemical devices",* Institute of physics, Chapter 2, 1992

[15] N. Sato, *"Electrochemistry at metal and semiconductor electrodes",* Elsevier science, Chapter 5, 1998

[16] S. Lamperski, C.W. Outwaite, *"A non-primitive model for the electrode | electrolyte interface based on the Percus-Yevick theory. Analysis of the different molecular sizes, ion valances and electrolyte concentrations",* Journal of electroanalytical chemistry 460, pp 135-143, 1999

[17] G.R. Langereis, *"An integrated sensor system for monitoring washing processes", PhD-* Thesis, University of Twente, 1999

[18] J. Wang, *"Analytical electrochemistry, second edition",* John Wiley & Sons, 2000

[19] W. Olthuis, W. Streekstra, P. Bergveld, *"Theoretical and experimental determination of cell constant of planar-interdigitated electrolyte conductivity sensors",* Sensors and Actuators B 24-25, pp 252-256, 1995

[20] E. Lust, A. Jänes, V. Sammelselg, P. Miidla*, "Influence of charge density and electrolyte concentration on the electrical double layer characteristics at rough cadmium electrodes",* Electrochemica Acta, 46, pp 185-191, 2000

[21] V.S. Muraldharan, *"Warburg impedance, basics revisited",* Anti-Corrosion Methods and Materials, Vol. 44 (1), pp 26-29, 1997

Chapter 5

Results and discussion*

5.1 Introduction

In the medical community, there is a considerable interest in ammonia analyzers, applicable for measuring ammonia levels in exhaled air as a diagnostic tool of certain diseases.[1] Measuring breath ammonia levels can be a fast diagnostic method for patients with disturbed urea balance, e.g. due to kidney disorder[2] or Helicobacter pylori bacterial stomach infection.[3-5] For such applications, often only a few hundred ml of exhaled air is available and, today, no suitable ammonia breath analyzer exists.[6] Furthermore, the analyzer should be extremely selective because the levels of ammonia are very low compared to the concentrations of interfering gasses, like O_2 and CO_2 levels.

Many air ammonia detectors have been reported in literature, based on different principles.[7-13] The most sensitive and selective systems, comprising laser setups, are not suited for miniaturization and integration on a chip and are therefore not applicable for measuring in the small available gas volumes. Direct gas measuring methods suitable for miniaturization have been shown, like tin oxide film[8] or conducting polymer film gas sensors.[9] These methods have been applied for measuring ammonia concentrations[10-12] but most of them show poor selectivity and inadequate detection limits and are therefore not suited.

Other conventional air analyzing systems for measuring ambient gasses make use of gas samplers, like denuders or diffusion scrubbers.[14-16] These

**This chapter is submitted for publication to Lab-on-a-chip, 2004*

systems have the advantage that they can concentrate the ammonia by sampling a volume of gas into a smaller volume of liquid, where ammonium ions are formed. Many accurate ways to measure low ammonium concentrations have been shown.[17]

An indirect ammonia sensing system, accurate enough for breath analysis, has been developed at the Energy research Centre of the Netherlands, ECN, for environmental monitoring.[18] However, the apparatus requires a continuous analyte gas flow of 1 litre per minute for more than ten minutes. To make the existing setup suitable for breath analysis, a reduction of the analyte gas consumption and system response time is desired. This can be accomplished by miniaturization of the key components, also making the device more rugged and less sensitive to disturbances.[19,20]

The apparatus comprises a gas sampler, a separator and a detector.[18,21] After sampling ammonia into an acid sample solution, interfering acid gasses are removed in the selector part where only ammonia is transported into a purified water stream. The resulting ammonium concentration is quantified by an integrated electrolyte conductivity sensor. The system is schematically shown in figure 5.1.

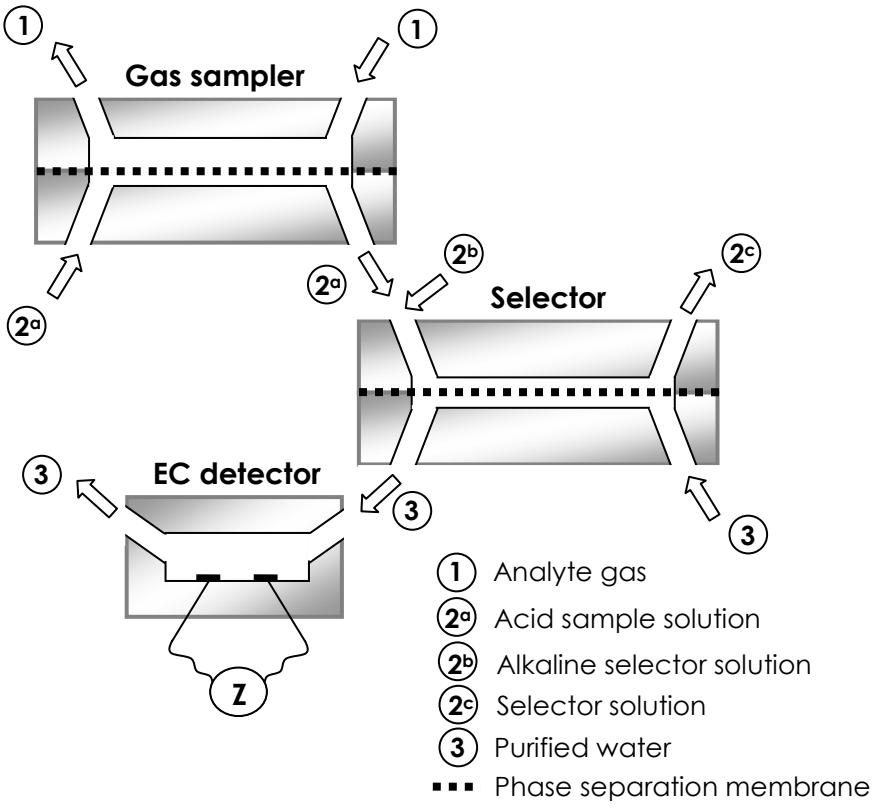

Figure 5.1. *Schematic of the air ammonia analyzer developed at ECN.*[18]

5.2 Theoretical

Normal ambient ammonia concentrations are in the low ppb range; an average of 2 ppb is assumed for the Dutch atmosphere.[18] The lower expected ammonia concentration for breath analysis is about 50 ppb.[2] Normal ambient CO_2 levels are about 300 ppm. Exhaled air can contain up to a hundred fold more, 30000 ppm or 3 $\%_V$.[21] The selectivity of the apparatus should be high enough to detect the lower ammonia detection limit, independent of the CO_2 concentration in the analyte gas.[5]

Ammonia is the main alkaline gas, both in environmental applications and in breath analysis. This is used in the detection principle to selectively measure gaseous ammonia. First, in the gas sampler, gasses are transported from the gas stream, through a micro-porous hydrophobic membrane, into an acid sample solution. In the acid solution, ammonia will react with water and form ammonium ions. This reaction is very fast and at low pH values, the equilibrium will cause almost all ammonia to be converted to ammonium.[22] Weakly acidifying gasses, like carbon dioxide, stay neutral in the acid solution. The overall reaction is given for ammonia and carbon dioxide in equation 5.1:

$$\begin{aligned} &NH_3(g) + H_3O^+(aq) \xrightarrow{pH=3} NH_4^+(aq) + H_2O(l) \\ &CO_2(g) + H_2O(l) \xleftrightarrow{PH=3} CO_2(aq) + H_2O(l) \leftrightarrow H_2CO_3(aq) \end{aligned} \qquad (5.1)$$

Subsequently, the sample solution is pumped into the selector where the pH is increased by adding a strong alkaline solution. The high pH value shifts the equilibrium, neutralizing the ammonium ions back to ammonia and dissociating sampled acid gasses like CO_2, as described by equation 5.2:[22]

$$\begin{aligned} &NH_4^+(aq) + OH^-(aq) \xrightarrow{pH=11} NH_3(aq) + H_2O(l) \leftrightarrow NH_3(g) + H_2O(l) \\ &H_2CO_3(aq) + 2OH^-(aq) \xrightarrow{pH=11} CO_3^{2-}(aq) + 2H_2O(l) \end{aligned} \qquad (5.2)$$

The selector is also formed by two opposite channels separated by a gas-permeable, water-repellent membrane, as illustrated in figure 5.1. The opposite channel contains purified water. The dissolved ammonia turns gaseous at the interface of the phase-separation membrane and passes through the membrane into the purified water where it partly dissolves. The dissolved ammonia reacts with water due to the dissociation equilibrium, as described in equation 5.3.

$$NH_3(g) + H_2O(l) \xleftrightarrow{PH=7} NH_3(aq) + H_2O(l) \leftrightarrow NH_4^+(aq) + OH^-(aq) \qquad (5.3)$$

All remaining ionized acid gasses are flushed out of the system as waste. The formed ammonium ions in the water stream are quantified using an electrolyte conductivity detector.[23]

5.3 Experimental

Miniaturized detection system

The system shown schematically in figure 5.1 has been realized as an integrated miniaturized detection system. The key components, the gas sampler, the selector and the electrolyte conductivity detector have been realized in one chip. The dimensions of the system have been optimized by simulating mass transport characteristics using the finite element program CFD-ACE from CFD Research Corporation. Theoretically the sensor should have a response time of one minute and a gas uptake of nearly 100%.

Both the gas sampler and the selector part comprise two opposite channels, separated by a gas-permeable, water-repellent membrane. A membrane, suitable for integration in a microfluidic gas detection system, is micro-porous polypropylene (PP). Such membranes are both gas-permeable and water-repellent and they can be glued to glass and silicon using epoxy glue. The thickness of commercial micro-porous PP membranes, acquired from Schleider & Schuell (PP 0.22 µm hydrophobic membrane), is about 150 µm. Previous research indicated that channels underneath the membrane should have a depth of more than 15 µm and a width of less than 1 mm to prevent clogging of the channel by buckling of the membrane into the channel.

To enhance the lower detection limit of the measurement system, the volume of sampled gas is much larger than the corresponding purified water volume. This ratio in volumes is called the concentration enhancement ratio. The lower detection limit can be optimized by making the volume of the gas sampler as large as possible with the selector volume as small as possible. Furthermore, a small selector volume reduces the flow-through time of the selector solution and therefore reduces the response time of the system.

Shallow channel structures, of 15 µm, have been etched in glass using wet chemical etching. Borofloat glass wafers are first cleaned in fuming nitric acid. A chromium or silicon mask layer is deposited and structured using standard photolithography and wet chromium or KOH etching. Subsequently, 15 µm deep channels are etched in the glass in a 10 % HF solution. The used photoresist is stripped from the wafer in acetone.

Through-holes and deep channels, like the gas channel with a depth of 100 µm, are made using powderblasting.[24] A photosensitive protective foil, Ordyl BF410, is laminated onto the wafer and structured using photolithography and developed in sodium carbonate. After powderblasting the through-holes with 9 µm aluminium oxide powder the foil is stripped in sodium carbonate and the wafer is ultrasonically cleaned in acetone to remove powder residue and diced.

A miniaturized EC detector, optimized for measuring low ion concentrations in small volumes, has been realized in previous research.[23] A comb-structured, two electrodes, conductivity detector with 95 electrode fingers with a width of 10 µm, a length of 1270 µm and a spacing between the fingers of 30 µm has been realized, resulting in a cell constant of 15 m^{-1}. After cleaning a Pyrex glass wafer, a negative image of the designed electrode structure is created on the wafer in photoresist using standard photolithography. After sputtering a tantalum adhesion layer, a platinum electrode layer is sputtered over the entire wafer. The electrode structure is realized using a lift-off step, by ultrasonically removing the photoresist layer. A glass cover to seal the electrodes is made by etching channels and powderblasting through-holes. The cover is glued over the electrodes using epoxy-glue. Two detectors are integrated in the system, one at the water inlet and one at the water outlet. The inlet detector is used as an indicator for changes other changes in the analyte gas, like temperature changes or pollutions in the purified water source.

The different parts are assembled by gluing the two glass parts together with the membrane in between. Fluid and gas connectors as well as wires are connected to the in- and outlet holes and the bond pads of the electrodes, respectively. A photo of the integrated ammonia measurement system is shown in figure 5.2.

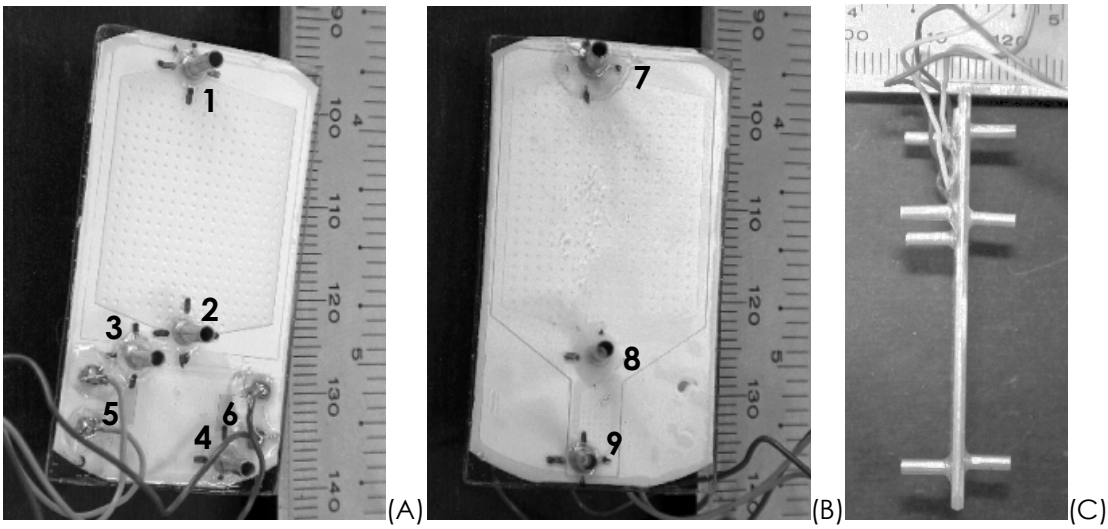

(A) (B) (C)

Figure 5.2. *Photographs of an assembled miniaturized ammonia analyzer, showing (A) a top view, (B) bottom view and (C) side view of the chip with: 1-gas outlet, 2-gas inlet, 3-purified water inlet, 4-water outlet, 5-EC detector at the water inlet, 6-EC detector at the water outlet, 7-sample solution inlet, 8-alkaline selector solution inlet and 9-solution outlet.*

Measurement setup

A 50 ml/min analyte gas flow is applied to the gas sampler. Pure nitrogen, pure CO_2 and a mixture of nitrogen with 10 ppm (±10 %) ammonia were acquired from Hoekloos. Gas flow was controlled using Bronkhorst Hightech mass flow controllers, EL-flow F-110C. The mass flow controllers used for the ammonia and the CO_2 source have a maximum flow of 3 ml/min with a minimum controllable flow of 2 %, which is 60 µl/min. The nitrogen flow is controlled with a 100 ml/min mass-flow controller. The mass-flow controllers should always be open, at least at 2 %, to prevent back flow of the analyte gas, resulting in minimum attainable ammonia and CO_2 concentrations of 12 ppb and 1000 ppm (0.1 $\%_V$) respectively, at a 50 ml/min gas flow.

The three liquid flows, the acid sample solution, alkaline selector solution and purified water flow, are pressure driven using CMA 102 microdialysis syringe pumps connected to a personal computer. Deionised water was purified by an ion exchange column filled with Baker mixed bed ion exchange resin.

The conductance between the electrodes in the detector is measured with home-made interface electronics, connected to the same computer. The measurement frequency of the interface electronics is 1 kHz at a 66 mV_{rms} sinusoidal measurement signal. A measurement and control program is written in Labview to be able to adjust flow settings and perform

measurements, simultaneously. A schematic of the used measurement setup is shown in figure 5.3.

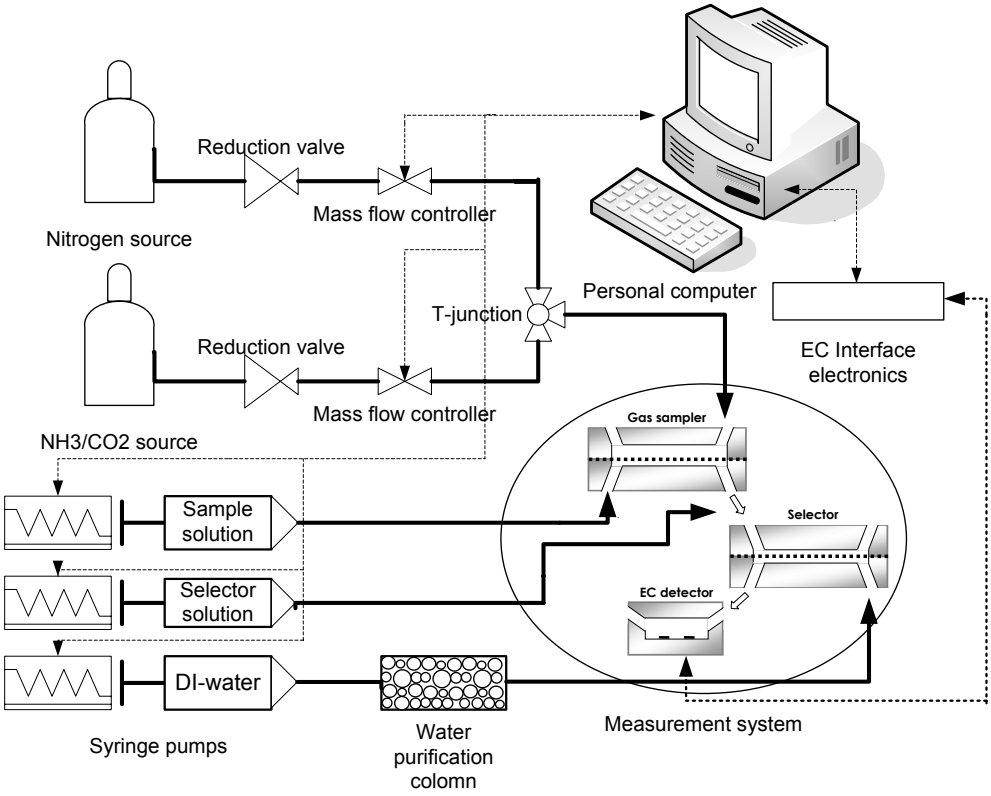

Figure 5.3. *Schematic representation of the used measurement setup.*

Measurement protocol

A 325 µM $NaHSO_4$ sample solution, with a pH of 3.5, is pumped through the gas sampler at 16 µl/min. A 0.1 M KOH solution is added to the selector, with a pH of 13.0, at a flow rate of 4 µl/min. The purified water is pumped into the selector at a flow rate of 2 µl/min. Prior to the experiments, a calibration measurement is performed with the electrolyte conductivity detectors. A solution with a known ammonium hydroxide concentration is flushed through the detector.

5.4 Results and discussion

The calibration result of the detector is shown in figure 5.4A. For the higher concentration range, the used measurement frequency is relatively low. This can be noticed in the inset in figure 5.4A, from the flattening of the curve at concentrations above 100 µM. The lower conductance at these higher electrolyte concentrations causes an increased influence of the double layer capacitance at the electrode-electrolyte interface. The interface electronics does not measure at the optimal frequency anymore. For lower ion concentrations, up to 100 µM, the relation between the concentration and the measured conductance is linear within 2 %.

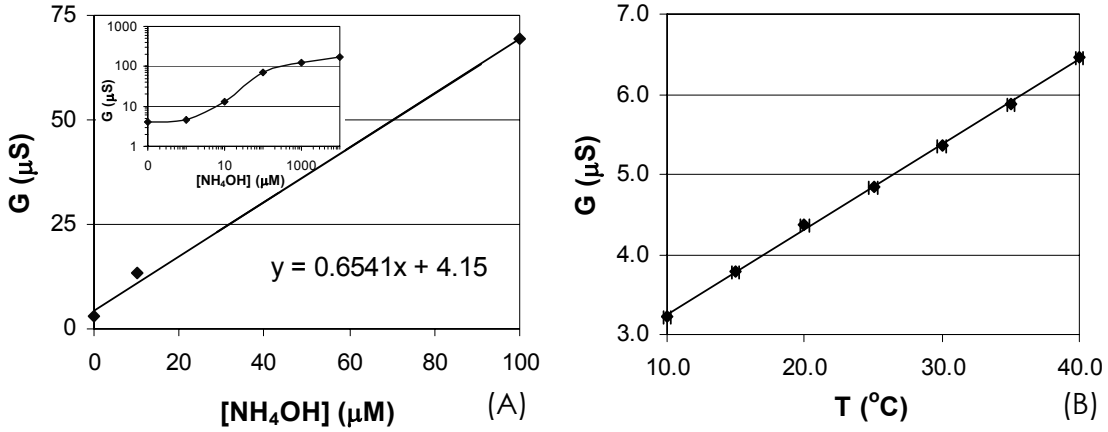

***Figure 5.4**. EC detector calibration with NH_4OH solutions at room temperature(A) and temperature dependence of the purified water conductance between 10 and 40 degrees Celsius (B).*

It should be noted that this calibration is only valid at room temperature, 20˚C, since electrolyte conductivity is also a function of the temperature. The temperature dependence of the conductance measured with purified water is plotted in figure 5.4B, showing a temperature dependence of 2.4 ± 0.3 %/˚C with respect to the conductance at 20˚C.

The first experiment conducted with the measurement system is an ammonia sensitivity test. The system is first flushed with pure nitrogen for an hour. Once the output signal of the detectors becomes stable, after cleaning of the selector channels and detector electrodes with purified water, ammonia is added to the nitrogen carrier gas. The measurement result obtained with an increasing ammonia concentration is shown in figure 5.5.

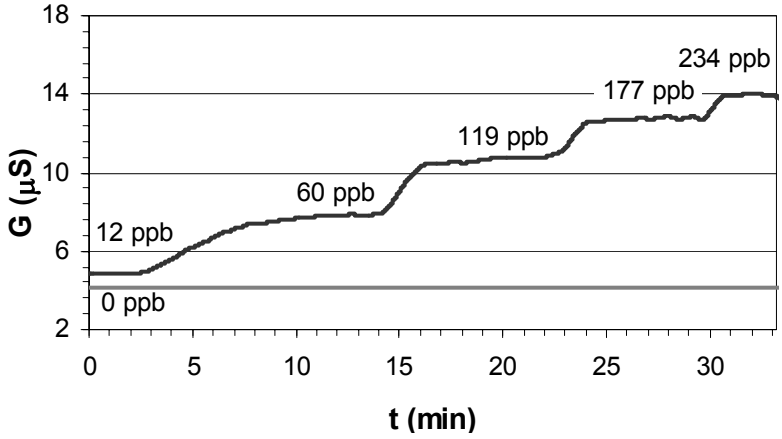

***Figure 5.5.** Ammonia sensitivity experiment showing the measured conductance of the two detectors, at the water inlet (—) and the water outlet (—), as a function of the ammonia concentration in the analyte gas.*

The sensor responds to an increase in ammonia concentration. The response time of the device seems to be a function of the ammonia concentration. This is an artefact caused by the analyte gas preparation setup shown in figure 5.3. Teflon® tubing is used as interconnect to transport the gasses from the mass-flow controllers to a T-junction that is connected with the gas inlet of the measurement system. When making very low ammonia concentrations, the flow from the source is so slow that it takes more than a minute before the desired gas composition actually reaches the sensor. Diffusion inside the tubing causes dispersion of the step in concentration. The response time, the time needed for the signal to reach 90% of the end value, is thus several minutes. When the flow from the ammonia source is higher, the response time of the measurement system itself becomes the dominant factor, resulting in a response time of about 1.6 minutes.

In order to determine the detection limit of the system, the ammonium concentration corresponding to the measured conductance values is plotted in figure 5.6 as a function of the applied ammonia concentration. The ammonium concentration is determined in two ways. First, the calibration measurement is used, of which the result is shown in figure 5.4A. Secondly, the concentration is calculated, assuming that all ammonia will be transported into the purified water where it will react with water according to the equilibrium reaction shown in equation 5.3. The error bars indicate three times the standard deviation of the conductance over one minute, taken from figure 5.5.

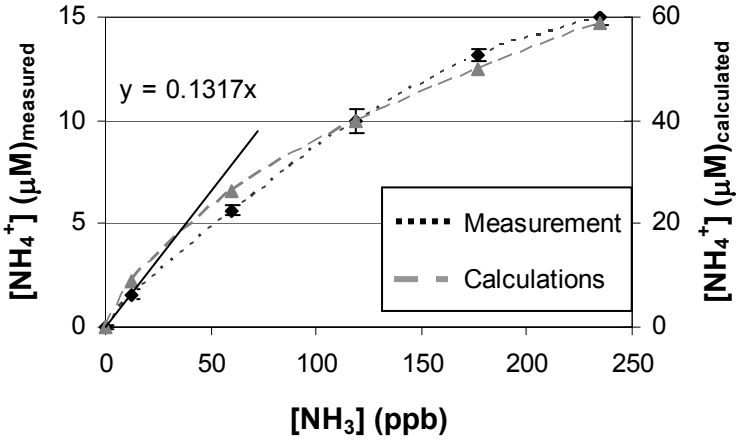

Figure 5.6. *Conductance as a function of the applied ammonia concentration with a linear fit through the lowest concentrations.*

With the linear fit through the lowest concentrations and the three-times-standard deviation value of the response to 12 ppb, which is calculated to be 0.14, the theoretical detection limit is calculated to be 1.1 ppb. This lower detection limit can be lowered by reducing the deviation in output signal, which seems to be caused mainly by flow variations inside the system. Especially gas flow variations largely influence the conductance signal.

Further, it is shown that the measured ammonium concentration, the left axis in figure 5.6, is a factor of four lower that the theoretically expected concentration, the right axis in figure 5.6. This can be explained by the fact that not all ammonia from the analyte gas is transported to the purified water stream. In order to investigate what causes the non-optimal functionality, both the selector and the gas sampler parameters have been adjusted. To test the selector part, the flow velocity of the purified water stream is varied. A 50 ml/min analyte gas flow with an ammonia concentration of 90 ppb is applied. The result is shown in figure 5.7. The efficiency of the measurement system is plotted as a function of the water flow velocity. The efficiency is determined by calculating the ammonium concentration with the calibration result shown in figure 5.4 and with the equilibrium of the reaction of ammonia with water in the purified water, shown in equation 5.3. It should be noted that the concentration factor, the analyte gas to purified water volume ratio, changes when the gas or the purified water flow velocity is changed.

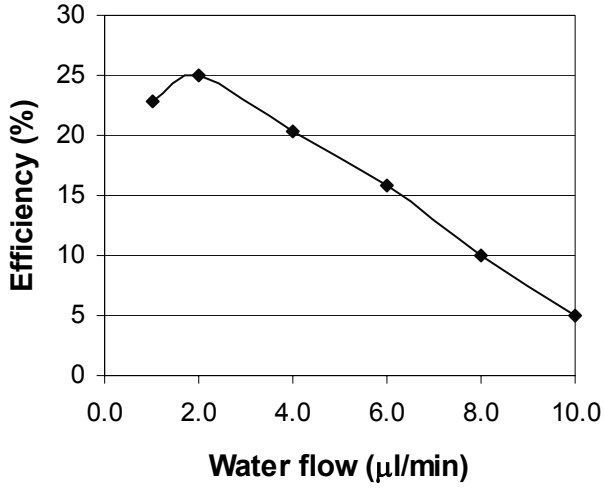

Figure 5.7. *Ammonium concentration in the detector as a function of the water flow.*

In figure 5.7, it is shown that the efficiency of the selector is optimal at a purified water stream of 2 µl/min. Both a higher and a lower water flow results in a reduced system efficiency. Thus, the 2 µl/min used in the experiment that resulted in figure 5.5 does not limit the efficiency of the selector. It should be noted that a reduction in water flow makes the system slower and therefore more sensitive to disturbances like temperature changes. This might cause the unexpected reduction in efficiency at the lower water flow rate. When the water flow velocity is increased, the efficiency is reduced significantly. The time available for the ammonium ions that form in the water stream to be transported away from the membrane interface becomes too short and therefore the uptake of ammonia is limited.

These results indicate that the non-optimal efficiency shown in figure 5.6, where the water flow was 2 µl/min and the efficiency 25 %, is caused by the gas sampler. To investigate whether this hypothesis is valid, the analyte gas flow, with a constant quantity of ammonia, is varied. The ammonium concentration is determined by measuring the conductance, using the calibration result, and by calculation using the equilibrium of the reaction of ammonia with water in the purified water, shown in equation 5.3. From the difference in the two ammonium concentrations, the efficiency of the gas sampler is calculated as a function of the gas flow, shown in figure 5.8.

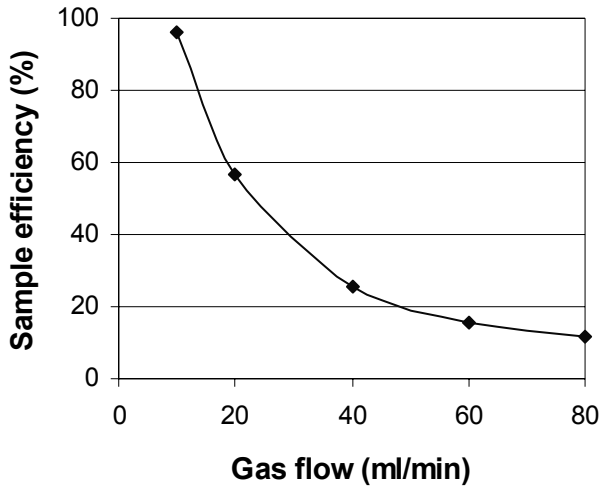

***Figure 5.8**. Efficiency of the gas sampler as a function of the analyte gas flow.*

The efficiency of the measurement system significantly decreases when the gas flow is increased. The uptake of ammonia into the sample solution is far from optimal when the residence time of the analyte gas is too short.

Although simulation results indicate a nearly optimal gas uptake for a gas flow up to 300 ml/min, the result shown in figure 5.8 proof otherwise. There are two possible explanations for this. First, the wide shape of the gas sampler might cause most of the gas to go straight through the middle of the channel. This would cause much of the analyte gas to have a lower residence time, reducing the ammonia uptake.

A second explanation can be found in less than optimal mass transport. The reaction of ammonia with water is fast. However, when ammonia will absorb in the membrane and stick to the walls of the pores, the ammonia transport towards the sample solution interface is reduced. Also, diffusion of ammonia from the analyte gas to the membrane is slower since ammonia in the membrane is not directly removed by the reaction with the sample solution, lowering the concentration gradient.

Although the efficiency is not as optimal as desired, the system is fast and accurate enough as a diagnostic tool for breath analysis. For such a system, however, it is very important that it selectively responds to ammonia. In exhaled breath, carbon dioxide levels are much higher than in normal air, as discussed in the introduction. To investigate the selectivity of the measurement system, the conductance response to a 50 ml/min analyte gas of nitrogen containing known partial pressures of CO_2 concentrations is determined. The result is shown in figure 5.9.

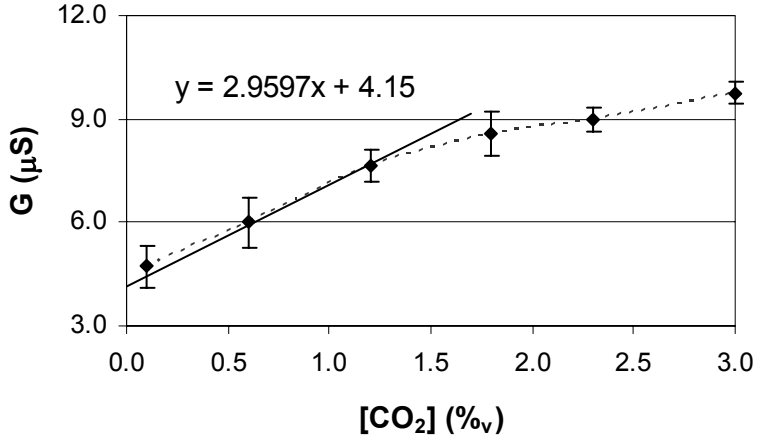

Figure 5.9. *Conductance measurement result with CO_2 with a linear fit to the lower concentrations.*

Concluding from these results, the measurement system does respond to increasing partial CO_2 pressures in the analyte gas. The maximum tested CO_2 concentration, 3 %v, corresponds to the higher level that can be found

in exhaled breath. The resulting conductance value can be compared with the ammonia measurement result shown in figure 5.4 and corresponds to an ammonia concentration of about 90 ppb. This means the selectivity of the system towards 3 $\%_V$ of CO_2 and ammonia is about 330000. It was our goal to reach a selectivity of 600000, so that the conductance response to the CO_2 level in exhaled breath would be comparable with the desired ammonia detection limit of 50 ppb. Although this selectively is not reached completely, exhaled CO_2 levels are relatively stable.[25] Therefore it still seems possible to detect 50 ppb of ammonia.

With the linear fit to the lower carbon dioxide concentration responses, an estimation of the system response to normal atmospheric CO_2 concentrations can be made. A concentration of 300 ppm or 0.03 $\%_V$ corresponds to a conductance of 4.24 µS. This equals the response of the system to an ammonia concentration of 1.0 ppb, according to the results shown in figure 5.4 and 5.6. This means that the system can be used for environmental monitoring in areas where the ammonia concentration is in the low-ppb range.

5.5 Conclusions

A miniaturized measurement system for low gaseous ammonia concentrations has been realized on a chip. The system comprises three key components; a gas sampler that converts gaseous ammonia to dissolved ammonium ions, a selector that removes interfering gasses like CO_2 and a detector that quantifies the electrolyte concentration that is directly proportional to the ammonia concentration in the analyte gas. A phase separation membrane is integrated by gluing polypropylene membranes between two glass chips comprising micromachined channels.

Although the gas sampler proved to perform less than optimal in sampling ammonia from the analyte gas, the detection limit of the system is calculated to be 1.1 ppb. The response time of the measurement system is determined to be 1.6 minutes. In environments with normal acidifying gas concentrations the selectivity of the system is sufficient to measure ammonia concentrations in the low-ppb range. The system is even sufficiently selective to ammonia to be used in environments that contain elevated carbon dioxide levels, like exhaled air. The lower ammonia concentration expected in diagnostic breath analysis applications, 50 ppb, is detectable.

The system comprises two electrolyte conductivity detectors, one to determine the conductance of the water that is pumped into the system and one to quantify the ammonium concentration as a result of the ammonia uptake. This first detector can be used as an indicator for sudden changes in input boundary conditions like pollution in the water flow or changes in temperature. It is shown that the temperature dependency of the water conductance is nearly linear at temperatures in the range from 10 to 40 degrees Celsius.

The system can be further optimized by increasing the efficiency of the gas sampler. Structures in the gas channel that help guiding the gas flow could be helpful. Another possible solution would be to use a longer and smaller channel. This would reduce the difference in residence time of gas flowing through the middle and along the sides of the channel.

5.6 References

[1] W. Ament, J.R. Huizenga, E. Kort, T.W. van der Mark, R.G. Grevink, G.J. Verkerke, *"Respiratory ammonia output and blood ammonia concentration during incremental exercise",* International Journal of Sports Medicine 20, pp 71-77, 1999

[2] L.R. Narasimhan, W. Goodman, C. Kumar, N. Patel, *"Correlation of breath ammonia with blood urea nitrogen and creatinine during hemodialysis",* PNAS 98 (8), pp 4617-4621, 2001

[3] B. Marshall, J.R. Warren, *"Unidentified curved bacillus and gastric Epithaeium in active chonic gastritis",* Lancet 1, pp. 1273-1275, 1993

[4] J. C.E. Underwood, *"General and Systematic Pathology",* Churchill Livingstone Inc, 2nd edition, pp 414-415, 1996

[5] D.J. Kearney, T. Hubbard, D. Putnam, *"Breath ammonia measurement in Helicobacter pylori infection",* Digestive diseases and sciences 47 (11), pp 2523-2530, 2002

[6] E. Verpoorte, *"Microfluidic chips for clinical and forensic analysis",* Electrophoresis 23, pp 677-712, 2002

[7] S.G. Buckly, C.J. Damm, W.M. Vitovec, L.A. Sgro, R.F. Sawyer, C.P. Koshland, D. Lucas, *"Ammonia detection and monitoring with photofragmentation fluorescence",* Applied optics 37 (36), pp. 8382-8391, 1998

[8] R.K. Sharma, P.C.H. Chan, Z. Tang, G. Yan, I-M. Hsing, J.K.O. Sin, *"Investigation of stability and reliability of tin oxide thin-film for integrated micro-machined gas sensor devices",* Sensors and Actuators B 81, pp 9-16, 2001

[9] F. Zee, J.W. Judy, *"Micromachined polymer-based chemical gas sensor array",* Sensors and Actuators B 72, pp 120-128, 2001

[10] M. Aslam, V.A. Chaudhary, I.S. Mulla, S.R. Sainkar, A.B. Mandale, A.A. Belhekar, K. Vijayamohanan, *"A highly selective ammonia gas sensor using surface-ruthenated zinc oxide",* Sensors and Actuators A 75, pp 162-167, 1999

[11] I. Laehdesmaeki, A. Lewenstam, A Ivaska, *"A polypyrrole-based amperometric ammonia sensor",* Talanta 43, pp 125-134, 1996

[12] V.V. Chabukswar, S. Pethkar, A.A. Athawale, *"Acrylic acid doped polyaniline as an ammonia sensor",* Sensors and Actuators B 77, pp 657-663, 2001

[13] J. Maier, *"Electrochemical sensor principles for redox-active and acid-base-active gases",* Sensors and Actuators B 65, pp 199-203, 2000

[14] P.K. Simon, P.K. Dasgupta, Z. Vecera, *"Wet effluent denuder coupled liquid/ion chromatography systems",* Analytical Chemistry 63, pp 1237-1242, 1991

[15] P.F. Lindgren, P.K. Dasgupta, *"Measurement of atmospheric sulfur dioxide by diffusion scrubber coupled ion chromatography",* Analytical Chemistry 61, pp 19-24, 1989

[16] C.B. Boring, R. Al-Horr, Z. Genfa, P.K. Dasgupta, *"Field measurement of acid gases and soluble anions in atmospheric particulate matter using a parallel plate wet denuder and an alternating filter based automatic analysis system",* Analytical Chemistry 74, pp. 1256-1268, 2002

[17] G. Schultze, C.Y. Liu, M. Brodowski, O. Elsholz, *"Different approaches to the determination of ammonium ions at low levels by flow injection analysis",* Analytica Chimica Acta 214, pp 121-136, 1988

[18] J.W. Erisman, R. Otjes, A. Hensen, P. Jongejan, P. v.d. Bulk, A. Khlystov, H. Möls and S. Slanina, *"Instrument development and application in studies and monitoring of ambient ammonia",* Atmospheric Environment 35, pp 1913-1922, 2001

[19] A. van den Berg, T.S.J. Lammerink, *"Micro Total Analysis Systems: Microfluidic Aspects, Integration Concept and Applications",* Topics in Current Chemistry 194, pp. 21-50, 1997

[20] A. Manz, N. Graber, H.M. Widmer, *"Miniaturized total chemical analysis systems – a novel concept for chemical sensing",* Sensors and Actuators B 1, pp 244-248, 1990

[21] R.M. Berne, M.N. Levy, *"Physiology",* Mosby, 4th edition, 1998

[22] B.H. Timmer, K.M. van Delft, R.P. Otjes, W. Olthuis, A. v.d. Berg, *"A miniaturized measurement system for ammonia in air",* Analytica Chimica Acta 507 (1), pp. 139-145, 2004

[23] B.H. Timmer, W. Sparreboom, W. Olthuis, P. Bergveld and A. v.d. Berg, *"Optimization of an electrolyte conductivity detector for measuring low ion concentrations",* Lab on chip 2 (2), pp. 121-124, 2002

[24] S. Schlautmann, H. Wensink, R.B.M. Schasfoort, M. Elwenspoek, A. v.d. Berg, *"Powder Blasting Technology as an Alternative Tool for Microfabrication of Capillary Electrophoresis Chips with Integrated Conductivity Electrodes",* Journal of Micromechanics and Microengineering 11(4), pp 386-389, 2001

Chapter 6

Solid-state phase separation membrane*,#

6.1 Introduction

This chapter comprises two parts. First, a description is given of an alternative for the micro-porous polypropylene membrane; a silicon nitride membrane realized using micro system technology. Secondly, the anodic bonding process of these silicon nitride layers to glass is investigated.

6.2 Membrane preparation

In this section, a silicon nitride membrane is dealt with. After an introduction, simulation results show that reduction of the membrane thickness is beneficial for reducing gas transport times. In the experimental section it is described how thin membranes can be realized using silicon and siliconnitride micromachining, followed by the results and discussion section and finalized with conclusions.

6.2.1 Introduction

The ammonia measurement system described in chapter 3 of this thesis[1] comprises a gas sampler, a selector and an electrolyte conductivity sensor. Both the gas sampler and the selector make use of a hydrophobic micro-porous membrane. This membrane is used as a phase-separating interface layer. The used membranes must be both gas-permeable and water-repellent so the pores stay filled with gas and no ions can pass through. Suited materials are micro-porous Teflon® (PTFE) or polypropylene (PP) membranes, as shown in appendix B.

**Section 6.2 is presented on a poster at the μTAS conference, 2001*
#Section 6.3 is presented on a poster at the MME conference, 2002

For a fast response time, the thickness of the conventional membrane becomes a limiting factor when using very shallow channels. Micro-porous membranes can not be made very thin because this would cause loss of structural integrity. An alternative, microfabricated membrane that is very thin, water-repellent and gas-permeable is presented in this chapter. A silicon nitride, Si_3N_4, membrane with a thickness of 1 µm is made porous using micro system technology and is rendered hydrophobic with a Fluorocarbon coating.[2,3]

6.2.2 Theoretical

The response time of the ammonia analyzer can be improved significantly by reducing the dimensions of the apparatus. For instance, the required residence time of the analyte gas is determined by the speed at which ammonia is transported from the gas channel, through the membrane, into the sample solution where it will react with the acid to form ammonium ions. According to Fick's second law of diffusion, a reduction in channel depth by a factor of x, results in a decrease of required transport time by a factor of x^2. However, there are two other parameters that significantly influence mass transport. First, the analyte gas and the sample solution are pumped through the system by pressure driven pumping, resulting in a parabolic flow profile. The flow velocity in the centre of the channel is higher than at the edges, influencing the ammonia distribution inside the channel. Secondly, there is a difference in gas diffusivity between gas inside the membrane and in the channel. Hydrophobic micro-porous membranes, made of materials like Teflon® (PTFE) or polypropylene (PP), do not react with ammonia but they cause a decrease in effective diffusion rate because the flux through the membrane is a function of the porosity of the membrane.[4]

The influence of the membrane thickness on the mass transport, when taking convective mass transport and the membrane porosity into account, is simulated in a CFD simulation software package, CFD-RC. A 2D model is made of a cross-section of a miniaturized channel with a depth of 100 µm. First, a conventional polypropylene membrane is used, with a thickness of 150 µm and a pore size of 0.2 µm. An inflow of air containing 10 ppm ammonia is applied to the channel with an average flow of 1 m/s. The membrane has a porosity of 70 % and does not react with any of the available gases. Underneath the membrane is an acid sample solution where the ammonia will be converted to ammonium ions. This is a fast reaction and therefore this is modelled as an ammonia sink boundary-layer

in the simulations. Figure 6.1 shows the ammonia profile at equilibrium found in the described simulation.

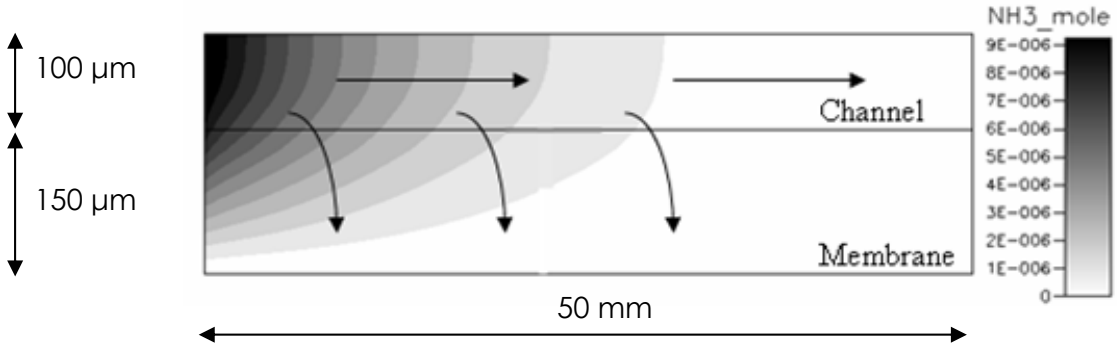

Figure 6.1. *Ammonia distribution simulation result for the "thick" PP membrane.*

The data points from the images are further analyzed to calculate the amount of ammonia in a slice of the channel, such as shown in figure 6.1, as a function of the distance from the inlet. It is found that it would take a channel length of 4.6 mm before 90 % of the ammonia is removed from the channel, in this particular case.

The required channel length can be shortened significantly by reducing the diffusion time required for transport of ammonia through the membrane. This is simulated again in CFD-RC by reducing the thickness of the membrane. The length of the channel that is required to remove 90 % of the ammonia from the channel at an average flow velocity of 0.5, 1.0 and 2.0 m/s is plotted against the membrane thickness in figure 6.2.

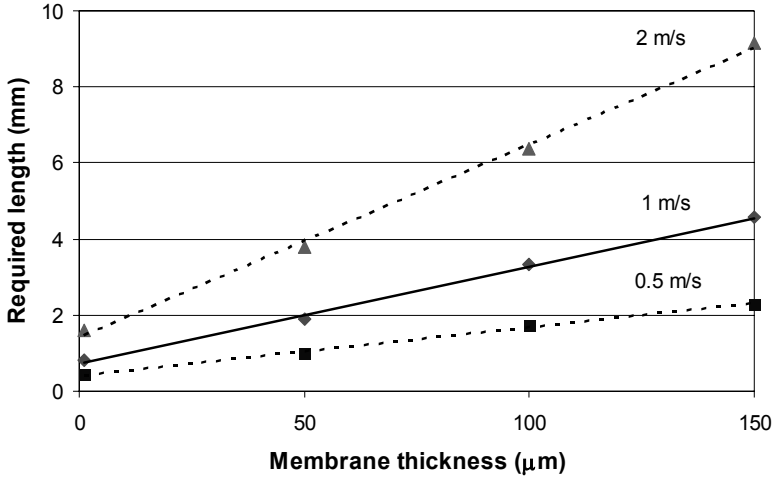

Figure 6.2. *Channel length required to remove 90% of the ammonia from the analyte gas as a function of the average flow velocity and the thickness of the membrane between the gas channel and the ammonia sink layer.*

It is found that the required channel length is a linear function of the membrane thickness. For an average flow of 1 m/s, a reduction of the membrane thickness from 150 µm to 1 µm would reduce the required channel length from 4.6 mm to 0.5 mm. Furthermore, the required length appears to be linearly dependent on the average flow velocity, for the used flow range. This can be used for optimizing the channel geometry for different flow velocity values.

In order to prevent water, and thus ions, to pass through the membrane, a hydrophobic membrane material should be used. A very suitable material for making membranes in silicon micromachining is silicon nitride, Si_3N_4, because it is very strong and silicon technology compatible. However, the water contact angle of LPCVD grown silicon nitride, the proposed membrane material, is measured to be 41˚. This means that the material is hydrophilic, as discussed in detail in appendix B. A solution to render this material hydrophobic is to apply a coating to the membrane.[2,3] One method is coating with 3M FC 722 fluorocarbon coating. The water contact angle of a silicon nitride layer with a thin spin-coated FC layer was measured to be about 115˚, dependent on the surface roughness.

The bubble point pressure can be measured to determine the maximum allowable pressure difference over the membrane.[5] The determined bubble point pressure should always be higher than the pressure difference over the membrane during operation, so that no water is pressed through the pores in the membrane, as described in appendix B.

6.2.3 Experimental

A 1-µm thick alternative for the micro-porous membranes is developed using micro system technology. First, a silicon substrate wafer is cleaned and a 1-µm thick layer of LPCVD Si_3N_4 layer is grown on both sides of the wafer. Standard photolithography is used to define pores in the nitride layer. The nitride layer is etched in an Elektrotech PF 340 etcher using anisotropic dry RIE etching with a CHF_3/O_2 plasma at 10 mTorr (1.33 Pa) and 75 W power. Subsequently, a channel is created underneath the membrane by etching the silicon underneath the nitride layer, using an isotropic SF_6 plasma etch process at 150 mTorr (20 Pa) and a power of 100 W. The etch rate of silicon in this plasma is sufficiently larger than the Si_3N_4 etch rate, enabling the nitride layer to act as the masking material for the silicon etch, so no new photolithography and aligning step is required and the channel is auto-

aligned to the membrane. A cover wafer is made in Pyrex glass and is structured using powderblasting.[6]

Through the isotropic nature of the silicon etch process, under-etch will cause the holes underneath the pores in the nitride layer to interconnect, resulting in a buried channel underneath the nitride membrane. A schematic representation of the proposed technique is shown in figure 6.3.

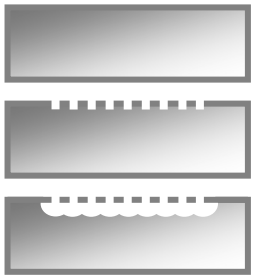

- A silicon substrate wafer is cleaned and a 1-µm LPCVD Si_3N_4 layer is grown.
- Pores are made using photolithography and dry etching in CHF_3/O_2 plasma.
- Silicon is etched underneath the membrane in SF_6/N_2 plasma

Figure 6.3. *Schematic representation of the membrane-channel process scheme.*

A 1:1 mixture of 3M FC722 coating and FC40 coating solvent is applied to the membrane by dip-coating in order to render the membrane hydrophobic. The coating layer is cured for 15 minutes at 100 ˚C. A contact angle measurement is performed on the silicon nitride membrane before and after the coating is applied, as well as a water bubble point pressure measurement and a gas pas-though measurement. Multiple layers of coating have been applied to determine whether a thickening of the coating layer and probably a denser covering increases the resulting hydrophobicity.

6.2.4 Results and Discussion

Membranes have been fabricated using the method described in the previous section. Square, 5 µm wide pores with a 5 µm distance and 2 µm wide pores with a 2 µm distance between the pores are made. Figure 6.4 shows the result of the photolithography process. Special test structures are added to the mask layout to test different dimensions and to determine the development of the under-etch profile. Figure 6.5 shows a picture of a part of such a test structure with an under-etch of 5 µm through 15 µm or 10 µm wide pores. Smaller pores result in less underetch.

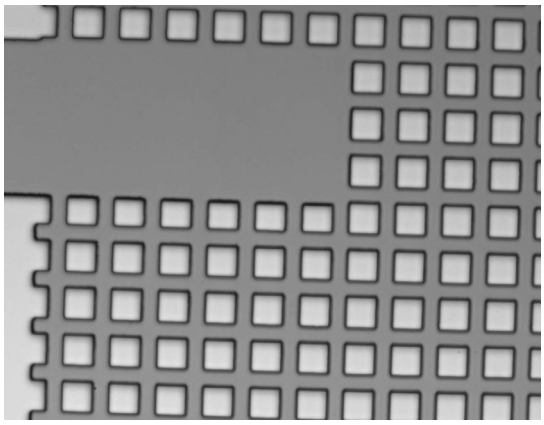

Figure 6.4. *Developed photoresist with square 5µm pores.*

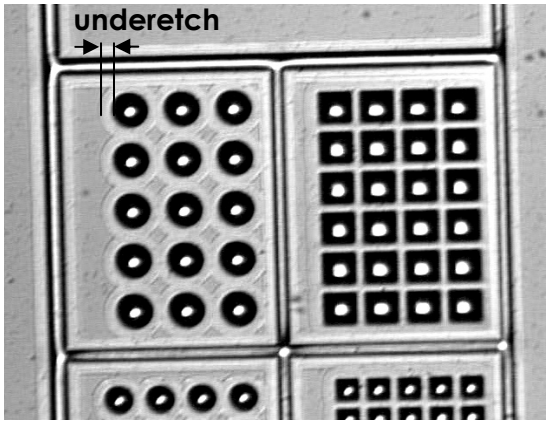

Figure 6.5. *Test structure with 15 µm and 10 µm wide holes showing 5 µm silicon under-etch.*

In order to etch the pores in the nitride layer, a plasma mixture of CFH_3 and O_2 took 15 minutes to etch through the 1-µm thick layer. An underetch of 10 µm, required to completely combine all holes to channels, was realized using a SF_6 plasma during 20 minutes of etching. Figure 6.6 shows a SEM image of the resulting membrane. Figure 6.7 shows a microscope image of a cross-section of the membrane and channel.

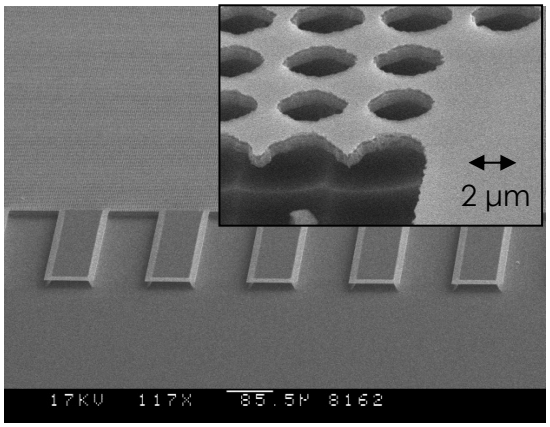

Figure 6.6. *Resulting Si_3N_4 membrane with inset of square 2 µm pores.*

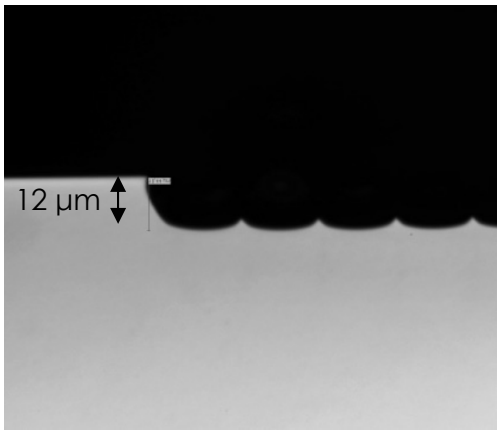

Figure 6.7. *Cross-section of the membrane showing the underetch profile.*

Contact angle measurements have been performed to determine the hydrophobicity of the membrane before and after applying the coating, as shown in figure 6.8. The images indicate a change in contact angle from 56±5° to 109 ±3°.

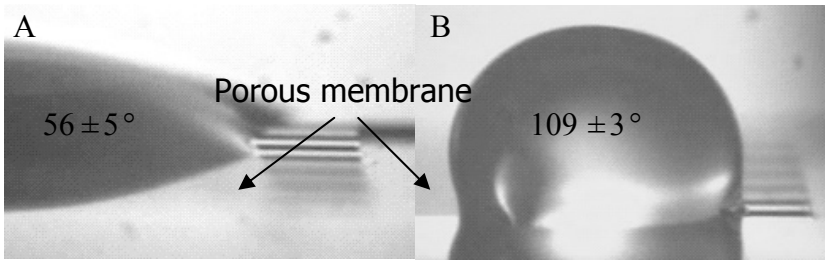

Figure 6.8. *Contact angle before (A) and after (B) applying hydrophobic coating.*

After rendering a small test piece of the membrane hydrophobic, the membrane characteristics are determined using the bubble point method. The bubble point pressure increases with subsequent application of hydrophobic coating layers, while gas can still easily pass through the membrane, as shown in figure 6.9. Two possible effects responsible for this increase are a decrease in effective pore-size and a higher membrane wetting pressure caused by an increased hydrophobicity.

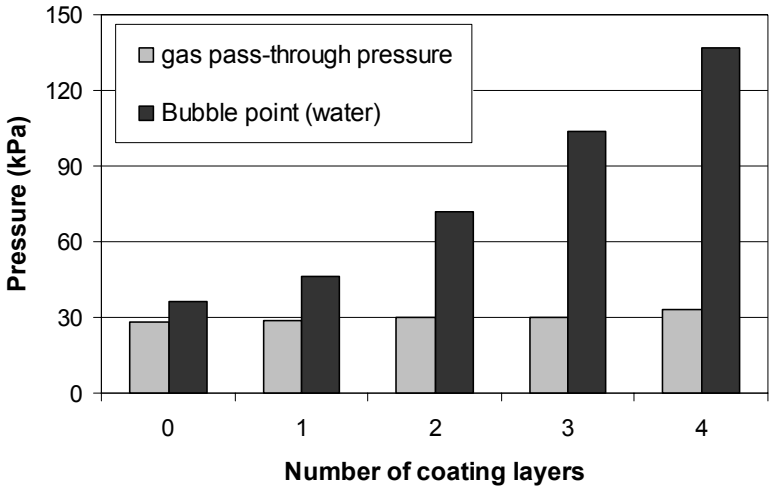

Figure 6.9. *Bubble point measurement and gas pass-through measurements after applying subsequent coating layers to the Si_3N_4 membrane.*

It should be noted that these results have been obtained with a small piece of membrane, typically 250 µm by 250 µm. It turned out to be very difficult to make a large membrane, of the order of several tens of mm^2, without defects that could be rendered hydrophobic by applying a FC coating. We never managed to do so.

6.2.5 Conclusions

A micromachined channel covered with a porous Si_3N_4 membrane is realized as an alternative for a miniaturized gas sampler. The membrane has a thickness of 1 µm, which will significantly reduce the time required for the analyte gas to diffuse through the membrane, compared to commercial available membranes that are hydrophobic and porous, like 150 µm thick PP membranes. Although a reduction in required gas diffusion time can be expected according to the simulation results shown in figure 6.1, it should be noted that this gas diffusion time is by far the smallest time constant of the total ammonia measurement system. A reduction in membrane thickness will not significantly shorten the system response time.

Contact angle, gas pass-through pressure and bubble point pressure measurements show that it is possible to render the micromachined porous membrane gas-permeable and water-repellent. This makes the membrane in principle suited for the described ammonia detection system. Technologically, the presented method proved too demanding to be useful for our applications.

6.3 Anodic bonding of a Si_3N_4 membrane to glass

In the first section of this chapter it is described how to create a membrane with micromachining. To fix this membrane between two channels, a cover with the second channel has to be bonded on top of the nitride layer. This can be accomplished using a structured glass cover that is fixated on the membrane using anodic bonding. The optimal parameters for the bonding process, bond temperature and voltage, depend on the thickness of the membrane layer.[7] It is shown in this section that it is possible to bond a glass wafer on a 1-µm "thick" silicon nitride membrane layer.

6.3.1 Introduction

In integrated miniaturized chemical systems, micro channels are used to transport liquids and gasses. Channels can be created, for example, using micromachining, by structuring glass or silicon wafers that are bonded together. A very strong bond method is anodic bonding, which is widely used for bonding glass to silicon.

Many micromachined system components, like valves, pumps or microphones, make use of membranes. A very suitable material for making membranes in silicon micromachining is silicon nitride, Si_3N_4, because it is

very strong and silicon technology compatible. When the membrane material is silicon nitride, Si_3N_4,[8,9] a glass wafer has to be bonded to a silicon nitride layer on a silicon substrate. This process, however, is not as trivial as bonding of glass to silicon, especially when the nitride layer gets rather thick like the membrane proposed in the previous section of this chapter. In literature, no data is found about anodic bonding of nitride layers thicker than 180 nm.[4,7] A method is required to qualify the bond that results from the anodic bonding process in order to optimize the bonding parameters for bonding glass to a "thick" 1-µm silicon nitride layer.

6.3.2 Theoretical

In the anodic bonding process, the two chips that should be bonded together are placed in the right position. The chips are heated to a temperature between 250 and 450˚C. At this elevated temperature sodium oxide in the glass is dissociated and the glass behaves as an electrolyte. Once the chips are heated, an electric potential is applied over the stack. The two wafers are attracted by the applied electric field.[10-13] Due to the high electrostatic pressure, induced by the applied electrical field during bonding, small cavities are pulled closed.[9,14,15] The process is illustrated for glass on silicon in figure 6.10.

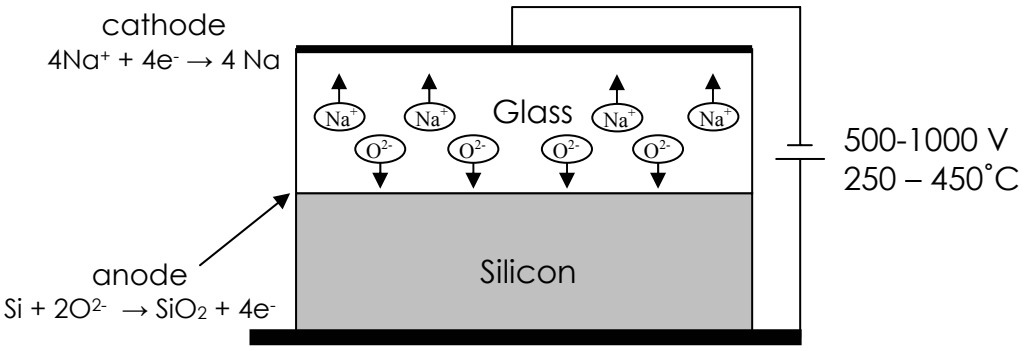

Figure 6.10. *Anodic bonding of silicon to glass*

Due to the electric field, the mobile sodium ions are attracted towards the cathode. The glass at the cathode becomes accumulated by these ions, whereas the oxygen ions migrate from this depletion region towards the bonding interface. Here oxygen reacts with the silicon surface to form the final strong bond.[7,10-12]

With a standard anodic bonding setting of 800 Volt at an elevated temperature of 400˚C, only a very weak bond was formed between the nitride layer and the glass. To optimize the parameters in order to obtain a

strong bond, a test method is required to investigate the bond strength. A non-destructive integrated bond test method is used to determine the strength of the bond between the two substrates.

Methods to determine the strength of the bond are the gap closure method[12,13,16] or the crack propagation analysis method.[17,18] In the latter, a blade with a thickness h (m) is inserted into the edge of the bonded wafer pair. Because the two wafers are separated locally a crack will propagate into the interface. The length of this crack r (m) is a measure for the strength of the bond. This method can be adjusted to make it a non-destructive test method suited for anodic bonding parameter optimization, similar to the gap closure method. A non-bondable metal elevation is created that functions as a pre-inserted "blade". The elevation is made using micro-system technology techniques, like patterning of thin metal layers using the lift-off technique. The proposed test method is illustrated in figure 6.11, where the non-bonded distance, r (m), is an indication of the bond strength.

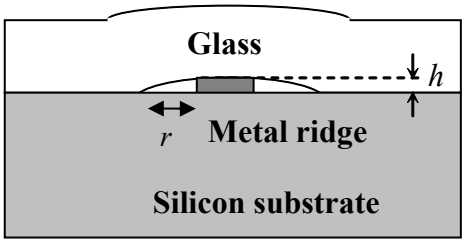

Figure 6.11. *Non-destructive integrated fracture surface energy measurement.*

6.3.3 Experimental

Prior to the bonding process, the surface of the nitride layer is wet oxidized at 1100˚C for 30 minutes to enhance bonding.[4,9,19] A platinum layer of 150 nm, with an underlying titanium adhesion layer of 30 nm, is sputtered onto the substrate, as the metal ridge layer. This layer is patterned using lift-off to form a non-bondable metal strip on the silicon nitride membrane layer. Subsequently, the silicon test wafer and an unstructured Pyrex glass wafer are diced to 1 by 1 cm square chips. Subsequently, the chips are cleaned for ten minutes in fuming nitric acid. After rinsing in deionised water and dry spinning, the chips are rinsed in acetone and dried again by spin drying. The glass part is put on top of the silicon nitride part and placed on a hot plate for a few minutes. Before bonding to the nitride layers, a bond is made between the glass chip and a bare silicon substrate wafer at 800 V and 400˚C as a reference. Thereafter, bonding is performed between glass

and silicon nitride at temperatures of 300, 350 and 400˚C. The applied voltage is varied between 900 and 1500 Volt with incremental steps of 200 Volt.

Through the glass top wafer, the distance between the bonded area and the elevated metal strip can be measured under a microscope, as illustrated in figure 6.12. This distance will decrease with increasing bond strength, as is described in the theoretical section.

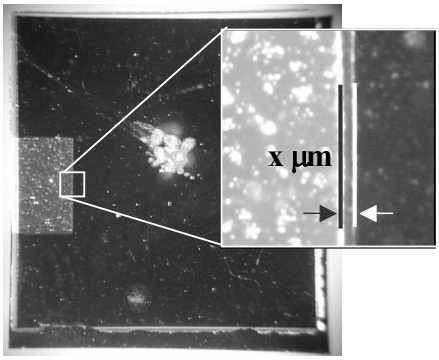

Figure 6.12. *Photograph of a test chip comprising a bonded glass chip and a silicon chip with a non-bonded metal elevation. The bondgap is measured under a microscope. The close-up shows the bond gap.*

6.3.4 Results and discussion

Standard anodic bonding settings, 400˚C and 800V, did not result in a strong bond between the glass and silicon nitride layer. With the test devices described in the experimental section, the influence of the temperature and the applied voltage is investigated. The result is shown in figure 6.13.

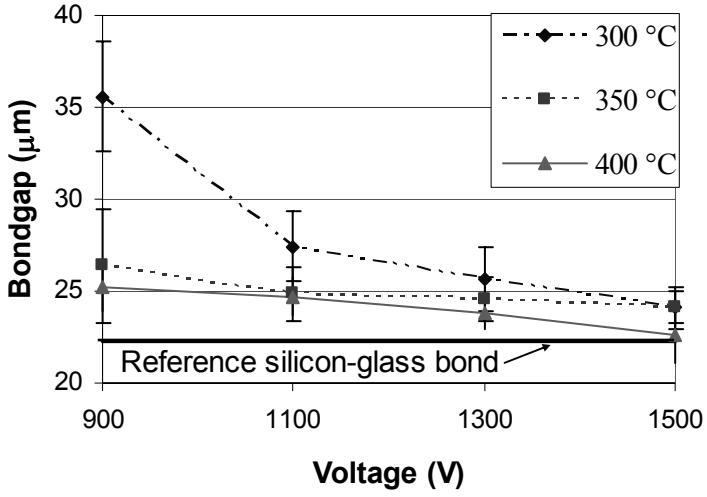

Figure 6.13. *Measured bond gap as a function of the bond temperature and the applied voltage*

It is found that bonding can be enhanced by increasing both the temperature and the applied voltage. The bond obtained at 1500 V and 400˚C proved to be close to the bond strength of bare silicon to glass, strong enough to hermetically seal the channel structure.

6.3.5 Conclusions

A glass cover has to be bonded onto the silicon nitride membrane layer to realize a channel-membrane-channel structure. This can be realized with anodic bonding. Bonding parameters have been optimized with a non-destructive bond strength test method. It is shown that an increasing bond temperature and applied voltage increase the bond strength. Glass covers are strongly bonded to the 1 μm thick nitride layer at 400˚C and 1500 V when the nitride layer is first oxidized in a wet oxidation furnace at 1100˚C for 30 minutes.

6.4 References

[1] B.H. Timmer, K.M. v. Delft, R.P. Otjes, W. Olthuis, A. v.d. Berg, *"A miniaturized measurement system for ammonia in air",* Analytica Chimica Acta 507 (1), pp. 139-145, 2004

[2] H.V. Jansen, J.G.E. Gardeniers, J. Elders, H.A.C. Tilmans, M. Elwenspoek, *"Application of fluorocarbon polymers in micromechanics and micromachining",* Sensors and Actuators A 41, pp 136-140, 1994.

[3] H.J.Qi, Y.B. Fu, D. Wang, X.X. Yang, K.Y. Sui, Z.L. Ma, *"SEM study of fluorocarbon films by R.F. sputtering of PTFE targets on PET substrates"*, Surface and coatings technology 131, pp 171-180, 2000

[4] R.W. Schofield, A.G. Fane, C.J.D. Fell, *"Gas and vapour transport through microporous membranes. I. Knudsen-Poiseuille transition",* Journal of membrane science 53, pp 159-171, 1990

[5] M. Mulder, *"Basic principles of membrane Technology"* Kluwer Academic Publishers, Dordrecht, The Netherlands, Second edition, Chapter IV.3, 1996

[6] S. Schlautmann, H. Wensink, R.B.M. Schasfoort, M. Elwenspoek, A. v.d. Berg, *"Powder Blasting Technology as an Alternative Tool for Microfabrication of Capillary Electrophoresis Chips with Integrated Conductivity Electrodes",* Journal of Micromechanics and Microengineering 11(4), pp 386-389, 2001

[7] S. Weichel, R. de Reus, S. Bouaidat, P.A. Rasmussen, O. Hansen, K. Birkelund, H. Dirac, *"Low-temperature anodic bonding to silicon nitride",* Sensors and Actuators A 82, pp. 249-253, 2000

[8] C.J.M. van Rijn, W. Nijdam, S. Kuiper, G.J. Veldhuis, H. van Wolferen, M. Elwenspoek, *"Microsieves made with laser interference lithography for micro-filtration applications",* Journal of Micromechanics and Microengineering 9, pp 170-172, 1999

[9] S. Kuiper, M. de Boer, C. van rijn, W. Nijdam, G, Krijnen, M. Elwenspoek, *"Wet and dry etching techniques for the release of sub-micrometre perforated membranes",* Journal of Micromechanics and Microengineering 10, pp 171-174, 2000

[10] T.M.H. Lee, D.H.Y. Lee, C.Y.N. Liaw, A.I.K. Lao, I-M. Hsing, *"Detailed characterization of anodic bonding process between glass and thin-film coated silicon substrates",* Sensors and Actuators A 86, pp. 103-107, 2000

[11] A. Bethold, *"Low-temperature Wafer-to-wafer bonding for microchemical systems",* PhD-thesis Delft, the Netherlands, 2001

[12] J.A. Plaza, J. Esteve and E. Lora-Tamayo, *"Effect of silicon oxide, silicon nitride and polysilicon layers on the electrostatic pressure during anodic bonding",* Sensors and Actuators A 67, pp. 1181-184, 1998

[13] J. A. Plaza, J. Esteve and E. Lora-Tamayo, *"Non-destructive in situ test for anodic bonding",* Sensors and Actuators A 60, pp. 176-180, 1997

[14] Pomerantz, D.I., US Patent No. 3,397,278

[15] G. Wallis, D.I. Pomerantz, *"Field assisted glass-metal sealing",* Journal of Applied Physics 40 (10), pp. 3946-3949, 1969

[16] M.T. Blom, N.R. Tas, G.Pandraud, E. Chmela, J.G.E. Gardeniers, R. Tijssen, M. Elwenspoek, *"Failure mechanism of pressurized microchannels, model and experiments",* Jounal of micromechanical systems 10 (1), pp. 158-164,2001

[17] S. Tatic-Lucic, J. Ames, B. Boardman, D. McIntyre, P Jaramillo, L. Starr, M. Lim, *"Bond-quality characterization of silicon-glass anodic bonding",* Sensors and Actuators A 60, pp. 223-227, 1997

[18] W.P. Maszara, G. Goetz, A. Caviglia and J.B. McKitterick, *"Bonding of silicon wafers for silicon-on-insulator"*, Journal of Applied Physics 64 (10), pp. 4943-4950, 1988

[19] A. Cozma, B. Puers, *"Characterization of electrostatic bonding of silicon and Pyrex glass", Journal of Micromechanics and Microengineering* 5, pp. 98-102, 1995

Chapter 7

Alternative gas sampler*

7.1 Introduction

In the medical community, there is a considerable interest in ammonia analyzers, applicable for measuring ammonia levels in exhaled air as a diagnostic tool of certain diseases.[1] Measuring breath ammonia levels can be a fast diagnostic method for patients with disturbed urea balance, e.g. due to kidney disorder[2] or Helicobacter pylori bacterial stomach infection.[3-5] For such applications, often only a few hundred ml of exhaled air is available and, today, no suitable ammonia breath analyzer exists.[6]

Many air ammonia detectors have been reported in literature, based on different principles.[7-13] The most sensitive and selective systems, comprising laser setups, are not suited for miniaturization and integration on a chip and are therefore not applicable for measuring in the small available gas volumes. Direct gas measuring methods suitable for miniaturization have been shown, like tin oxide film[8] or conducting polymer film gas sensors.[9] These methods have been applied for measuring ammonia concentrations[10-12] but most of them show poor selectivity and inadequate detection limits and are therefore not suited.

Other air analyzing systems for measuring ambient ammonia, or other gasses, make use of gas samplers, like denuders or diffusion scrubbers.[13-15] A volume of gaseous ammonia is sampled into a smaller volume of liquid,

**This chapter is accepted for publication as a technical note in Lab-on-a-Chip, 2004*

where ammonium ions are formed.[16] Many accurate ways to measure low ammonium concentrations have been shown.[17] An ambient ammonia (sub-ppb level) detection system developed at the Energy research Centre of the Netherlands (ECN)[18] is such a system, which is very selective and highly accurate. The apparatus comprises a gas sampler, a separator and a detector. In the detector only ammonium ions are present in deionised water that are quantified using an electrolyte conductivity detector. Although this apparatus requires several litres of analyte gas for detection, its very selective measurement principle is suited for miniaturization into a lab on a chip approach.[19] One component, a miniaturized EC detector that can to measure low ion concentrations in less than 200 nl of liquid, has been realized in previous research.[20] Here we present and characterize a miniaturized gas sampler that can be used in the miniaturized ambient ammonia detection system.

Sampler principle

Instead of using a phase-separation membrane, as used in the "AMINA" principle discussed in chapter three of this thesis, the ammonia uptake in the presented gas sampler is realized by directly mixing the analyte gas with the sample liquid, in this case purified water, without an intermediate membrane layer. A reaction chamber is integrated to allow the ammonia to react with the water. Subsequently, the carrier gas has to be removed from the system because gas bubbles would otherwise disturb the EC measurement. Therefore, a degasser is integrated in the sampler structure.

There are many ways to remove gas bubbles from a liquid stream. The most convenient way, used in the laboratory to degas liquids, is vacuum degassing, where membranes are applied in order to keep the liquid volume fixed.[21-23] Integration of a vacuum pump in a chip is not yet demonstrated so other techniques have been tried to remove gas bubbles from micro-fluidic systems, like piezoelectric actuators for removing gas bubbles ultrasonically.[24] However, when the only goal is to remove gas bubbles from the liquid stream, it is far easier to integrate a gas outlet hole that is sealed with a micro-porous hydrophobic membrane and generate an over-pressure inside the liquid channel, resulting in removal of the gas. Therefore a flow restrictor is integrated to increase the gas pressure underneath the membrane. A schematic drawing of the described sampler with the degasser is shown in figure 7.1. It comprises a mixer where the analyte gas is mixed with a sample liquid, a reaction chamber, a gas outlet

sealed with a micro-porous, water-repellent membrane and a liquid outlet with a flow restrictor. The EC detector is placed at the liquid outlet of the sampler.

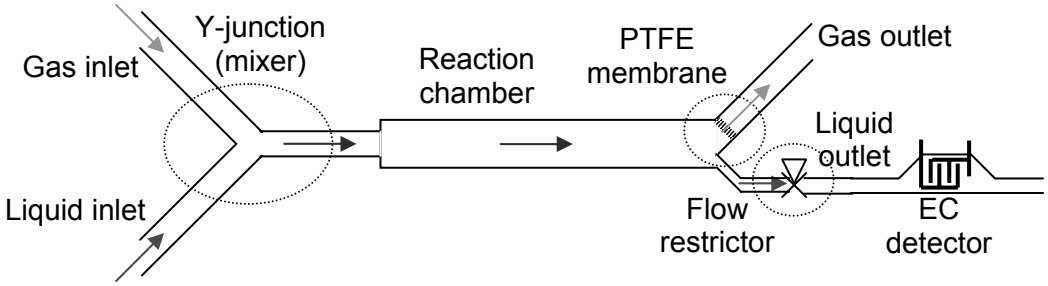

Figure 7.1. *Schematic of the gas sampler with integrated degasser.*

7.2 Experimental

Sampler / degasser processing

The proposed system was realized in glass on silicon technology. A channel between the gas and liquid inlet and the gas outlet provides some time for the reaction between the gas and the liquid. A large round hole with a diameter of 1.5 mm is placed at the end of this channel to vent the carrier gas. The flow restrictor and the liquid outlet are placed behind the gas outlet. The total design is shown in figure 7.2.

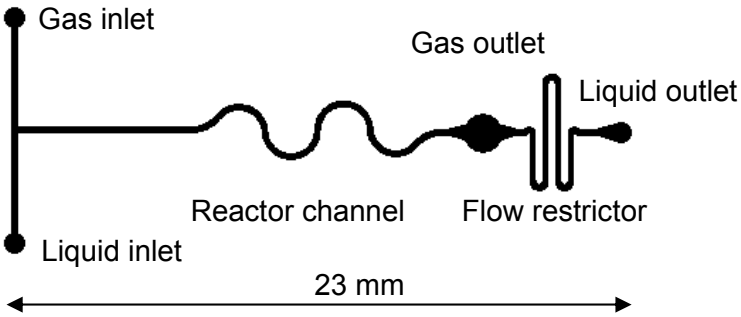

Figure 7.2. *Gas sampler mask design.*

The sampler was made in a rapid prototyping process, using powderblasting.[25] This technique can be used to make channels and through-holes in brittle materials, like glass or silicon. Here we used a 10 cm Pyrex glass wafer as a functional layer. An Ordyl BF410 photosensitive protection foil was laminated to the glass wafer and structured using UV-photolithography. Photo masks for the channel structure and the through-holes were designed with a computer program, CLEwin, and printed on transparencies using a standard HP 930C inkjet printer. The minimal lateral

feature size of the technique will be used, which is about 200 µm. After developing the protective foil, the wafer was processed in the powderblasting apparatus. The resulting channels have a depth of 25 µm and a width of about 220 µm, measured with a Dektak profilometer. The widening of the channel was mainly caused by the poor quality of the mask. The protective foil was removed in sodium carbonate and after a cleaning step in fuming HNO_3 the wafer was rinsed in water and dried. A second protective foil was applied to the wafer to form the masking layer for the through-holes. The foil was developed and the wafer processed again by powderblasting. After stripping the foil, the wafer was cleaned ultrasonically in acetone to remove powder residue, cleaned in fuming HNO_3, rinsed in water and dried again. The structured glass wafer was then bonded anodically to a silicon substrate wafer at 400°C and 800 V for 30 minutes in an EV-501 anodic bonder. Thereafter the chips are diced. The process scheme is shown in figure 7.3.

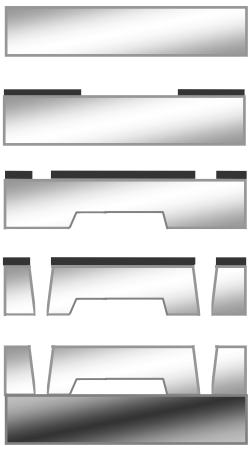

- Protective foil is laminated to a cleaned glass wafer and structured using photolithography.
- Channels are made by removing 25 µm of glass using powder-blasting and subsequently the protective foil is removed in sodium carbonate.
- The process is repeated on the back side to make through-holes.
- The wafer is bonded anodically to a silicon substrate and is diced to chips and cleaned.

***Figure 7.3**. Sampler fabrication process scheme.*

Flow restrictor design

A gas outlet is used to vent the carrier gas and to prevent gas bubbles to be transported towards the liquid outlet. A water-repellent, gas-permeable membrane is used to keep the liquid in the sampler. A suitable membrane is micro-porous hydrophobic PTFE, that was obtained from Millipore (Fluoropore 0.5 µm membrane filter).

To design the flow restrictor, both the pressure difference required for removing the residue gas from the system and the maximum pressure over the membrane, at which water will penetrate the pores, have to be determined. This can be done by a technique applied in the membrane separation industry to test the porosity of a membrane,[26] the so-called

bubble point detection method. A piece of membrane was clamped between two home-made Perspex holders with sealing rubber O-rings. A pressure sensor, Kulite Semiconductor Products pressure transducer XTL-190N 7 BAR, was placed gastight into the inlet of the holder.
To determine the maximum allowed pressure over the membrane, the water pass-through pressure, the membrane is first wetted and then a water column is pressed through the membrane using a gas pressure. The pressure difference required to press the water through the pores can be determined because, when all water is pressed out, gas will go through the membrane and gas bubbles will appear. The minimum required pressure over the membrane to remove the gas bubbles from the sampler, the gas pass-through pressure, can be determined in the same way by using a non-wetted membrane and leaving out the water column. This technique is described in detail in appendix B.

Once the water and gas pass-through pressures are known, the flow restrictor can be designed. The pressure difference over a channel can be calculated using the Poiseuille equation[27] that relates the pressure difference to the flow through and the hydraulic resistance of the channel:

$$\Delta P = Q \cdot R = Q \cdot \frac{2\eta L(\text{perimeter})^2}{(\text{cross}-\text{sectional area})^3} = Q \cdot \frac{8\eta L(w+h)^2}{w^3 h^3} \qquad (7.1)$$

with ΔP the pressure difference over the membrane (Pa), Q the flow velocity (m^3/s) and R the fluidic resistance ($Pa \cdot s/m^3$). The fluidic resistance is dependent on the viscosity of the solution, η ($Pa \cdot s$, 10^{-3} $Pa \cdot s$ for water) and the geometry of the channel, the length L (m), width w (m) and height (m).[28]

The bubble point pressure with water was determined to be 170 kPa and the gas pass-through pressure to be about 2 kPa. The pressure difference over the membrane should lie between these two boundary values. The flow restrictor was designed to yield a pressure of about one-third of the bubble point pressure, 60 kPa, at a liquid flow rate of 20 µl/min. In combination with the channel parameters given before (w = 220 µm and h = 25 µm), the required length of the channel was calculated to be 15 mm.

Measurement protocol

As indicated in the introduction, the total miniaturized air analyzer system will be used for measuring ammonia concentrations. Therefore, the non-selective gas sampler presented here is tested using ammonia in a nitrogen carrier gas while the gas will be sampled in purified water. For use as a real-life air ammonia analyzer, a separation step has to be included to reach the required selectivity, as described in chapter three of this thesis.[18,19] However, in the experiment described in this chapter, no other gasses, like CO_2 and SO_2, are present that would interfere with the measurements.

Ammonia has a very high solubility in water, 31.3 mol/l at a temperature of 293 K.[29] The diffusion rate of ammonia in gas is very high because it is a small molecule, $1.21 \cdot 10^{-5}$ $m^2 \cdot s^{-1}$.[30] By using very small micromachined channels, 25 by 220 µm, the diffusion length is also small. Therefore the assumption is made that almost all ammonia will dissolve very rapidly, well within the residence time of the gas in the sampler, about 10 ms. Once dissolved, ammonia will react with water to form ammonium ions.

Pure nitrogen and a mixture of nitrogen with 10 ppm (±10 %) ammonia were acquired from Hoekloos. Gas flow was controlled using Bronkhorst Hightech mass flow controllers, EL-flow F-110C. The mass flow controllers have a maximum flow of 3 ml/min with a minimum controllable flow of 2 %, which is 60 µl/min. Therefore, gas mixtures of nitrogen with ammonia concentrations between 10 and 0 ppm can be realized by mixing the two gasses. Both the ammonia and the nitrogen source should always be open, at least at 2 %, to prevent in-diffusion of CO_2 into the tubing (30 cm of PTFE tubing, 0.8 mm ID 1.6 mm OD), reducing the maximum and minimum attainable ammonia concentration to 9.8 and 0.2 ppm respectively, dependent of the flow velocity.

Pre-cleaned, deionised water was purified by an ion exchange column filled with Baker mixed bed ion exchange resin and pumped directly into the sampler. The water flow was controlled using a CMA-102 microdialysis syringe pump with a maximum flow of 20µl/min. The EC detector was connected to the liquid outlet of the sampler, using 0.3 mm ID PTFE tubing and connectors acquired from Lee. Home-made interface electronics is used to measure the conductivity of the sample liquid after gas sampling.

The total system was first cleaned by flushing with pure nitrogen and purified water for several hours. Then, the analyte flow was set at 1.0 ml/min and the water flow at 20 µl/min. This resulted in an elevated ammonia concentration due to the difference in volume of a factor of 50, resulting in an enhanced detection limit.

7.3 Results and Discussion

In order to calculate the ion concentration from the conductance of the water stream measured with the EC detector,[20] a calibration curve is made. An ammonium hydroxide solution with an ammonium concentration of 100 µM is mixed with on-line purified water to create lower ammonium concentrations and is subsequently flushed through the EC detector. The resulting conductivity is measured for several minutes. The average conductivity value is plotted against the concentration in figure 7.4. A best fit line is drawn in Excel that will be used as the relation for calculating the ion concentration from experimental conductivity values.

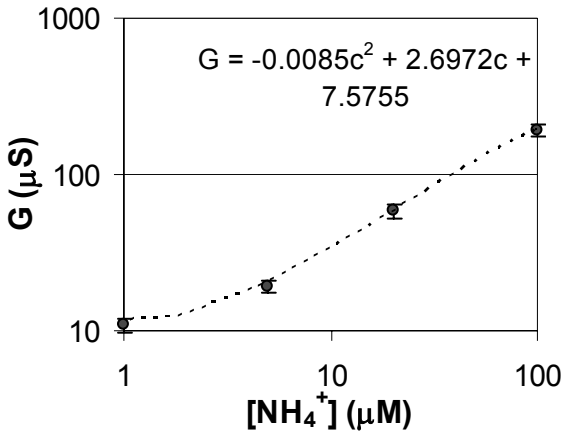

Figure 7.4. *Calibration curve showing the relation between the ammonium concentration and the measured conductance.*

Subsequently, the gas sampler is tested for the ammonia sampling ability via the measurement described in the measurement protocol. Ammonia detection was started at the higher ammonia concentration of 9.6 ppm. After stabilization of the system, the concentration was lowered to 6.7, 4.6, 3.3, 1.8 and 0.6 ppm, respectively. The lowest concentration corresponds to 27 nmol/l of analyte gas. The conductance values measured with the EC detector during the described experiment are shown in figure 7.5.

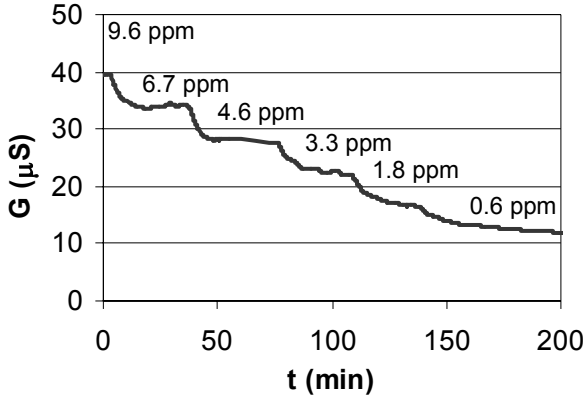

Figure 7.5. *Conductance response to different ammonia concentrations.*

It is observed that the ammonia concentration in the analyte gas directly influenced the conductance of the sample solution at the outlet of the sampler. When the ammonia concentration in the analyte gas is lowered, the conductance of the liquid at the output of the sampler is reduced. With the presented gas sampler, the conductivity difference between 1.8 and 0.6 ppm is measurable, so the detection limit of the described system lies below 1.8 ppm. Unfortunately it was not possible with the used setup to test lower ammonia concentrations.

The theoretically expected ammonium concentration in the water flow can be calculated as a function of the ammonia concentration of the sampled analyte gas. The ammonia concentration can be converted to the number of moles per litre, knowing that the molar gas volume at room temperature is $2.45 \cdot 10^{-2}$ m^3. Parameters like the concentration enhancement of 50, due to the ratio between the gas flow and the liquid flow, and the ammonium ion formation due to the dissociation equilibrium should be taken into account.

Using the fitted curve found in figure 7.4, it is possible to calculate the ammonium concentration from the measured conductance. Both the theoretically and experimentally determined values are plotted as a function of the initial ammonia concentration in figure 7.6.

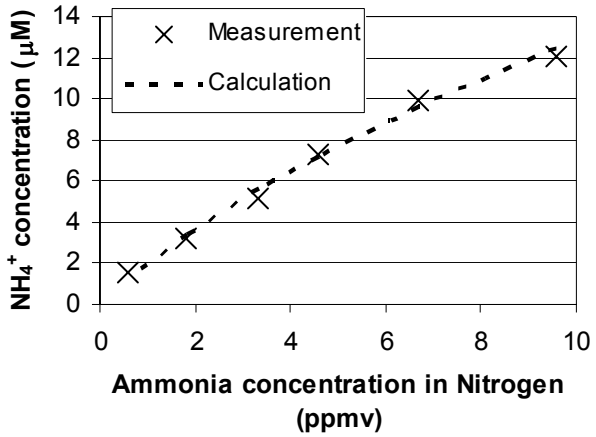

Figure 7.6. *Ion concentration of the sample solution at the outlet of the sampler, as a function of the ammonia concentration in the analyte gas, both calculated and measured.*

The calculated ammonium concentrations are comparable to the measured values. The difference between the two curves is maximal 7 %. However, the system is rather slow; it takes up to 15 minutes for the conductivity to stabilize where it only takes a few seconds for the water to flow through the sampler. This delay is caused by the relatively large volume in the interconnecting tubing between the outlet of the sampler and the EC detector. Reducing the volume between the sampler and the detector by integration of the EC sensor would drastically shorten the response time of the presented system. It should be noted that a response time of about 15 minutes corresponds to a total gas consumption of 15 ml, which makes the presented gas sampler potentially applicable for breath analysis applications.

For the higher ammonia levels, all measured ammonium concentrations are within 7 % of the calculated values. This is within the error of the ammonia concentration in the gas source: 10 ppm ±10 %. The ammonia concentration is believed to be slightly unstable over time due to adsorption of ammonia to the gas cylinder wall.

7.4 Conclusions

An ammonia gas sampler is demonstrated, based on direct mixing of analyte gas into a sample solution. A degasser is integrated to remove carrier gas bubbles from the sample liquid flow. The degasser consists of a large venting hole sealed with a micro-porous water-repellent PTFE membrane and a flow restrictor behind the hole to create an over-pressure

over the membrane. The lowest ammonia concentration tested with the sampler with integrated degasser is 0.6 ppm (27 nmol/l in the analyte gas), resulting in a response within the detection limit of the used EC detector. The measured ion concentrations are within 7 % of the calculated values, except for the lowest measured concentration. The system has a response time of about 15 minutes which is rather slow. This is mainly caused by the large dead volumes in the tubing and interconnecting parts. Integration of the EC detector in the sample channel would significantly reduce the volume between the sampler and the detector and therefore the response time. During the 15 minutes response time, only 15 ml of gas is used which makes the presented gas sampler applicable for breath analysis applications. In a future design, the detection limit will be further improved to make the system suited as a diagnostic tool.

7.5 References

[1] W. Ament, J.R. Huizenga, E. Kort, T.W. van der Mark, R.G. Grevink, G.J. Verkerke, "*Respiratory ammonia output and blood ammonia concentration during incremental exercise*", International Journal of Sports Medicine 20, pp 71-77, 1999

[2] L.R. Narasimhan, W. Goodman, C. Kumar, N. Patel, "*Correlation of breath ammonia with blood urea nitrogen and creatinine during hemodialysis*", PNAS 98 (8), pp 4617-4621, 2001

[3] B. Marshall, J.R. Warren, "*Unidentified curved bacillus and gastric Epithaeium in active chonic gastritis*", Lancet 1, pp. 1273-1275, 1993

[4] J. C.E. Underwood, "*General and Systematic Pathology*", Churchill Livingstone Inc, 2nd edition, pp 414-415, 1996

[5] D.J. Kearney, T. Hubbard, D. Putnam, "*Breath ammonia measurement in Helicobacter pylori infection*", Digestive diseases and sciences 47 (11), pp 2523-2530, 2002

[6] E. Verpoorte, "*Microfluidic chips for clinical and forensic analysis*", Electrophoresis 23, pp 677-712, 2002

[7] S.G. Buckly, C.J. Damm, W.M. Vitovec, L.A. Sgro, R.F. Sawyer, C.P. Koshland, D. Lucas, "*Ammonia detection and monitoring with photofragmentation fluorescence*", Applied optics 37 (36), pp. 8382-8391, 1998

[8] R.K. Sharma, P.C.H. Chan, Z. Tang, G. Yan, I-M. Hsing, J.K.O. Sin, "*Investigation of stability and reliability of tin oxide thin-film for integrated micro-machined gas sensor devices*", Sensors and Actuators B 81, pp 9-16, 2001

[9] F. Zee, J.W. Judy, "*Micromachined polymer-based chemical gas sensor array*", Sensors and Actuators B 72, pp 120-128, 2001

[10] M. Aslam, V.A. Chaudhary, I.S. Mulla, S.R. Sainkar, A.B. Mandale, A.A. Belhekar, K. Vijayamohanan, "*A highly selective ammonia gas sensor using surface-ruthenated zinc oxide*", Sensors and Actuators A 75, pp 162-167, 1999

[11] I. Laehdesmaeki, A. Lewenstam, A Ivaska, "*A polypyrrole-based amperometric ammonia sensor*", Talanta 43, pp 125-134, 1996

[12] V.V. Chabukswar, S. Pethkar, A.A. Athawale, "*Acrylic acid doped polyaniline as an ammonia sensor*", Sensors and Actuators B 77, pp 657-663, 2001

[13] P.K. Simon, P.K. Dasgupta, Z. Vecera, "*Wet effluent denuder coupled liquid/ion chromatography systems*", Analytical Chemistry 63, pp 1237-1242, 1991

[14] P.F. Lindgren, P.K. Dasgupta, "*Measurement of atmospheric sulfur dioxide by diffusion scrubber coupled ion chromatography*", Analytical Chemistry 61, pp 19-24, 1989

[15] S-I. Ohira, K. Toda, S-I. Ikebe, P. K. Dasgupta, "*Hybrid microfabricated device for field measurement of atmospheric sulfur dioxide*", Analytical Chemistry 74, pp. 5890-5896, 2002

[16] C.B. Boring, R. Al-Horr, Z. Genfa, P.K. Dasgupta, "*Field measurement of acid gases and soluble anions in atmospheric particulate matter using a parallel plate wet denuder and an alternating filter based automatic analysis system*", Analytical Chemistry 74, pp. 1256-1268, 2002

[17] G. Schultze, C.Y. Liu, M. Brodowski, O. Elsholz, "*Different approaches to the determination of ammonium ions at low levels by flow injection analysis*", Analytica Chimica Acta 214, pp 121-136, 1988

[18] J.W. Erisman, R. Otjes, A. Hensen, P. Jongejan, P. v.d. Bulk, A. Khlystov, H. Möls and S. Slanina, "*Instrument development and application in studies and monitoring of ambient ammonia*", Atmospheric Environment 35, pp 1913-1922, 2001

[19] B.H. Timmer, K.M. van Delft, R.P. Otjes, W. Olthuis, A. v.d. Berg, "*A miniaturized measurement system for ammonia in air*", Analytica Chimica Acta 507 (1), pp. 139-145, 2004

[20] B. Timmer, W. Sparreboom, W. Olthuis, P. Bergveld and A. v.d. Berg, *"Optimization of an electrolyte conductivity detector for measuring low ion concentrations",* Lab on chip 2 (2), pp. 121-124, 2002

[21] T. Leiknes, M.J. Semmens, *"Vacuum degassing using microporous hollow fiber membranes"*, Separation an purification Technology, 22-23, pp 287-294, 2000

[22] A. Sengupta, P.A. Peterson, B.D. Miller, J. Scheider, C.W. Fulk, Jr., *"Large-scale application of membrane contactors for gas transfer from or to ultrapure water",* Separation an Purification Science 14, pp 189-200, 1998

[23] Akira Ito, Kazuaki Yamagiwa, Masato Tamura, Michio Furusawa, *"Removal of dissolved oxygen using non-porous hollow-fiber membranes",* Journal of Membrane Science 145, pp 111-117, 1998

[24] Zhen Yang, Sohei Matsumoto, Ryutaro Maeda, *"A prototype of ultrasonic micro-degassing device for portable dialysis system",* Sensors and Actuators A 95, pp 274-280, 2002

[25] S. Schlautmann, H. Wensink, R.B.M. Schasfoort, M. Elwenspoek, A. v.d. Berg, *"Powder Blasting Technology as an Alternative Tool for Microfabrication of Capillary Electrophoresis Chips with Integrated Conductivity Electrodes",* Journal of Micromechanics and Microengineering 11(4), pp 386-389, 2001

[26] M. Mulder, *"Basic principles of membrane Technology",* Kluwer Academic Publishers, Dordrecht, The Netherlands, Second edition, Chapter IV.3, 1996

[27] W.M. Deen, *"Analysis of Transport Phenomena",* Oxford university press, Chapter 5, 1998

[28] F.M. White, *"Fluid Mechanics",* McGraw-Hill, 1979

[29] R.C. Weast, *"CRC Handbook of chemistry and physics",* The chemical Rubber Co., 65th ed., 1984

[30] R. Chang, *"Physical chemistry for chemical and biological sciences",* University Science Books, 3rd ed., chapter 11, 2000

Chapter 8

Conclusions and recommendations

8.1 Conclusions

The conclusions of the different subjects, discussed in the different chapters of this thesis, are given for each chapter:

Chapter 1:

Miniaturization and integration of chemical sensors and sensor systems give rise to new applications. Especially when only small analyte volumes are available, miniaturization and integration can be very beneficial. This approach seems suitable to make the ammonia measurement system developed at ECN[1] applicable for other applications than environmental monitoring, e.g. diagnostic breath analysis.

Chapter 2:

Ammonia has been present in the earth's atmosphere from the very beginning and it may even have been an important component in the evolution of life itself. Today, there are many sources of ammonia and application areas for ammonia detectors and measurement systems. When very small concentrations are to be measured, e.g. less than 2 ppb for environmental monitoring and 50 ppb for breath analysis, solid state ammonia sensors are not sensitive enough. Optical methods that make use of lasers are often too expensive and very large. When the reagent consumption and response time can be decreased, the "AMINA" measurement principle seems very suited as a small ambient ammonia sensing device for small analyte volumes.[1]

Chapter 3:
The "AMINA" principle is an indirect chemical method for measuring ambient ammonia without interference of acidifying gasses, even when these gasses have a much higher concentration level.[2] In potential, the method is suitable for miniaturization.

Chapter 4:
The ammonia measurement system developed at ECN[1] is made up of fluid and gas channels, separated by micro-porous, phase-separation membranes. Channels can be made very shallow and small in materials like silicon and glass using micro system technology. A method to integrate a membrane in a micro-channel structure is demonstrated.

The miniaturization of the channels in the system reduces mass transport distances in the system and therefore the required time constants of the different parts of the system. When the parts are integrated on one chip, this results in a reduced system response time. In the gas sampler, the distances that gas molecules have to travel in the channel to reach the membrane interface are reduced significantly. The reduction in channel depth by a factor of 20, from 2 mm to 100 µm, was simulated to result in a reduced time to take up 99.9 % of the available ammonia from the analyte gas by a factor of 65. A major advantage of the reduced gas uptake time is the correlated reduction in required analyte gas volume. The channel depth and length can be shortened to lower the internal volume of the channel and the time constant for the gas flow is reduced. In the system that is optimized to have a response time of one minute, the maximum theoretical gas volume required for one measurement is reduced from 20 liters to 300 ml.

A detector that is suitable for quantifying low ion concentrations in a small volume is presented. Theory on the cell constant of the used planar interdigitated electrolyte conductivity sensors is combined with theory on electrochemical effects at the electrode-electrolyte interface to come to a better description of the sensor. It is known that the double layer capacitance decreases significantly with decreasing electrolyte concentration. Taking this into account it is now possible to predict the sensor response even for low concentrations. A sensor is realized that is optimized for low electrolyte concentrations with a cell constant as low as

8.8 m^{-1} and a total detector area of 0.075 cm^2. The maximum measured resistance value for pure deionised water is about 220 kΩ at 1 kHz.

Chapter 5:
The miniaturized measurement system for low gaseous ammonia concentrations, presented in chapter four of this thesis, has been realized on a chip. Although the gas sampler proved to be less than optimal in sampling ammonia from the analyte gas, the detection limit of the system is calculated to be 1.1 ppb. The response time is determined to be 1.6 minutes with a gas flow of 50 ml/min. The required gas volume for one measurement is therefore reduced to less than 2 % of the gas consumption of the large scale ammonia monitor this system is based on. For normal atmospheric environments, the selectivity of the system is sufficient to measure ammonia concentrations in the low-ppb range. The system is even sufficiently selective to ammonia to be used in environments containing elevated carbon dioxide levels, like exhaled air. The lower ammonia concentration expected in diagnostic breath analysis applications, 50 ppb, is easily detectable. It is shown that the water conductance increases linear with the temperatures in the range from 10 to 40 degrees Celsius with 2.4 ± 0.3 %/˚C compared to room temperature. To overcome this problem, a second detector is included to function as a temperature reference.

Chapter 6:
A micromachined channel covered with a 1-µm thick porous Si_3N_4 membrane is realized as a thin alternative for the membrane used in the AMINA-chip. The reduced thickness of the membrane will significantly shorten the time required for the analyte gas to diffuse through the membrane. Contact angle, gas pass-though pressure and bubble point pressure measurements show that it is possible to render the micromachined membrane water-repellent by coating the Si_3N_4 layer with a fluorocarbon coating. This makes the membrane in principle suited for the described ammonia detection system.

Anodic bonding parameters for bonding of a 1-µm Si_3N_4 to a glass cover have been optimized with a non-destructive bond strength test method. It is shown that increasing the bond temperature and the applied voltage increases the bond strength. The glass covers are strongly bonded to the nitride layer at 400˚C and 1500 V after the nitride layers are oxidized in a wet oxidation furnace at 1100˚C for 30 minutes.

Chapter 7:
A gas sampler that makes use of direct mixing between the analyte gas and the sample solution is presented. A degasser is implemented to remove the carrier gas after sampling. The degasser comprises a venting hole, sealed with a micro-porous water-repellent membrane and an integrated flow restrictor, resulting in complete gas removal. The gas sampler is shown to function very efficient in a test with an analyte gas of ammonia in nitrogen, sampled in purified water. An electrolyte conductivity sensor is placed at the outlet of the sampler to quantify the resulting ammonium concentration. The result is shown to correspond well with theoretical calculations.

8.2 Recommendations for future work

The ammonia measurement system, as described in chapter five, is shown to have a non-optimal efficiency. The system can be further optimized by increasing the efficiency of the gas sampler. Structures in the gas channel for guiding the gas flow could be helpful. Another possible solution would be to use a longer and smaller channel. This would reduce the difference in residence time of gas flowing through the middle and along the sides of the channel.

The main drawback of the "AMINA-chip" presented in this thesis is the time-consuming production process. Especially the assembly of the different glass parts and the membrane is rather demanding. The membrane is glued by hand between the two glass chips, as is the glass cover. This has to be done really careful because otherwise the system will leak and loose its functionality. Experiments have been conducted to simplify the three gluing steps.

In the first gluing step, the membrane is placed between the two glass parts. Although PP membranes can be glued to glass using epoxy glue, applying the glue in a controlled manner is a real challenge. In the channels of the measurement system, support poles are integrated to prevent the membrane from buckling into the channel. It would be much easier if the membrane could be glued to these support poles. It has been tried to apply a homogeneous thin glue layer to the structured glass chips using a glue laminator, as shown in figure 8.1. We did not succeed in applying a thin glue layer that covered the support poles without glue getting inside the channels. Although we did not succeed, this method

seems the best way to make the chip production process applicable for mass-production.

Figure 8.1 *Laminator for applying thin glue films to substrates (for non-industrial purposes).*

The second gluing process, the application of the glass covers that seal the electrolyte conductivity detectors, can be overcome by bonding of a silicon cover to the glass chip. Anodic bonding is a method that can create a strong bond between glass and silicon, as discussed in chapter 6 of this thesis. Channels and through-holes in silicon can be made with micromachining.[3] For aligning purposes, it is most convenient to bond a complete silicon wafer to the glass wafer. However, when the glass chips are completely covered with silicon, it is no longer possible to visually inspect the liquid flows inside the system. This drawback of the proposed method can be overcome by selectively removing the silicon, e.g. by etching away the silicon that covers the channels. This can be done with wet-chemical KOH etching but, in that case, concave corners have to be protected against underetching.[4,5] This can be done by creating special corner compensation structures on the etch mask.[6,7] An experiment with such structures has been conducted. A structured silicon wafer is bonded to a glass substrate by anodic bonding. The used mask design is realized in silicon nitride using photolithography and dry chemical nitride etching. The used mask is shown in figure 8.2(A). Subsequently, the silicon is removed by wet-chemical etching in KOH. During the etching process, the corner compensation structures are shortened, shown in figure 8.2(B), until the silicon is removed from the glass substrate and the corner compensation structures are completely removed, as shown in figure 8.2(C).

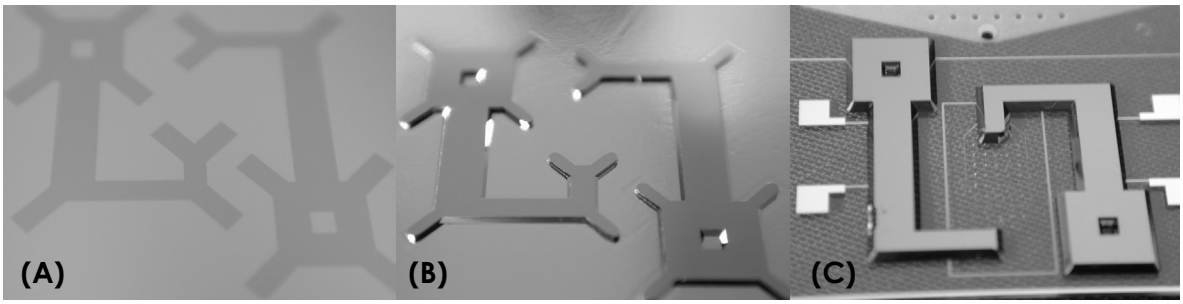

Figure 8.2 *Electrode cover that is made by anodic bonding and back-etching of silicon. Corner compensation structures are created in the siliconnitride masking material (A) that are reduced in length during KOH etching (B) until they are completely removed when the silicon is removed from the glass substrate (C).*

A third gluing step is the installation of interconnects. The system comprises interconnects to the different in- and outlets to attach the gas and liquid sources, as well as electrical wires to be able to connect the detectors to the interface electronics. It would be more convenient when all these connections could be made in one single step. This can be done by placing the chip in a special holder, like the one shown in figure 8.3. This holder was made as a prototype but the surface proved to be too rough. The pressure required to seal the o-ring fluid connectors caused the glass chips to break.

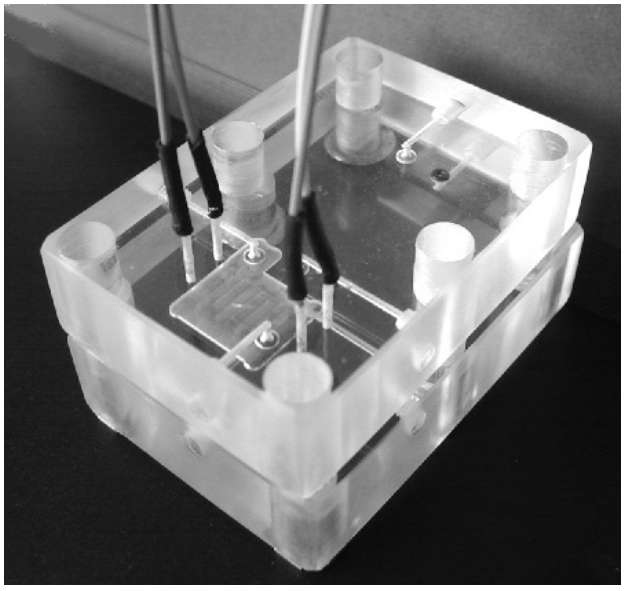

Figure 8.3 *Prototype chip holder with o-ring gas- and liquid connectors and spring electrode connectors.*

During experiments with the integrated ammonia measurement system, it has been observed that water starts to condensate in the gas chamber. This not surprising because the used membrane is permeable to gas but also to vapour. The difference in water vapour pressure between the sample solution and the analyte gas causes water vapour to permeate through the membrane into the gas stream. For the ammonia measurement system, this is not a real problem since the ion concentration in the detector is not significantly influenced by the sample solution flow rate. However, this evaporation process can be used to concentrate low ion concentration electrolyte samples, as shown in experiments that have been carried out with a controlled gas flow over a membrane to control the evaporation rate.[8]

8.3 References

[1] J.W. Erisman, R. Otjes, A. Hensen, P. Jongejan, P. v.d. Bulk, A. Khlystov, H. Möls and S. Slanina, *"Instrument development and application in studies and monitoring of ambient ammonia",* Atmospheric Environment 35, pp 1913-1922, 2001

[2] B.H. Timmer, K.M. van Delft, R.P. Otjes, W. Olthuis, A. v.d. Berg, *"A miniaturized measurement system for ammonia in air",* Analytica Chimica Acta 507 (1), pp. 139-145, 2004

[3] M. Madou, *"Fundamentals of microfabrication",* CRC press, 1997

[4] M. Bao, Chr. Burrer, J. Esteve, J. Bausells and S. Marco, *"Etching front control of <110> strips for corner compensation",* Sensors and Actuators A 37-38, pp 727-732, 1993

[5] O. Powell, H.B. Harrison, *"Anisotropic etching of {100} and {110} planes in {100} silicon",* Journal of Micromechanics and Microengineering 11, pp 217-220, 2001

[6] van Kampen and R F Wolffenbuttel, *"Effects of <110>-oriented corner compensation structures on membrane quality and convex corner integrity in <100>-silicon using aqueous KOH",* Journal of Micromechanics and Microengineering 5, pp 91-94, 1995

[7] P. Enoksson, *"New structure for corner compensation in anisotropic KOH etching",* Journal of Micromechanics and Microengineering 7, pp 141-144, 1997

[8] B.H. Timmer, K.M. van Delft, W. Olthuis, P. Bergveld, A. van den Berg, *"Micro-evaporation electrolyte concentrator",* Sensors and Actuators B 91, pp 342–346, 2003

Appendix A

Mass transport

A.1 Introduction

The response time of the ammonia measurement system is mainly determined by the time required for mass transport in the system. For instance, in the gas sampler, ammonia is transported from the gas stream, through the membrane, into the sample solution. In the sample solution underneath the membrane, ammonia is converted to ammonium ions, acting as an ammonia sink.[1] This causes a gradient in gas concentration inside the channel and the membrane, resulting in diffusive transport of ammonia towards the sample solution to overcome this concentration difference.[2,3]

The analyte gas, the sample solution, the alkaline selection solution and the purified water stream are pumped through the system at continuous flow. Besides diffusion in the z-direction of the channel, the depth, convective transport in the y-direction, the length of the channel, also contributes to the transport of mass. An illustration of the membrane-channel system is given in figure A.1.

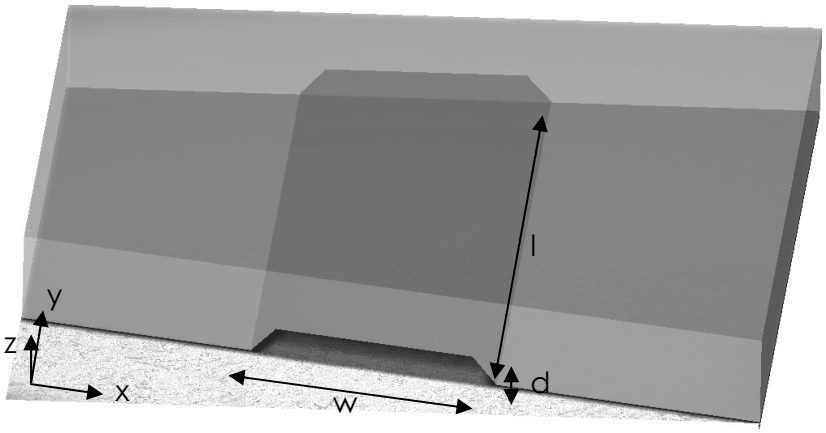

Figure A.1. Schematic representation of a channel above a membrane.

In this appendix, the influence of these two transport mechanisms is discussed for both gas and ion transport. The required theory about mass transport is described in the first section. Simulations that have been conducted to quantify gas transport and ion transport are shown in the second and third section respectively.

A.2 Diffusive and convective transport of gaseous ammonia

Diffusive transport is described by Fick's first law of diffusion, given in equation A.1 for one dimension,[2] in this case z. It states that the mass flux, J (mol/m^2·s), the net amount of solute that diffuses through a unit area per unit time, is proportional to the concentration gradient of the diffusing substance at time t of diffusion, $(\partial c/\partial z)_t$:

$$J \propto -\left(\frac{\partial c}{\partial z}\right)_t = -D\left(\frac{\partial c}{\partial z}\right)_t \qquad \text{(A.1)}$$

with D (m^2/s) is the diffusion coefficient of the diffusing substance.

In addition to diffusive mass transport, convection also influences the total transport of ammonia in the system. Whether convective mass transport is negligible compared to diffusive mass transport can be determined by calculating the dimensionless Peclet number, Pe, which works out to be the product of the system length, l (m), and mean fluid velocity, v (m/s), divided by the diffusitivity, D (m^2/s).[3] When Pe << 1, diffusion dominates mass transport and there is no bulk mixing. The Pe number is given in equation A.2.

$$Pe = \frac{l \cdot v}{D} \qquad \text{(A.2)}$$

The diffusivity of interest is the diffusion constant of gaseous ammonia in air, $1.21 \cdot 10^{-5}$ m^2/s.[2] In order to stay in the diffusion controlled regime, the Peclet number should stay below unity.

The macro scale device has a gas channel with a length of 1.5 meter and an average velocity of 4.2 m/s (1 l/min through a 2 mm * 2 mm channel),

resulting in a Peclet number of $6.9 \cdot 10^5$. This is far bigger than 1, implying that the convective mass transport does have influence on the total mass transport of ammonia towards the membrane. The miniaturized system will have a channel length in the order of centimetres. When the flow velocity is chosen comparable with the macro-scale gas channel, the Peclet number will be lowered two orders of magnitude but the mass transport is still significantly influenced by the convection.

The velocity of the gas inside the channel used to calculate the Peclet number can not be assumed to be constant over the entire channel. The flow velocity in a small channel at low flow rates results in a parabolic flow profile. The velocity of the flow, v (m/s), that goes through a channel with a certain length, L (m), when a pressure difference, ΔP (Pa), is applied over the channel, is a function of the viscosity of the gas or liquid, η (Pa·s), and the distance from the wall of the channel, r (m), as is given in equation A.3 for a circular capillary with a radius R (m).[2]

$$v = \frac{\Delta P}{4\eta L}(R^2 - r^2) \qquad \text{(A.3)}$$

However, equation A.3 only holds for a laminar flow profile, which is the case at low flow velocities and/or small channel dimensions. Whether the condition of laminar flow is fulfilled can be derived by calculating the Reynolds number, Re. The Reynolds number distinguishes between laminar flow, for a number below 2000, and turbulent flow, at numbers higher than 3500.[4,5] The Reynolds number can be calculated using equation A.4:

$$Re = \frac{\delta v \rho}{\eta} \qquad \text{(A.4)}$$

with δ (m) the hydrodynamic diameter of the channel and ρ the density of the gas or liquid (kg/m^3). The hydrodynamic diameter of a rectangular channel, with side length a and b (m), can be calculated using the equation A.5:

$$\delta = \frac{2ab}{a+b} \qquad \text{(A.5)}$$

For the case of gas flow through the macro rectangular channel with dimensions of 2 by 2 mm, a velocity of 4.2 m/s, a density of air of

1.293 kg/m^3 at atmospheric pressure and a viscosity of air $17.1 \cdot 10^{-6}$ Pa·s, the resulting Reynolds number is $6.4 \cdot 10^2$. This means that the flow regime is laminar and that the gas flow is parabolic. The miniaturized system has smaller channels so the Reynolds number will be even lower. Thus, in the miniaturized case, the flow profile will also be laminar. For the flow velocity consideration this implies that only at the sides of the channel, where the flow is very low, convective transport can be neglected. The total mass transport towards the membrane can thus not be solved with the simple 1D Fick's law shown in equation A.1.

Ammonia is continuously added by convective transport of analyte gas into the gas channel. This implies that the concentration gradient over the channel will be inhomogeneous over the length of the channel. As the analyte gas is transported along the channel, the concentration gradient decreases. For such cases, diffusion is expressed by Fick's second law, shown in equation A.6.[2]

$$\left(\frac{\partial c}{\partial t}\right)_z = D\left(\frac{\partial^2 c}{\partial z^2}\right)_t \qquad \text{(A.6)}$$

It is possible to add convective flux to this equation. For completeness, also the diffusion components in the x and y direction should be added to the equation. Since convection will only occur in the y direction, the total generalized diffusion equation in three dimensions can be written as:[6]

$$\left(\frac{\partial c}{\partial t}\right)_x = D\left(\frac{\partial^2 c}{\partial x^2}\right)_t + D\left(\frac{\partial^2 c}{\partial y^2}\right)_t + D\left(\frac{\partial^2 c}{\partial z^2}\right)_t - v_y\left(\frac{\partial c}{\partial y}\right) \qquad \text{(A.7)}$$

It is clear now that the velocity can not be assumed constant over the entire channel because a pressure driven flow in systems with a low Reynolds number results in a parabolic flow profile. This even makes the above equation more complex because the v_Y component is now a function of x and z. Solving this equation can best be done using a numerical solver in a software simulation package.

A.3 Simulation of ammonia transport

CFD-ACE, the finite element numerical solver from CFD Research Corporation, is used to investigate transport properties. Both diffusion and convection are taken into account. This software can be used to visualize parameters like flow, pressures, temperatures, and concentration profiles.

A.3.1 Macro scale gas sampler verification

The first conducted simulation was a flow velocity experiment to determine the flow profile in the channel, which should be parabolic according to the above discussion. The width of the channel is assumed such that the side walls have no effect so that a 2D model can be used. Although this assumption is not valid for the 2 mm by 2 mm macro channels, the miniaturized channels are much wider than they are deep. The actual influence on the simulation results is hard to predict. The velocity is higher in the centre and lower on the sides. It depends on the influence of the convective mass transport whether this will decrease or increase the total transport of mass.

A 2D model of the macro scale gas channel with a depth, d, of 2 mm and a length, l, of 1.5 meter is made in the simulation software geometry editor, the dimensions of the macro scale channel. A flow of 4.2 m/s is applied at the inlet of the channel, at the left. This is the average flow velocity inside the macro-scale gas sampler at normal operation, 1 l/min. The resulting flow profile from the simulation is shown in figure A.2.

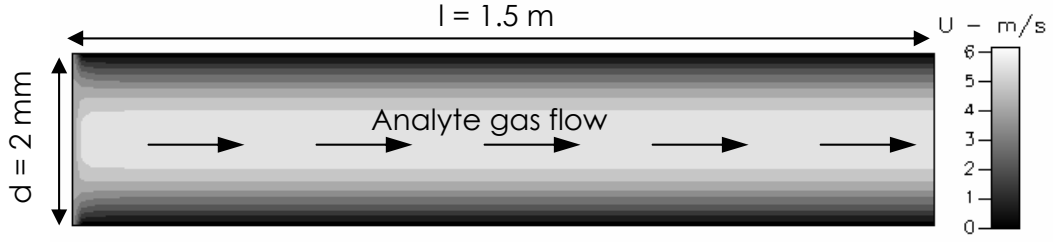

Figure A.2. *Flow profile inside the gas channel with pressure driven flow.*

After a certain entrance effect[5] the flow profile inside the channel is parabolic, as would be expected from the above discussion.

In the next conducted simulation, a gas mixture containing 80 % nitrogen and 20 % oxygen, approximately air, with 10 ppm of ammonia is used as the input gas. Because the reaction of ammonia with the sample solution is very fast, the ammonia concentration at the sample solution-membrane

interface is assumed zero. Because the membrane thickness is quite thin (150 µm) compared to the channel depth (2000 µm), the membrane is assumed to be negligible, concerning mass transport delay. Therefore, the ammonia concentration at the bottom of the gas channel is fixed at zero. The development of the ammonia concentration along this channel is shown in figure A.3.

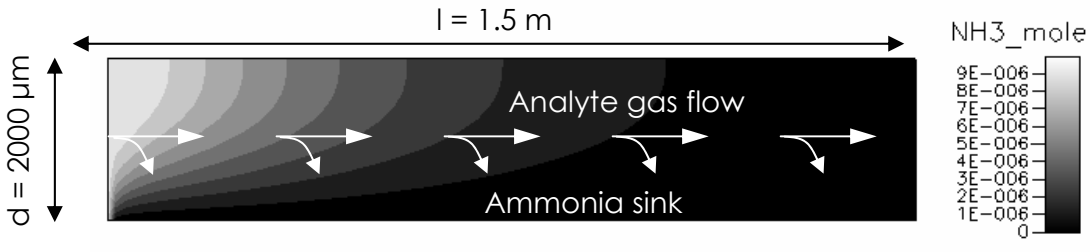

Figure A.3. *Ammonia concentration along the channel as a result of the ammonia sink function at the membrane interface at the bottom of the channel.*

The ammonia concentration along the channel can be copied from the simulation results for further analysis. The average ammonia concentration in a slice of the channel as a function of the distance from the inlet at the left of the channel, y (m), can now be determined. The amount of ammonia that is left in the channel is plotted as a function of the distance from the inlet, shown in figure A.4.

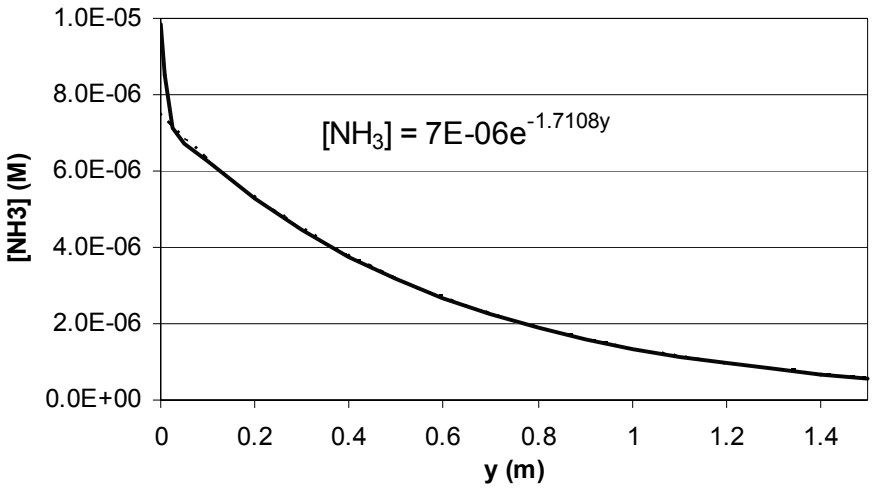

Figure A.4. *Average ammonia concentration as a function of the distance from the inlet.*

The decrease in ammonia concentration is an exponential function of the distance from the inlet. The simulation predicts a gas uptake after 1.5 m of about 95%, where an almost complete uptake of more than 99% is measured for the actual device. This might be caused by the assumption that the geometry can be simplified as a two dimensional problem.

A.4 Micro-scale gas sampler optimization

The next step is to simulate the miniaturized geometry that comprises a micro-channel. The depth of the gas channel, d_c, is about 100 µm. The used PP membrane has a thickness, d_m, of about 150 µm and is therefore not negligible in this situation. The simulation program can deal with porous media. Because ammonia does not react with the membrane material, the pores can be simulated as channels that only slow down diffusion and convection as a function of the porosity.[7–10] The porosity of PP membrane is about 70%, or 0.7. The ammonia sink layer is now simulated at the bottom of the membrane layer, at the interface with the sample solution.

The geometry is realized in the geometry editor of the simulation program CFD-ACE and simulations have been applied to determine the flow profile and the ammonia concentration in the system. First, a channel with a length of 10 mm is used to simulate the resulting flow profile in the channel and the membrane, shown in figure A.5. The top part of the image is the channel, where the analyte gas is pumped into with an average velocity of again 4.2 m/s. The lower part is the membrane with at the bottom of the membrane the ammonia sink layer.

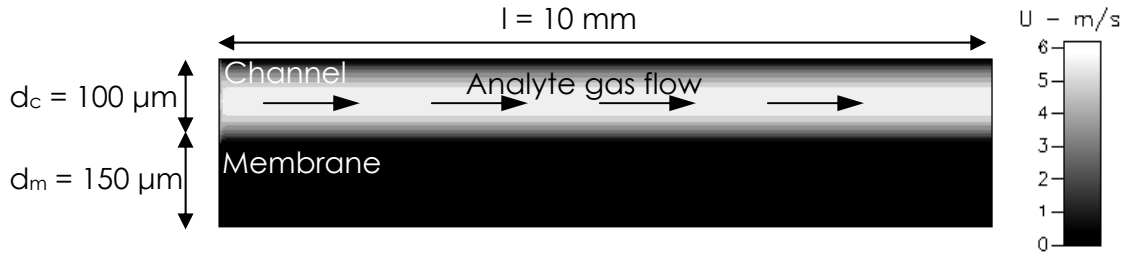

Figure A.5. *Flow profile inside the gas channel and the membrane with pressure driven flow through the channel.*

It is shown in figure A.5 that the flow profile in the channel is again parabolic, as expected from theory. Inside the membrane, there is very little flow. This seems plausible when looking at the actual membrane that is made up of thin layers of material, as is shown in appendix B. This limits convective flow.

With the same model of the miniaturized gas sampler, the ammonia concentration throughout the channel can be simulated in the same way as described for the macro scale gas sampler. A 4.2 m/s average flow of air with 10 ppm ammonia is applied to the gas channel. The resulting ammonia distribution is plotted in figure A.6.

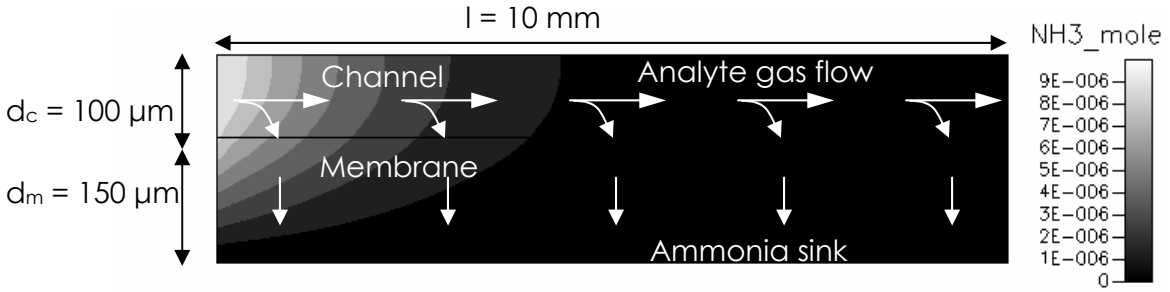

Figure A.6. *Ammonia concentration along the channel and the underlying membrane as a result of the ammonia sink function at the bottom of the membrane.*

Again, this data is copied to a spreadsheet program for further analysis. When the data points are plotted as a function of the distance from the inlet, as shown in figure A.7, the resulting ammonia concentration inside the system can be calculated.

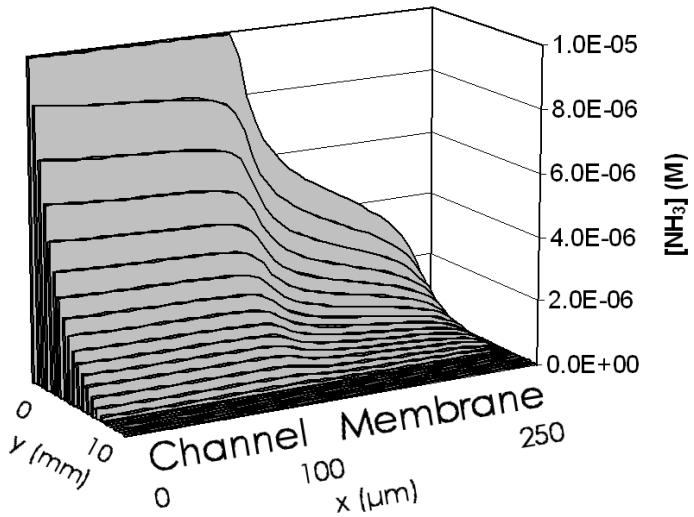

Figure A.7. *3D visualization of the ammonia concentration along the channel and the membrane.*

It is shown in this image that the membrane can not be neglected. In the channel, the left part of the figure, the distances are small compared to diffusion lengths and there is a small gradient in ammonia concentration towards the membrane. Inside the membrane, diffusion is slower and the diffusion length towards the ammonia sink layer is larger. Almost the complete gradient of ammonia concentration is present in the membrane.
Now, the amount of ammonia inside the channel can be determined as a function of the distance from the inlet along the channel by importing the simulation data in a spreadsheet program. The simulation result shown in figure A.7 showed that only 68 % of the ammonia was taken up after

10 mm. The simulation results are used in the optimization process discussed in the fourth chapter of this thesis. For the optimization, a gas uptake of 99.9 % is desired. Therefore, the length of the channel in the model is increased and the resulting ammonia consumption is shown in figure A.8 for a channel with a length of 50 mm.

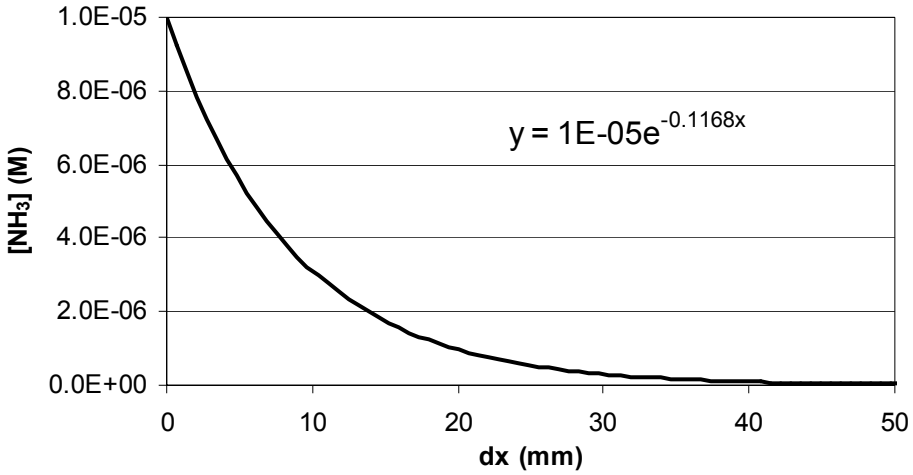

Figure A.8. *Average ammonia concentration in the system as a function of the distance from the inlet.*

It is shown in figure A.8 that the decrease in ammonia content in the gas channel is an exponential function of the distance from the channel inlet. It can be determined that a channel length of 59 mm is required to remove 99.9 % of the ammonia from the gas channel.

However, when the flow velocity is changed, the influence of the convective transport will alter compared to the diffusion component. At very low velocity, diffusion will dominate and at very high velocity, convective mass transport will dominate the flux of ammonia towards the membrane. Therefore, the time that is required to remove 99.9% is not a constant value. This makes it rather difficult to optimize the geometry of the system. The next simulations are used to investigate whether the required residence time can be assumed constant at velocity values around the 4.2 m/s used in the macro-scale device. The result is shown in figure A.9.

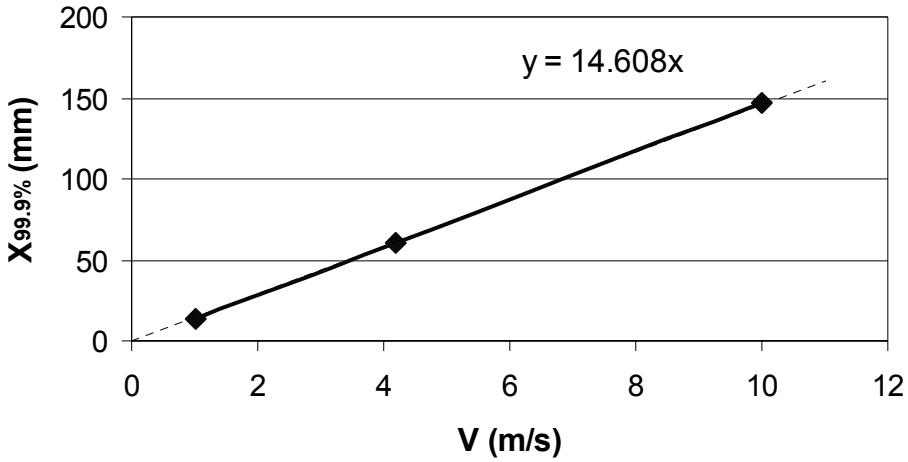

Figure A.9. *Channel length required to remove 99.9 % of the ammonia from the analyte gas in a 100 µm deep channel using a 150 µm thick membrane.*

At flow velocities from 1 to 10 m/s, it is shown that the residence time can be assumed independent of the flow velocity, without making a large error. The required residence time of the analyte gas in a 100 µm deep channel and a membrane thickness of 150 µm is 14.6 ms.

A.5 Simulation of ammonium transport

Once the analyte gas has passed the membrane, it comes in contact with the sample solution. An acid sample solution is used so that all the available ammonia is converted to ammonium ions, at least when the concentrations are not too high. In the previous section, the ammonia concentration at the interface between the sample solution and the membrane is assumed zero. This is only valid when the formed ammonium ions are transported from the interface fast enough. This section describes simulation experiments that investigate whether this assumption is legitimate.

A.5.1 Macro-scale gas sampler

In order to determine whether convection influences ionic mass transport in the sample solution, the Peclet number is calculated. First, this is done for the macro scale ammonia analyzer. The length of the sample channel is the same as the gas channel, 1.5 meter. The depth of the sample channel is 1/10th of the gas channel, 0.2 mm, resulting in an average flow velocity of $4.2 \cdot 10^{-3}$ m/s at a sample flow of 100 µl/min.[1] Ammonium ions in water have a diffusion constant of $1.96 \cdot 10^{-9}$ m^2/s.[2] With these values, equation A.2 results in a Peclet number of $3.2 \cdot 10^6$. This value is far bigger than 1, so convection does have a considerable influence on the total mass transport.[3] The

channels in the selector are shorter than the sample channel, but not so much that the Peclet number approaches unity.

Although it is possible to simulate porous media in CFD-ACE, it seemed not possible to model the water-repellent characteristic of the membrane used in the ammonia analyzer with normal simulation settings. Therefore, it is not suited for modelling the gas sampler as a whole. Instead, only the channel that comprises the sample solution is modelled, with an ammonium inflow at the upper interface layer.

The maximum ammonia concentration at the membrane interface in the macro-scale gas sampler is shown in figure A.3 to be equal to the initial ammonia concentration in the analyte gas flow of 10 ppm. Since one cubic meter of gas at atmospheric pressure contains 40.82 moles at room temperature, this ammonia concentration can also be expressed as $4.1 \cdot 10^{-7}$ M. The inflow of analyte gas is 1 l/min, or $1.67 \cdot 10^{-5}$ m^3/s. Therefore, the total ammonia input can be calculated to be $6.8 \cdot 10^{-9}$ mol/s.

The average ammonium concentration in the sample solution will be a thousand times higher than the sampled ammonia concentration due to the difference in flow rate between the analyte gas and the sample solution, or $4.1 \cdot 10^{-4}$ M. This ammonium influx is modelled as an inflow of an ammonium solution with a concentration of $4.1 \cdot 10^{-4}$ M. The flow rate can be calculated from the total ammonia inflow and the membrane surface area, $3 \cdot 10^{-3}$ m^2, to be $5.5 \cdot 10^{-6}$ m/s. The resulting ammonium distribution of this experiment is shown in figure A.10 for a channel length of 150 mm. The sample solution flow is set to $4.2 \cdot 10^{-3}$ m/s, as determined above.

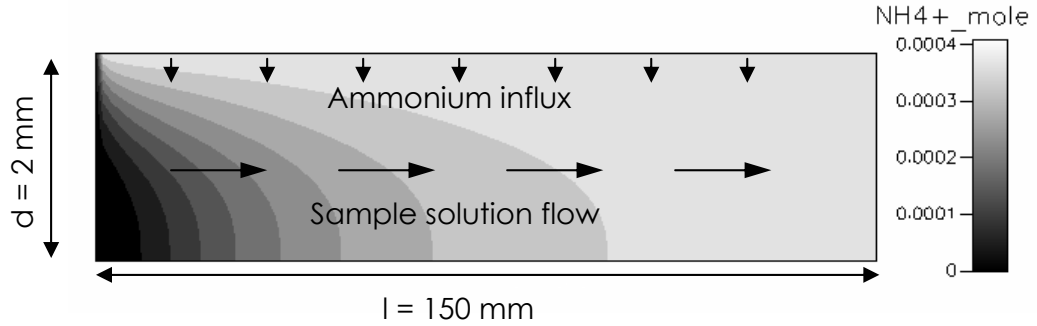

Figure A.10. *Ammonium profile development in the macro scale sample solution channel underneath the membrane.*

It is shown that, at the used flow rate, the ammonium is rather uniformly distributed over the channel after 150 mm. The sample solution channel in the macro scale gas sampler is even longer, 1.5 meters, so complete mixing can be expected. This situation does not equal the real situation, with a continuous ammonia flux towards the sample solution but a non-uniform ammonium concentration at the membrane interface. However, it is shown that diffusion and convection sufficiently transport ammonium into the whole channel depth.

A.5.2 Miniaturized gas sampler

The miniaturized selector channel will have the same length as the miniaturized gas channel, in the order of centimetres. The flow velocity will be in the same range as the macro-scale. The Peclet number is lowered two orders of magnitude due to the channel length reduction. The selector and detector channels will be shorter than the gas sampler but in the same order. Convection will thus be of influence on the mass transport of ions throughout the microfluidic system.

The model of the miniaturized ammonia analyzer was used to repeat the ammonium influx simulation. The ammonia influx can not directly be calculated in this case because the width of the channel is jet unknown. However, by defining the channel width as δy, the gas flow can be calculated to be the volume divided by the time constant: $l \cdot \delta y \cdot 100\mu m / \tau_{gas}$. This gas channel time constant was determined to be 14.6 ms. The length of the gas channel is the same time constant multiplied by the flow velocity, v_{gas} (m/s). With the ammonia concentration of 10 ppm, the total ammonia input can be calculated to be $4.1 \cdot 10^{-8} \cdot v_{gas} \cdot \delta y$ (mol/s).

The resulting ammonium concentration is determined by the concentration factor. The gas and the sample solution channel have the same length and width. The thickness of the sample solution channel will be fixed at the minimal suitable depth of 15 µm, see chapter 4 of this thesis. With these parameters, the concentration factor can be calculated to be $457 \cdot \tau_{sol}$, with τ_{sol} the mean residence time of the solution.

This residence time is the only parameter that is left unknown. It determines both the concentration factor and the flow velocity of the sample solution. In order to find an optimum, simulations have been conducted with different sample flow velocities. With the time constant that follows from the

chosen velocity, the concentration factor can be calculated, and thus the expected ammonium concentration. The resulting ammonia flow is the total ammonia input divided by the ammonium concentration and the membrane surface area, $l \cdot dy$ (m^2). The simulation result with a sample flow velocity of 4.2 mm/s, as used in the macro-scale gas sampler, is given in figure A.11 for a channel with a length of 3.3 mm.

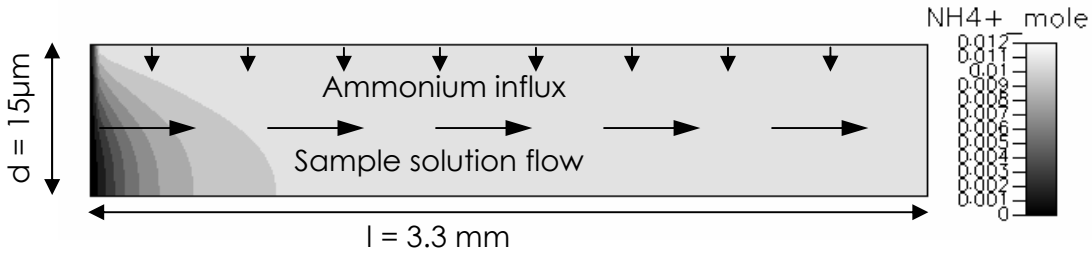

Figure A.11. *Ammonium level development in the miniaturized sample solution channel.*

The simulation data are exported to a spreadsheet program for further analysis. The difference in ammonium concentration directly underneath the membrane and at the bottom of the channel is determined as a function of the distance from the channel inlet. A concentration difference of 0.1 % is assumed as an indication for almost complete mixing. From the result, it can be determined that it takes 1.6 mm to reach total mixing, or 0.38 sec. The same simulation was performed with flow velocities around this value. The result is shown in figure A.12.

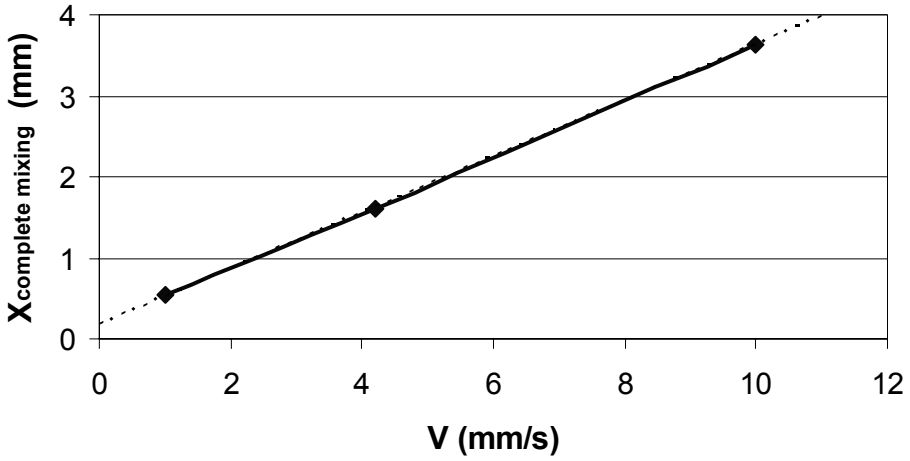

Figure A.12. *Minimum required liquid channel as a function of the flow velocity in the channel.*

It is shown in figure A.12 that the required channel length is again almost linear with the flow velocity, as for the gas channel, but there is a certain offset in the required channel length. This is caused by the time required for the ions to be transported in the channel. However, when taking this offset into account, the required time constant will always lie below about halve a second. No accumulation of ammonium ions underneath the membrane is expected when τ_{sol} is at least half a second.

Because the time offset is determined by the diffusion time required for transporting ions from the top to the bottom of the channel, the channel depth becomes a rather critical parameter. There is always some variation in the depth of the channels. Since diffusion time scales with the square of the depth, a τ_{sol} value of 1 second is used in the system optimization, discussed in chapter four of this thesis.

A.5.3 Selector

The selector channel in the macro scale device has a length of 200 mm, about 13 % of the gas sampler channel. The depth is the same as the sample solution channel, 0.2 mm. When looking at figure A.10, it seems that the mixing inside the channel after this distance is far from complete. Empirical data on the macro scale ammonia analyzer at ECN showed that 30 % of the ammonia in the sample stream is transported towards the detector. This seems plausible because the transport of ammonium towards the membrane is not optimal.

The channels in the miniaturized selector will have the same depth as the sample solution channel in the gas sampler, 15 µm, due to technical limitations. When the time constant of 1 second is applied again, total mixing is to be expected. This holds for both channels; the selector solution channel and the purified water channel.

A.6 References

[1] J.W. Erisman, R. Otjes, A. Hensen, P. Jongejan, P. v.d. Bulk, A. Khlystov, H. Möls and S. Slanina, *"Instrument development and application in studies and monitoring of ambient ammonia",* Atmospheric Environment 35, pp 1913-1922, 2001

[2] R. Chang, *"Physical chemistry for chemical and biological sciences",* University Science Books, 3rd ed., chapter 11, 2000

[3] W.M. Deen, *"Analysis of Transport Phenomena",* Oxford university press, New York, 1998

[4] P. Gravesen, J. Branebjerg, O.S. Jensen, *"Microfluidics – a review",* Journal of Micromechanics and Microengineering 3, pp 168-182, 1993

[5] M. Elwenspoek, T.S.J. Lammerink, R. Miyake, J.H.J. Fluitman, *"Towards integrated microliquid handling systems",* Journal of Micromechanics and Microengineering 4, pp 227-245, 1994

[6] P.W. Atkins, *"Physical Chemistry",* Oxford university press, Oxford, 5th edition,1994

[7] R. Ash, *"A note on permeation with boundary-layer resistance",* Journal of membrane science 186, pp 63-69, 2001

[8] I. Tarsiche, E. Hopirtean, D. Ciurcea, *"Design note, Least-squares analysis of ammonia diffusion through PTFE membranes",* Measurement Science and Technology 8, pp 1367-1371, 1997

[9] R.W. Schofield, A.G. Fane, C.J.D. Fell, *"Gas and vapour ransport through microporous membranes. I. Knudsen-Poiseuille transition"*, Journal of membrane science 53, pp 159-171, 1990

[10] H. Mahmud, A. Kumar, R.M. Narbaitz, T. Matsuura, *"Mass transport in the membrane air-stripping process using microporous polypropylene hollow fibers: effect of toluene in aqueous feed"*, Journal of membrane science 209, pp 207-219, 2002

Appendix B

Membrane characterization

B.1 Introduction

One of the most important parts of the ammonia measurement system is the phase-separation membrane. The membrane is used as an interface layer in the gas sampler, between the analyte gas and the sample solution, and in the selector, as an interface between the selector solution and the purified water stream. This chapter will discus the functionality of the membrane and characterization methods.

B.2 Membrane functionality

The function of the membranes in the "AMINA" principle is two-fold. First, the membrane is used to keep the liquid flows in place. All gas and liquid flows go through channels. The membrane is the boundary layer between the two flows in the sampler and in the selector. The membrane construction should be rugged enough to prevent the membrane from buckling into one of the two channels and clogging the device. This is easiest accomplished by using thick membrane layers or very stiff membrane materials. Especially Teflon®, PTFE, membrane, often used in gas extraction devices,[1-3] is very easily crumpled, which makes it hard to handle. Another membrane material that is used frequently in gas extractors is polypropylene, PP.[3-6] Such membranes are much stiffer and easier to handle.

The second function of the membrane, and probably the most important, is the specific permeability of the material.[7,8] Micro-porous membranes are used because gasses can pass through the pores in the membrane. Ions, however, should never be able to pass through the membrane because this would cause loss of the system functionality. This is accomplished by using hydrophobic materials, materials that are not wetted by water and

separate the gas phase inside the membrane with the water phase at the interface. This is very important because transport of ions through the membrane would drastically alter the ion concentration in the purified water stream inside the detector and disturb the EC measurement.

B.3 Porosity of a membrane

In order to transport gas through the membrane at a reasonable speed, the used membrane should be porous. Non-porous membranes do allow transport of gas through the membrane but this is rather slow.[9] The gas flux that will go through the pores of the membrane is not only determined by the thickness of the membrane but also by the amount of pores per unit of membrane surface area, the porosity.[10] Normally, membrane suppliers give a number for the porosity of a membrane. The membranes mentioned in this appendix have porosity values of about 70 %, or 0.7. One method to check the "openness" of the membrane is by visual inspection, using a microscope.[11] When the pore size becomes very small a scanning electron microscope, SEM, can be used. Figure B.1 shows SEM images of PTFE and PP membranes, acquired from Schleicher and Schuell (S&S).

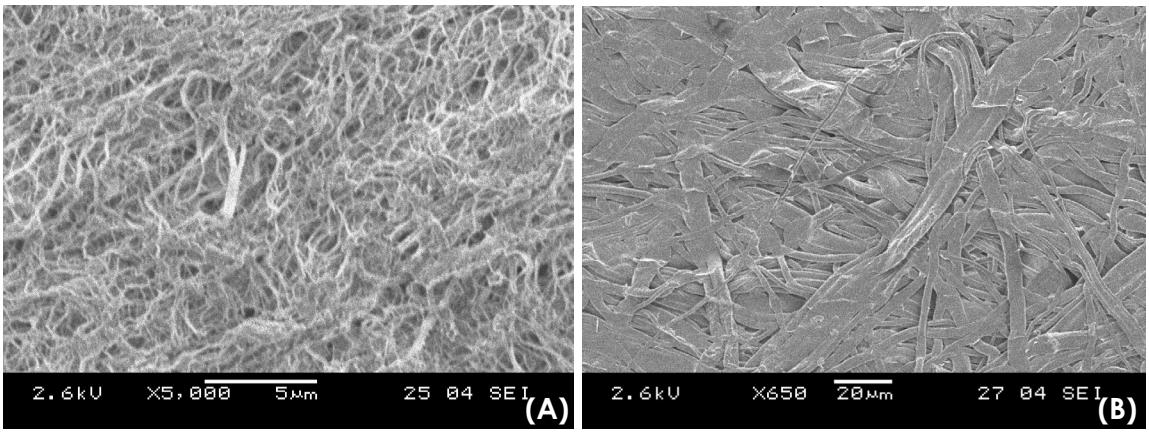

Figure B.1. *SEM pictures of (A) PTFE and (B) PP micro-porous hydrophobic membrane.*

Figure B.1 shows that the texture of the two materials is rather different. PTFE membranes are fish-net like structures that are very open. PP membrane seems constructed of overlapping sheets of material. Although the openness of the material seems less, from this image, the porosity value given by the manufacturer is the same.

B.4 Permeability of a membrane

A better way to determine whether a membrane is suited as a phase-separation layer is to investigate the pressure required to push gas or water through the membrane.[8] Since the suitable materials are highly porous, the material permeability to gasses is not so important in this situation. However, when the material itself is very permeable to ammonia, the gas is kept inside the membrane and released slowly, causing a delay in the ammonia measurement.

In order to function as a phase separation membrane between the gas inside the pores and the solution at the surface of the membrane, the pores have to stay filled with gas; no water may enter the pores. A technique that can be applied to characterize how resistant the membrane is against wetting is the bubble point detection method.[8,12-14] This technique is used in the chemical industry to check membrane filters for leakage. First, a membrane is completely wetted. Water-repellent membranes can be wetted in water under high pressure, by vacuum degassing or by prior wetting with a wetting agent, a low surface tension liquid, e.g. acetone. An increasing gas pressure is applied over the membrane until the water is pushed out of the membrane so that gas bubbles will appear on the other side of the membrane. The process is schematically shown in figure B.2.

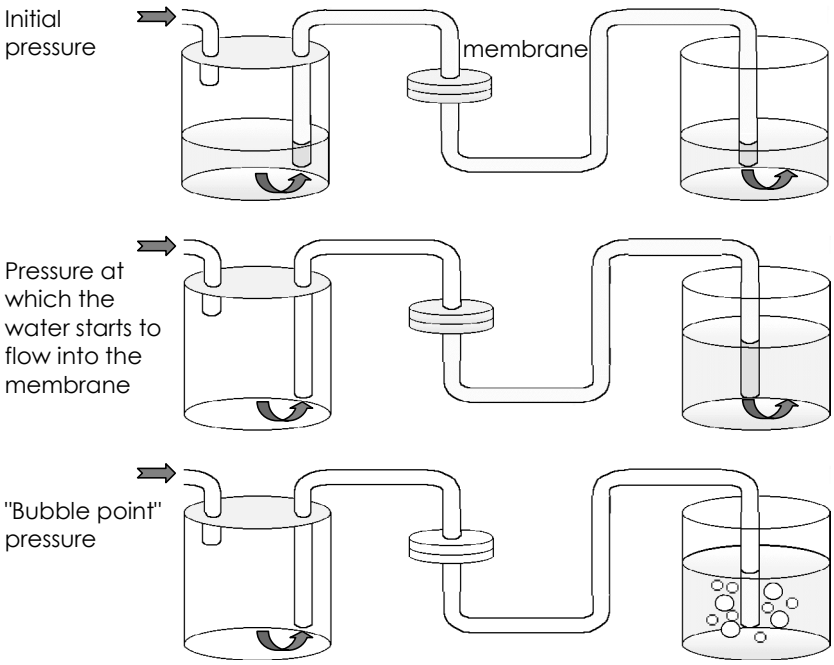

Figure B.2. *The bubble point method to determine the gas pressure at which the water is pushed out of a wetted membrane.*

This technique is used to measure the largest available pore size in the membrane. The effective pore-size of the membrane can be calculated using this bubble point pressure, ΔP (Pa), and equation B.1:

$$r_p = \frac{2\sigma_{sl}}{\Delta P} \cdot \cos(\varphi) \qquad (B.1)$$

with r_p the pore radius (m), σ_{sl} the interfacial surface tension between the solid and the liquid, at the water-membrane interface (N/m), and φ the contact angle at this interface.[8,13,15] The interfacial surface tension is the difference in surface tension of the used solution, in this case water with a surface tension of $7.3 \cdot 10^{-2}$ N/m, and the membrane material, here PTFE or PP with a surface tension of $1.8 \cdot 10^{-2}$ N/m and $2.9 \cdot 10^{-2}$ N/m respectively.[16]

Once the pressure is high enough to overcome the critical angle between the water front and the side of the pore, the water can penetrate the pore. For water and air, this critical angle is 0°.[8] The gas that presses against the water will pass through the membrane and appear on the outer side of the membrane as gas bubbles. This critical angle is reached easier in a wider pore. The process is visualised in figure B.3.[8]

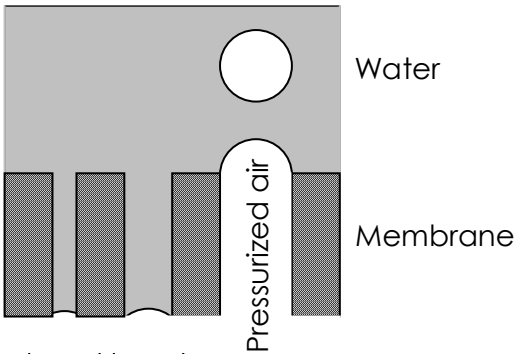

Figure B.3. *Principle of the bubble point detection method.*

The gas pass-through pressure should be very low, ensuring that gas is easily transported through the membrane. The water pass-through pressure should be very high, to ensure the required water-blocking characteristic of the membrane. Both micro-porous PTFE and PP have been tested for gas pass-through pressure and water pass-through pressure. The surface tension values are used to calculate the maximum effective pore size, using equation B.1. The pass-through pressures and the corresponding calculated pore size values are shown in table B.1.

Table B.1. *Gas and water pass-through pressure values.*

Membrane	Gas pass-through pressure (Pa)	Bubble-point pressure (Pa)	Calculated pore size (µm)
S&S PTFE 0.2 µm	$15 \cdot 10^2$	$1{,}7 \cdot 10^5$	0.65
Goretex PTFE 0.2 µm	$26 \cdot 10^2$	$1{,}8 \cdot 10^5$	0.61
S&S PP 0.2 µm	$8 \cdot 10^2$	$>1.9 \cdot 10^5$	<0.46

All three tested membranes only require a small pressure difference over the membrane to let a visually detectable gas flux pass through the membrane. It is difficult to see when the first gas bubbles appear, making these gas pas-through pressure data rather inaccurate maximal values.

The measured pressure difference required to push water out of the membrane is much higher than the gas pass-through pressures. Normally, in the chemical industry, lower surface tension liquids are used that result in a lower bubble point pressure. The high pressure differences found here might cause the membranes to deform during the experiments. The pore sizes that have been calculated from the bubble point pressure values also indicate this. Especially PTFE is a weak material that is easily deformed. The found pore sizes are larger than indicated by the suppliers. Although, the visual inspection of the membrane, shown in figure B.1, also indicates that the largest pores might be larger than 0.2 µm in diameter.

The conclusion that can be drawn from these results is that the maximum pressure difference over the membranes of the ammonia analyzer, both the macro scale device and the miniaturized version, should always stay well below the bubble point pressure of the used membrane since otherwise the material will loose the water-repellent characteristic that makes it a suitable phase-separating membrane for the described ammonia measurement system. A maximum allowable pressure difference of $1.7 \cdot 10^5$ Pa is used in the optimization process described in chapter 4 of this thesis.

B.5 Hydrophobicity of a membrane

Both mentioned membrane materials, PP and PTFE, are water-repellent, or hydrophobic. This literary means the material is "water hating". The material has little or no tendency to adsorb water. Hydrophobic materials have a low surface tension value and they lack active groups on the surface for formation of hydrogen-bonds with water. High surface tension liquids, like water, therefore tend to form discrete droplets on the surface. This causes the porous film to be non-permeable for water. Because the pores will stay filled with gas, no ions can diffuse through the membrane.

It depends on the surface tensions of the used materials if the surface is wetted by a certain liquid. Liquids that have low surface tension values will generally wet materials with higher surface tension values. Wetting is illustrated in figure B.4. When the angle between the surface of the material and a droplet of the liquid, called the contact angle, is 90 degrees or more, the material is called hydrophobic.[17] When the contact angle is less than 90 degrees the material is called hydrophilic (literally "water loving").

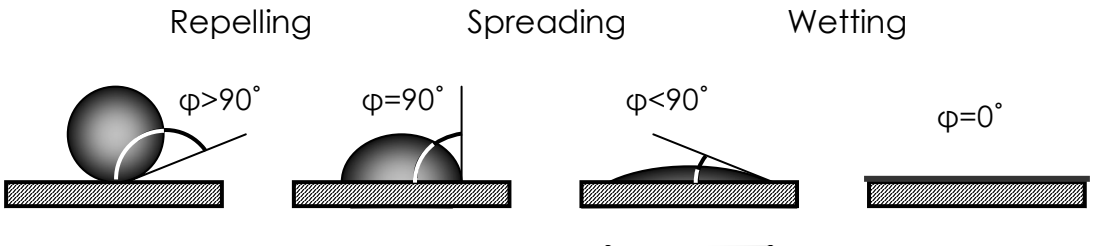

Figure B.4. *Wetting of solid surfaces: contact angle.*

With the hydrophobicity being an important parameter of the membrane, techniques have been investigated on measuring this parameter. Both the surface tension measurement and the contact angle measurement are of practical use. The two methods are related to each other by Young's equation;[15,18]

$$\cos(\varphi) = \frac{\sigma_{sv} - \sigma_{sl}}{\sigma_{lv}} \qquad \text{(B.2)}$$

relating the contact angle φ to the liquid-vapour surface tension, σ_{lv}, the solid-vapour surface tension, σ_{sv}, and the solid liquid surface tension, σ_{sl}. The used parameters are shown in figure B.5.[15]

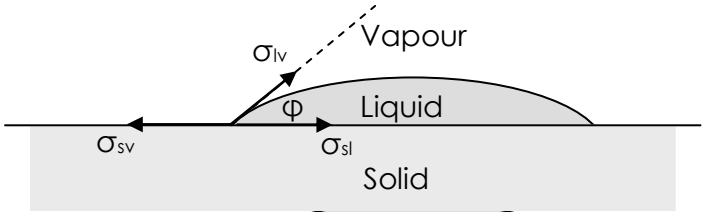

Figure B.5. *The parameters used in Young's relation.*

Although the relation between the contact angle and the surface tension is rather clear it is not practically easy to calculate the contact angle from the surface tension values because it is not possible to directly measure the solid-vapour and the solid-liquid surface tension. For our purpose, to determine whether a material is water-repellent, directly measuring the contact angle is a more suitable method.

Contact angle images have been made for both PTFE and PP membranes by taking an image from the side of a purified water droplet on the membrane surface using a video micro probe AS 14/50. Images are shown in figure B.6. The measured contact angles are 113˚ and 133˚ for PTFE and PP membranes, respectively. The standard deviation of the used technique is statistically determined to be about 4˚.

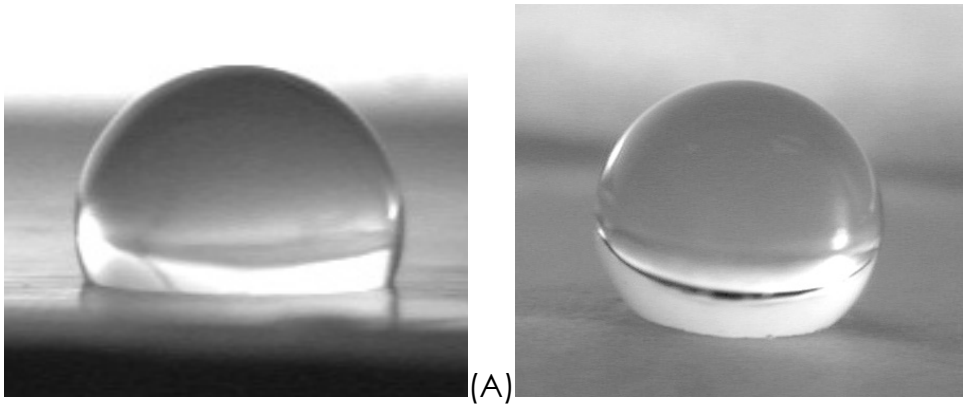
(A) (B)

Figure B.6. *Contact angle images of 0.2 µm porous PTFE (A) and 0.2 µm porous PP membranes with purified water.*

As shown in figure B.6, both tested material are water-repellent. When comparing these characteristics with the water pass-through pressure values shown in table B.1, it is clear that the higher contact angle value of the PP membrane also results in a higher bubble point pressure. Apparently, the material is more hydrophobic than PTFE although it has a higher surface tension. This might be caused by the roughness of the material, which is known to enhance the water-repellency of hydrophobic materials.[15]

B.6 References

[1] J.W. Erisman, R. Otjes, A. Hensen, P. Jongejan, P. v.d. Bulk, A. Khlystov, H. Möls and S. Slanina, *"Instrument development and application in studies and monitoring of ambient ammonia",* Atmospheric Environment 35, pp 1913-1922, 2001

[2] L. Thöni, E. Seitler, A. Blatter, A. Neftel, *"A pssive sampling method to determine ammonia in ambient air",* Journal of Environmental Monitoring 5, pp 96-99, 2003

[3] A. Gabelman, S-T Hwang, *"Hollow fiber membrane extractors",* Journal of membrane science 159, pp 61-106, 1999

[4] H. Mahmud, A. Kumar, R.M. Narbaitz, T. Matsuura, *"A study of mass transfer in the membrane air-stripping process using microporous polypropylene hollow fibers",* Journal of membrane science 179, pp 29-41, 2000

[5] S_I. Ohira, K. Toda, S_I. Ikebe, P.K. Dasgupta, *"Hybrid microfabricated devices for field measurement of atmospheric sulfur dioxide"*, Analytical Chemistry 74, pp 5890-5896, 2002

[6] P.v. Zweigbergk, R. Lindahl, A. Östin, J. Ekman, J-O. Levin, *"Development of a diffusive sampling method for determination of methyl isocyanate in air",* Journal of Environmental Monitoring 4, pp 663-666, 2002

[7] R.W. Schofield, A.G. Fane, C.J.D. Fell, *"Gas and vapour transport through microporous membranes. I. Knudsen-Poiseuille transition",* Journal of membrane science 53, pp 159-171, 1990

[8] M. Mulder, *"Basic principles of membrane Technology"* Kluwer Academic Publishers, Dordrecht, The Netherlands, Second edition, Chapter IV.3, pp162-18, 1996

[9] G.S. Patil, M. Bora, N.N. Dutta, *"Emperical correlations for prediction of permeability of gases/liquids through polymers",* Journal of membrane science 101, pp 145-152, 1995

[10] S. Srebnik, "Theoretical model of the porosity of copolymer membranes", Journal of membrane science 184, pp 97-106, 2001

[11] I. Masselin, L. Durand-Bourlier, J-M. Laine, P-Y. Sizaret, X. Chasseray, D. Lemordant, *"Membrane characterization using microscope image analysis",* Journal of membrane science 186, pp 85-96, 2001

[12] Porous Materials Inc., *"Automated bubble point tester",* Filtration & Separation 33 (5), p 370, 1996

[13] E. Jakobs, W.J. Koros, *"Ceramic membrane characterization via the bubble point technique",* Journal of membrane science 124, pp 149-159, 1997

[14] A. Hernandez, J.I. Calvo, P. Pradanos, F. Tejerina, *"Pore size distributions in microporous membranes. A critical analysis of the bubble point detection method",* Journal of membrane science 112, pp 1-12, 1996

[15] A. Torkkeli, A. Häärä, J. Saarilahti, H. Härmä, T. Soukka, P. Tolonen, *"Electrostatic transportation of water dropets on superhydrophobic surfaces"*, Proceedings of IEEE International Conference on Micro Electro Mechanical Systems, MEMS 2001, pp 475 – 478, 2001

[16] Internet source: http://www.gewater.com/library/tp/772_Hydrophilicity_and.jsp

[17] D.Y. Kwok, C.N.C. Lam, A. Li, A. Leung, R. Wu, E. Mok, A.W. Neumann, *"Measuring and interpreting contact angles: a complex issue"*, Colloids and surfaces A 142, pp 219-235, 1998

[18] R. Chang, *"Physical chemistry for chemical and biological sciences",* University Science Books, 3rd ed., chapter 11, 2000

Summary

The development of a miniaturized and integrated measurement system for gaseous ammonia is described in this thesis. The measuring principle, "AMINA", is an indirect method for selectively measuring ammonia that makes use of pH-transitions, electrolyte conductivity detection and phase-separating membranes. It is based on an environmental ammonia monitor developed by the Energy research Centre of the Netherlands, ECN. Reduction of the analyte gas volume and reagents consumption as well as an increase in speed would offer opportunities for new applications, e.g. diagnostic breath analysis. This was accomplished by miniaturization of the commercially available "AiRRmonia", in the project that resulted in this thesis. The key elements, a gas sampler, selector and electrolyte conductivity detectors, were realized on a chip using micro system technology. The system dimensions were optimized using mass-transport simulations. The conductivity detector with planar interdigitated electrodes was optimized for measuring low ion concentration in a small volume. Ultimately, an integrated sensing chip was realized with an analyte gas consumption that is reduced by a factor of more than 100 and a response time that is reduced from about 20 to 1.6 minutes, using a gas flow of 50 ml/min. The sensing chip has a calculated lower ammonia detection limit of 1.1 ppb. This detection limit and the small analyte gas consumption make the sensing chip suitable for measuring breath ammonia, where lower concentration levels of about 50 ppb can be found. Under normal atmospheric conditions the selectivity of the system is sufficient to measure ammonia concentrations in the low-ppb range. The system is even sufficiently selective to be used in analyte samples that contain elevated carbon dioxide levels, like exhaled air. The characteristics of the presented sensing device could be further optimized by increasing the efficiency of the used gas sampler. Two alternatives are proposed; a direct gas-liquid mixer with an integrated degasser that is shown to effectively sample ammonia from an analyte gas and a thin micromachined membrane with a self-aligning buried channel, resulting in decreased mass transport distances.

Samenvatting

In dit proefschrift is de ontwikkeling van een verkleind en geïntegreerd meetsysteem voor ammoniak beschreven. Het gebruikte "AMINA" principe is een indirecte, selectieve meetmethode voor ammoniak waarbij gebruik gemaakt wordt van pH-overgangen in vloeistofstromen, geleidbaarheidsdetectoren en fase-scheidings membranen. Het is gebaseerd op een ammoniakmonitor ontwikkeld door het Energie Onderzoek centrum van Nederland, ECN. Vermindering van het analysegas- en reagentiaverbruik en tevens versnellen van het systeem maakt nieuwe applicaties mogelijk, b.v. diagnostische ademanalyse. Dit is bereikt door de commercieel verkrijgbare "AiRRmonia", te verkleinen, zoals beschreven in dit proefschrift. De belangrijkste onderdelen, een gassampler, scheider en geleidbaarheidsdetectoren, zijn met micro-systeemtechnologie op een chip gerealiseerd. De dimensies van de gebruikte kanalen zijn geoptimaliseerd met massatransport simulaties. De detectoren, met integreerbare kamstructuur elektroden, zijn geoptimaliseerd voor het meten van lage ion concentraties in een klein volume. Deze componenten zijn vervolgens geïntegreerd in een meetchip, waarbij de gas consumptie met meer dan een factor 100 verkleind is en de responstijd van 20 naar 1.6 minuten teruggebracht is, bij een gasconsumptie van 50 ml/min. De meetchip heeft een berekende detectieondergrens voor ammoniak van 1.1 ppb. Deze ondergrens en het kleine benodigde gasvolume maken de meetchip geschikt voor het meten van ammoniak in adem, waar een ondergrens van 50 ppb verwacht kan worden. Voor normale buitenlucht is de selectiviteit van de meetchip voldoende voor het meten van ammoniakconcentraties in het laag-ppb bereik. Ook in situaties met een verhoogde CO_2 concentratie, zoals in adem, is de selectiviteit voldoende. De eigenschappen van het systeem zouden verder verbeterd kunnen worden door de effectiviteit van de gebruikte gassampler te verhogen. Hiervoor zijn twee alternatieven uitgewerkt; een directe gas-vloeistof mixer met ingebouwde ontgasser, waarmee ammoniak effectief opgenomen kan worden uit een gasstroom, en een dunner membraan gemaakt met microsysteemtechnologie, voor het verkleinen van massatransport afstanden.

Dankwoord

Dit proefschrift was nooit tot stand gekomen zonder de hulp en steun van een heleboel mensen, die ik hierbij allemaal hartelijk wil bedanken. Het is voor mij onmogelijk goed werk te leveren zonder me geregeld goed te ontspannen zodat ik me goed blijf voelen. Hierbij heb ik steun gehad van mijn vriendin, Chantal, mijn familie en mijn vrienden; o.a. Martijn, Bastiaan & Anita, Collin & Kristel en Edwin, en de dinsdagavond-fietsvrienden.

Ook een goede werksfeer is erg belangrijk. Alle collega's die hieraan hebben bijgedragen, zoals bijvoorbeeld Sebastiaan & Dorothee, Erik, Sjouke Ed en Annie, maar natuurlijk ook alle andere BIOS collega's, hartelijk dank. Ik mag mijzelf ook erg gelukkig prijzen met alle zeer gemotiveerde studenten die zich gedurende de vier jaar van het promotie project voor mij ingezet hebben. Dit zijn: twee groepen D1 studenten: Sven, Tristan en Menno en Floris, Alfons, Anne en Frank, twee IOO studenten, Wouter en Wabe (verantwoordelijk voor delen van hoofdstuk 4), een HBO-afstudeerster, Tzvetelina (verantwoordelijk voor een deel van hoofdstuk 6), en een afstudeerder, Erik.

Er missen hier echter een paar erg belangrijke mensen, personen die, naast het "goede-sfeer maken", voor het project en mijn persoonlijke ontwikkeling binnen het "onderzoeker zijn" veel bijgedragen hebben. Wetenschap moet je leren, dat werd mij snel duidelijk bij interessante discussies met mensen als Theo, Niels en later Jan. Studenten begeleiden leerde ik vooral van Bart en Emiel. Op het technische vlak heb ik veel gehad aan de hulp van Ad, Johan, Ton en vooral Koen. Tenslotte was het project nooit geslaagd, en sowieso al nooit opgestart, zonder de inbreng van mijn begeleiders, Piet, René, Ron en vooral Wouter en Albert.

Bedankt allemaal voor de afgelopen vier jaar, ook al die mensen die ik hier niet bij naam genoemd heb.

Björn

List of publications

Accepted journal papers

I. S. Böhm, B.H.Timmer, W. Olthuis, P. Bergveld, "*A closed loop controlled electrochemically actuated micro dosing system*", J. Micromech. Microeng. 10, pp 498-504, 2000

II. B.H. Timmer, W. Sparreboom, W. Olthuis, P. Bergveld and A. v.d. Berg, "*Optimization of an electrolyte conductivity detector for measuring low ion concentrations*", Lab on a chip 2 (2), pp. 121-124, 2002 (**Chapter 4 of this thesis**)

III. B.H. Timmer, K.M. v. Delft, W. Olthuis, P. Bergveld, A. van den Berg, "*Micro-evaporation electrolyte concentrator*", Sensors and Actuators B 91, pp 342–346, 2003

IV. B.H. Timmer, K.M. v. Delft, R.P. Otjes, W. Olthuis, A. v.d. Berg, "*A miniaturized measurement system for ammonia in air*", Analytica Chimica Acta 507 (1), pp. 139-145, 2004 (**Chapter 3 of this thesis**)

V. B.H. Timmer, W. Olthuis, A. v.d. Berg, "*Sampling small volumes of ambient ammonia using a miniaturized gas sampler*", accepted for publication in Lab on a chip. (**Chapter 7 of this thesis**)

In preparation for publication

VI. B.H. Timmer, W. Olthuis, A. v.d. Berg, "*Ammonia sensors and their applications, a review*", submitted to Sensors and Actuators B. (**Chapter 2 of this thesis**)

VII. B.H. Timmer, W.W. Koelmans, K.M. v. Delft, W. Olthuis, A. v.d. Berg, "*Selective low concentration ammonia sensing in a microfluidic lab-on-a-chip*", submitted to Lab-on-a-chip. (**Chapter 5 of this thesis**)

Conference contributions

I. S. Böhm, B.H. Timmer, W. Olthuis, P. Bergveld, "*A closed loop controlled electrochemically actuated micro dosing system for in situ sensor calibration*", MicroTAS 2000, Enschede (NL), poster and proceedings contribution, pp. 347-350, 2000.

II. B.H. Timmer, J.G. Bomer, K.M. v. Delft, R.P. Otjes, W. Olthuis, P. Bergveld, A. v.d. Berg, "*Fluorocarbon coated micromachined gas sampling device*", MicroTAS 2001, Monterey (USA), poster and proceedings contribution, pp. 381-382, 2001 (**The first part of chapter 6 of this thesis**)

III. B.H. Timmer, W. Sparreboom, W. Olthuis, P. Bergveld, A. v.d. Berg, "*Planar interdigitated conductivity sensors for low electrolyte concentrations*", SeSens, Veldhoven (NL), poster and proceedings contribution, pp. 878-883, 2001

IV. B.H. Timmer, W. Olthuis, P. Bergveld, A. v.d. Berg, "*Miniaturization of an ammonia detector - from gas to conductivity*", Annual MESA+ meeting, Hengelo (NL), poster presentation, 2001

V. B.H. Timmer, W. Olthuis, P. Bergveld, A. v.d. Berg, "*Miniaturization of an ammonia detector - from traces of gas to conductivity*", Sense of contact, Woudschoten (NL), poster and proceedings contribution, 2002

VI. B.H. Timmer, K.M. v. Delft, W. Olthuis, P. Bergveld, A. v.d. Berg, "*Micro evaporation electrolyte concentrator*", The 9th International Meeting on Chemical Sensors, Boston (USA), oral presentation and proceedings contribution, pp. 103, 2002

VII. W. Olthuis, E.J. Faber, B.H. Timmer, P. Bergveld, "*Optimized design rules for electrolyte conductivity sensors*", The 9th International Meeting on Chemical Sensors, Boston (USA), part of a proceedings contribution, pp. 189, 2002

VIII. B.H. Timmer, W. Olthuis, P. Bergveld, A. v.d. Berg, "*Miniaturization of an ammonia sampler*", NanoTech 2002, Montreux (CH), poster, 2002

IX. B.H. Timmer, K.M. v. Delft, T.D. Dermendjieva-Jansink, W. Olthuis, P. Bergveld, A. v.d. Berg, "*Non-destructive test for anodic bonding characterisation of "thick" silicon nitride bonded to glass*" MME 2002, Sinaia (RO), poster and proceedings contribution, pp. 339-341, 2002 (**The second part of chapter 6 of this thesis**)

X. B.H. Timmer, "*Miniaturization of an analyser for trace amounts of ammonia*", NWO congres Studiegroep Analytische Scheikunde, Lunteren (NL), oral presentation, 2002.

XI. B.H. Timmer, K.M. v. Delft, T.D. Dermendjieva-Jansink, W. Olthuis, P. Bergveld, A. v.d. Berg, "*Non-destructive test for anodic bonding characterisation of "thick" silicon nitride bonded to glass*", Annual MESA+ meeting, Enschede (NL), poster, 2002

XII. B.H. Timmer, W. Olthuis, P. Bergveld, A. v.d. Berg, "*Miniaturization of a gas sampler for low ammonia concentrations*", Sense of Contact 5, Veldhoven (NL), poster and proceedings contribution, 2003

XIII. B.H. Timmer, K.M. v. Delft, R.P. Otjes, W. Olthuis, P. Bergveld, A. v.d. Berg, "*Towards a miniaturized ambient ammonia detection system*", microTAS 2003, Squaw Valley (USA), poster and proceedings contribution, pp. 81-84, 2003

XIV. B.H. Timmer, K.M. v. Delft, R.P. Otjes, W. Olthuis, P. Bergveld, A. v.d. Berg, "*Towards a miniaturized ambient ammonia detection system*", Annual MESA+ meeting, Enschede (NL), poster, 2003

XV. B.H. Timmer, W.W. Koelmans, K.M. v. Delft, W. Olthuis, A. v.d. Berg, "*Selective low concentration ammonia sensing in a microfluidic lab-on-a-chip*", Sense of Contact 6, Wageningen (NL), poster and proceedings contribution, 2004

XVI. B.H. Timmer, W.W. Koelmans, K.M. v. Delft, W. Olthuis, A. v.d. Berg, "*Selective low concentration ammonia sensing in a microfluidic lab-on-a-chip*", submitted to μTAS 2004